JOINT EUROPEAN TORUS JET

JET–P(94)48

Many Authors

JET Papers presented at the 15th IAEA Conference on Plasma Physics and Controlled Nuclear Fusion Research

(Seville, Spain, 26 September–1 October 1994)

JET Papers presented at the 15th IAEA Conference on Plasma Physics and Controlled Nuclear Fusion Research

(Seville, Spain, 26 September–1 October 1994)

Many Authors

JET-Joint Undertaking, Culham Science Centre, OX14 3DB, Abingdon, UK

Preprint of Papers to be published in the Proceedings of
15th IAEA Conference on Plasma Physics and Controlled Nuclear Fusion Research
(Seville, Spain, 26 September-1 October 1994)

JET Papers presented at the
15th IAEA Conference on
Plasma Physics and Controlled Nuclear Fusion Research
(Seville, Spain, 26 September–1 October 1994)

The New Experimental Phase of JET and Prospects for Future Operation

The JET Team
(presented by D Stork)

JET Joint Undertaking, Abingdon, Oxfordshire, OX14 3EA, UK.

THE NEW EXPERIMENTAL PHASE OF JET AND PROSPECTS FOR FUTURE OPERATION

The JET Team
(presented by D Stork)

JET Joint Undertaking,
Abingdon, Oxon, OX14 3EA, UK.

ABSTRACT

The upgrade of the Joint European Torus (JET) to install the Pumped Divertor (PD) machine configuration has been recently completed. The initial results from the JET-PD device are reviewed with emphasis on Divertor issues; confinement and power threshold in H-mode; high β_p plasmas; steady-state H-modes; high performance results and non-inductive current drive. Consequences for the future operation of JET are described. Finally, the JET programme in the near-, medium- and longer terms is discussed.

1. INTRODUCTION – A NEW MACHINE

The shutdown of the JET experimental device to perform the upgrade to the 'Pumped Divertor (PD)' configuration was completed successfully at the end of January 1994. During this shutdown, an exceptionally large number of new components and facilities were installed in the Tokamak vessel and its associated power and control systems. Taken as a whole, these modifications comprise in essence a completely new machine and this paper overviews the first experimental results from this new machine.

The cross section of the JET-PD configuration is shown in fig.1. The principal in-vessel modifications include: internal divertor coils to enable a wide range of plasma equilibria and divertor geometries to be investigated; a new toroidally continuous array of Carbon Fibre Composite (CFC) divertor tiles for improved power handling; a toroidally continuous cryopump to allow the study of fuelling strategies and impurity control mechanisms; the replacement of the previous 'belt' limiters with poloidal limiters at discrete locations on the toroidal circumference; a new Lower Hybrid Current Drive (LHCD) launcher connected to 24 klystrons giving an eventual launch capability of 10MW; and a new set of Ion Cyclotron Radio Frequency (ICRF) antennae arranged in four current strap modules to allow phased operation for Fast Wave Current Drive (FWCD) and designed to couple to the plasma at larger distances. In addition, the power supply and position control systems have been modified substantially to give the capability of sweeping the X-point and divertor strike points at 4Hz to increase the wetted area of the target for long pulse high-power heating studies, a facility designed to complement the improved, carefully aligned tiles. The Neutral Beam Injection (NBI) system has also been modified slightly to incorporate a facility for vertical steering on some of the ion sources, to allow central power deposition in plasma equilibria displaced above the vessel midplane. The NBI system is now a mixed energy (80keV/140keV) system, and will have an eventual injection capability of 22MW. The fuelling and conditioning systems of the machine have also been upgraded; featuring new glow discharge electrodes; new beryllium evaporator heads (4 in number); and toroidally-symmetric gas fuelling in the divertor region. Finally, an extensive range of new diagnostics, specifically designed to provide a detailed analysis of the divertor region, have been installed. Most of thje existing diagnostics had also to be modified for compatibility with the PD configuration and several were completely upgraded.

The operation of the JET-PD device was commissioned in the period February to end-April 1994, and the experimental campaign began in May 1994. The programme

to date has been divided between; evaluating the methods of running the new machine; benchmarking conditions to be expected in the 'Mark II' divertor configuration, due to be installed in 1995 (see section 9), so that assumptions in the design could be verified; and a programme of experiments, covered in detail elsewhere in these proceedings, grouped under the broad headings of *'Divertor Physics'* [1],[2], *High performance studies'* [3], and *'Tokamak concept improvement'* [4].

This paper initially reviews the general features of JET-PD operation. The technical aspects of the programme for Divertor Physics, are then briefly described. The confinement properties of the H-mode in various regimes are discussed. The development of long-pulse steady-state H-modes outlined and the High Performance work overviewed. The non-inductive current drive studies are also covered in brief. Finally, the future JET programmes in the short, medium and long term are outlined.

2. GENERAL OVERVIEW OF JET-PD OPERATION

2.1 Vacuum and vessel conditions

The JET-PD vacuum vessel is baked at 250°C during operations. This is a lower temperature than JET used up to 1992 (300°C) and has been constrained to date by the need to remain prudent during the first few months of operation. Vacuum integrity has been maintained at this temperature, the value of which has been limited until safety analyses could establish that, in the event of an air leak, the increased heat transfer to the divertor coils by conduction and convection could be overcome by cooling the vessel fast enough before over-ageing of the coil epoxy occurs. This has now been verified [5], and baking of the machine to 300-320°C should commence at the end of September 1994. The divertor tiles are carried on water-cooled supports and these keep the tiles at around 40°C ***between*** pulses. The surface conditions are thus different from those in the original JET machine. In addition, the inner wall has much less area covered with carbon tiles, than in the 1991-2 JET configuration.

These significant changes have not altered the basic high quality vacuum obtained in JET. Table 1 shows that the quality of the vacuum after the initial glow discharge is very similar to that in previous campaigns, and that the important partial pressures are significantly reduced when the Pumped Divertor cryopump is cooled to liquid nitrogen and liquid helium temperatures.

TABLE 1
Vacuum conditions in JET-PD (vessel at 250°C)

Typical values of → after ↓	Mass 18 (mbar)	Mass 20 (mbar)	Mass 28 (mbar)	Mass 44 (mbar)
He GDC only	2.10^{-8}	$1.5\ 10^{-8}$	1.10^{-8}	$3\text{-}5\ 10^{-10}$
Fresh beryllium evaporation	4.10^{-9}	$3.5\ 10^{-9}$	$3\ 10^{-9}$	5.10^{-10}
Cryopump with LN_2 + LH_e (No Be evap)	1.10^{-9}	$6.5\ 10^{-10}$	$2\ 10^{-9}$	Below detection limit

2.2 Operating space

During the initial 4 months of the Experimental Campaign the JET-PD device has been operated at $1.0 \leq I_p \leq 4.0$MA and $1.0 \leq B_T \leq 3.4$T in a variety of configurations. These range from small volume, high aspect ratio (A ~ 3.7)

plasma at 1MA, through 2MA slim high clearance plasmas for Divertor physics studies to fat plasmas at 4 MA. An example of six of these configurations is shown in fig.2, indicating the flexibility of the coil set.

In all these configurations, the measured error fields are much lower than obtained in the old JET configuration, being around 0.2-0.4 gauss compared to 1.7 gauss in the 1991-2 High Performance configuration [6]. This is a result of highly accurate installation of the divertor coils, since a displacement of ± 2mm in these coils would lead to an error field ~ 0.2 gauss. These lower error fields have already opened up a possibility of low density operation ($\langle n_e \rangle \sim 1\ 10^{19} m^{-3}$) at low q ($q_{95} < 2.5$) without the risk of locked modes. This regime remains to be properly exploited. The range at low q is especially important as the plasma volume in the JET-PD configuration is lower (by ~ 30 %), leading to a lower q(a) for similar plasma current.

Initial investigations have covered several operating regimes including low density 'Hot Ion' discharges [3], medium density steady-state H-modes and detached plasmas [2]. In all regimes, the striking difference from previous JET operation is the significantly increased recycling. This high edge fuelling has led to the ubiquitous appearance of ELMy behaviour in the JET H-modes. Investigation of ELMs, which is still continuing, is covered in section 4 and also in ref [3].

Impurities do not seem to be a significant problem in the new JET operation however. Radiated powers remain relatively low (20-30% of input power) and Z_{eff} is usually < 2-2.5 except in certain unusual circumstances. The contamination of nickel is low, in spite of the larger area of plasma-facing metal wall.

3. DIVERTOR PHYSICS STUDIES

3.1 Power handling of the JET-PD target

The power handling of the JET-PD target tiles has been evaluated in comprehensive initial studies. The ***horizontal*** target tiles have excellent alignment (maximum error ~ ± 0.3mm) and are carefully designed to avoid the incidence of power on tile edges. Infrared thermography of the strike zones on the tiles shows that, even without plasma sweeping, a total conducted energy of 40MJ to the tiles brings the peak temperature of the strike zones to only ~ 1000°C. This is shown for a series of 14MW NBI heated plasmas in fig.3. The performance achieved is a considerable improvement over the 10-15MJ of conducted power at which carbon bloom temperatures were previously reached on the JET X-point tiles even in ELMy H-modes [7]. This has resulted in improved access to longer pulse lengths at high power.

The situation is even better when divertor sweeping is applied. In these cases, even at high input powers, a quasi-stationary tile temperature can be achieved. Figure 4 shows traces from a discharge with 25MW of combined heating power in a typical JET-PD ELMy H-mode regime. The application of divertor sweeping at 13s brings the maximum temperatures at inner and outer zones into a cyclic pattern with peak temperatures in the range of 550-650°C even after 3 seconds and a total of ~ 72MJ energy conducted to the tiles. This behaviour has been exploited in the development of the long pulse ELMy H-modes (section 5). The application of the sweeping has ***not*** so far been found to be correlated with, or a cause of, ELM behaviour.

3.1.1 Operation with reverse fields

The imbalance between the power conducted to the inner and outer strike zones in the normal direction of the ion ∇B drift (towards the X-point) can be up to 40% in the ELMy H-modes, with more power conducted to the outer zone. In previous JET campaigns it has been

observed [8], that the power conducted to the strike zones was more equal in the case of ion ∇B drift away from the X-point ('reversed' ∇B operation). This has been coupled with the observation of more equal densities at the strike zones in the reversed ∇B case, giving higher radiated power at the inner zone; a more favourable carbon bloom behaviour; and the possibility of having both zones in the same divertor regime [9].

A series of experiments in the JET-PD have been carried out to compare the characteristics of 'normal' and 'reversed' ∇B divertors. The results are covered in detail in [1] and are still under investigation. The clearest trend is seen by comparing L mode discharges where the imbalance in power loading between the strike zones can be seen to be strongly dependent on B_T and q_{cyl}. Results in line with the previous JET findings are produced at low q and low B_T, where the power conducted to the strike zones is more equal for the reversed ∇B case. On the other hand at higher q and B_T, the power loading asymmetries are worse in the reversed ∇B case. The conclusion from D_α asymmetries is that the B_T reversal affects directly the density redistribution between the two strike zones rather than the power distribution into the two divertor channels. The conclusion for JET-PD operation is that the choice of best operating regime (normal or reversed ∇B) will depend on factors other than a straightforward power equalisation criterion. The data were taken with the equilibrium shown in fig.2(c).

3.2 Operation with the PD cryopump

Previous JET operation with near steady-state in the ELMy H-mode has avoided the carbon bloom by using ELMs partly to transport impurities out of the edge plasma [7], and partly to spread the power loading on the tiles and reduce temperatures [10]. The 18 sec ELMy H-modes described in ref [10] suffered from steadily rising density and falling confinement as the edge recycling increased. One of the missions of the JET-PD divertor cryopump work is to overcome this and the pump has been used extensively in recent operation.

The speed is the pump for molecular deuterium is ~ $170 m^3 s^{-1}$, including the input conductances. The particle removal rate has been measured as high as $8\ 10^{21}\ D \cdot s^{-1}$ in Ohmic plasmas with $\langle n_e \rangle \sim 4\ 10^{19} m^{-3}$ when the X-point strike zone is near the pump entrance. The variation of this removal rate with strike zone position is illustrated in fig.5 which exhibits an increasing particle removal rate as the strike zones are swept nearer to the entrance of the pump. In this case the approximately constant gas feed is unable to maintain the requested plasma density.

The particle removal rate is still sufficient, even when the strike zone is ~ 20cm from the pump entrance, to cope adequately with the particle input from 10MW of NBI heating (~ $10^{21}\ D \cdot s^{-1}$) with a factor ~ 3 in hand at moderate densities ($n_e \sim 6\ 10^{19} m^{-3}$). The experience with the pump is described in more detail in [1]. An additional facility of the cryopump, which has not yet been commissioned, is the use of argon frosting of the liquid helium-cooled surfaces to permit the study of helium exhaust in the divertor of a high performance plasma.

4. CONFINEMENT IN THE JET-PD H-MODE REGIMES

4.1 L-H transition power threshold behaviour

The power threshold for transition from L-H mode has been measured in the new machine in both the normal (towards the X-point) ∇B drift direction (+ve

∇B) and the reversed (away from X-point) ∇B drift direction (-ve ∇B). The results show, when plotted against $n_e B_T$ sign (∇B), that the thresholds are roughly unchanged from the 1991-2 carbon tile data with the +ve ∇B configuration, but slightly lower than the 1991-2 carbon tile data with -ve ∇B (see fig.6). The data are consistent with the ASDEX-U scaling for positive ∇B [11] if a plasma surface area of 150-180 m^2 is taken. The possibility of a separate density scaling has been investigated and is described in [12] where definite evidence for scaling is presented.

4.2 Energy confinement in ELMy and ELM-free H-modes

4.2.1 ELM behaviour and density profiles

In previous JET operation, ELMs were rarely encountered in the H-mode [10], only being present either just above the L-H transition threshold; with extremely strong gas puffing; at high β or with hydrogen plasmas. In the present high recycling conditions of JET-PD, the ELMy H-mode (as shown in fig.4) is the norm. Long ELM-free periods (> 1 second) can only be obtained with some specialised preparation. The ELMs have the characteristics of the 'giant' ELMs identified on other machines such as DIIID [13] and ASDEX-U [14]. These include an ELM frequency which increases with input power and tends to reduce with plasma current.

During the ELM free period, the edge density builds up very quickly in the high recycling conditions. An edge pressure limit very similar to previous ***high performance*** JET plasmas (Hot Ion and high β_P VH modes [15], [16]) is rapidly achieved but with a hollow density profile and a lower edge temperature. The appearance of the ELMs then sheds the edge density and clamps the edge pressure. At present, the resolution of edge T_e and n_e measurements, which comes from LIDAR analysis, is not sufficient to establish unequivocally whether the edge pressure is ballooning limited. The ELM free period does have some of the right systematic dependencies however. ELM stability (as measured by the period to the first ELM following the L-H transition) is improved by increasing the shear at the edge or by increasing the triangularity of the equilibrium. These effects, typical of the stabilisation of ballooning modes, are discussed in detail in [3].

An example of the density profiles is shown in fig.7. In figs 7(a) and (b) one can see the measure of the density control which can be achieved with the cryopump. Density profiles in 2 discharges with 10MW NBI heating, one with cryopump, one without, are compared in the steady ELMy phase. A 30% reduction in density and a factor ~ 3 reduction in D_α recycling light is seen with the pump on. The reduced density and improved heating profile give a slightly better confinement enhancement, in the opposite direction to scaling predictions such as the ITER93HP law, which have favourable scaling with density [17]. The profiles of density contrast strongly with those achieved at the end of a long ELM-free period (fig.7(b)) at the same power level. These are unfavourable for NBI heating and the achievement of good central parameters. The ELM-free discharge, one of a series of double null plasmas [4], did not reach a higher confinement enhancement in steady-state, probably due to a combination of poor power deposition profile and high edge recycling.

The density build-up in an ELM-free period can be controlled by careful programming and this is being achieved in the JET-PD Hot Ion H-mode development (section 6 and ref [3]). Fig.8 shows comparison of profiles in two discharges with 17-18MW input power, a 4MA high density H-mode and a 2.5MA Hot Ion H-mode. The cryopump was in operation for both discharges. The production of slightly peaked density profiles at low densities can be seen in the Hot Ion shot which

maintains low edge density even with intense heating. In the 4MA high density discharge, the increased ELM-free period obtained with higher current results in an initially unfavourable density profile which then flattens with the onset of ELMs. The better beam penetration in the Hot Ion discharge leads to improved central temperatures and neutron yields (see section 6).

4.2.2 Confinement overview

An overview of the confinement enhancement in JET-PD ELMy and ELM-free H-modes is shown in figs 9 and 10. The data are plotted against the predictions of the ITER89-P L-mode scaling law [18], as they are measurements for the ***total*** stored energy. The fast particle content of the diamagnetic energy (W_{dia}) ranges from ~ 20% for the high power discharges at 1.5 MA to < 5% for the high power 4 MA plasmas. The dataset average is around 10%.

In figs 9 and 10, the measured diamagnetic energy confinement time ($\tau_{E,dia}$) is plotted against the prediction from the ITER89-P law ($\tau_{E,ITER89P}$). It may be seen that the bulk of the data lies in the ranges

$$1.6 \cdot \tau_{E,ITER89P} < \tau_{E,dia} < 2.2 \cdot \tau_{E,ITER89P} \quad \text{(ELMy)}$$

and $$2.0 \cdot \tau_{E,ITER89P} < \tau_{E,dia} < 2.4 \cdot \tau_{E,ITER89P} \quad \text{(ELM free)}$$

The ELMy dataset is dominated by steady-state and quasi-steady-state discharges ($dW_{dia}/dt \sim 0$). The ELM-free dataset is not in steady state, but a limit of $dW_{dia}/dt < 0.4\ P_{in}$ has been applied. The confinement is generally maintained up to high values of loss power.

The small confinement advantage of the ELM-free over the ELMy H-mode is still under investigation, but may be due to a combination of poor deposition profiles and high recycling which are encountered. in this dataset. The exception to this is the good performance of the Hot Ion H-modes, predominantly at 2.5 MA. These are covered in more detail in section 6.1.

4.3 Confinement at high β

Confinement at high values of poloidal beta (β_p) and normalised toroidal beta (β_N) have been studied in a campaign aimed at investigating the development of '*Advanced Tokamak*' scenarios with high fraction of bootstrap current. These are described in detail in [4]. The plasmas with high bootstrap current fraction obtained in the 1991-2 JET campaign at 1 MA (70% bootstrap current) and 1.5 MA (50% bootstrap current) were generated at high q(a) (> 10) and low values of β_N [16]. The present experiments have aimed to bring these plasmas into a more reactor-relevant regime of medium q and high β_N.

As indicated previously, the high recycling in the JET-PD machine has limited the ELM-free periods and this has been especially severe at low current values. Consequently, the elevated confinement values relative to L-mode (H_L>3) achieved in the 1991-2 campaign have not yet been repeated. The ELMy discharges obtained have confinement approximately equal to the JET-DIIID H-mode scaling law [19] and, as a result, the 'efficiency' of achieving high β_p is now much lower. Nevertheless, values of β_p = 2.1 have been recorded with 26 MW of combined NBI and ICRF power at 1 MA, and the discharges in the new configuration are not transient but present 'quasi-steady-state' conditions for 5-10 energy confinement times [4].

The confinement enhancement in the H-mode does not increase with β_p for the ELMy plasmas (fig.11). In marked contrast to the results obtained both in JT-60U [20] and the JET 1991-2 campaign [16], confinement appears to degrade as $P^{-0.5}$ in this dataset. There does appear to be some marginal gain in

confinement enhancement with increasing β_p for discharges which have achieved longer ELM-free periods in the JET-PD (also shown in fig.11). These latter discharges being performed in a double-null configuration [4].

The new JET results constitute a significant enlargement of the parameter domain, moving the high β_p plasmas closer to the reactor relevant domain, as indicated on fig.12. For example, $\beta_p = 1.6$ has been achieved in quasi-steady-state together with $\beta_N \sim 3$ and confinement enhancement relative to ITER89-P L-mode of around 2. Such discharges are close to the previous β_N limit established in JET [21]. In these discharges the plasma relaxes from a peak $\beta_N \sim 3.2$ with the accompaniment of low-n MHD activity. The limit $\beta_N \sim 4 \cdot l_i$ appears to apply, in common with limits previously established in DIIID plasmas [22]. This relaxation is accompanied by a decline in the confinement enhancement of around 10%.

5. STEADY-STATE H-MODES WITH ENHANCED CONFINEMENT

Reactor studies such as the ITER-EDA [23] have focused on the requirement for ignition in enhanced confinement regimes with confinement enhancement above L mode scalings (H_L) between 1.6 and 2.0. The ELMy H-mode, with its measured propensities for achievement of steady-state densities, impurity and helium expulsion [24] and the spreading of power conducted to the divertor, is an obvious candidate for extrapolation to a reactor. An important part of the JET-PD programme is the development and study of such modes to regimes of high performance and fusion power.

5.1 Long pulse ELMy H-mode

The combined advantages of the JET-PD target power handling, the divertor cryopump and the high recycling conditions reached routinely in the divertor, have enabled the production of long pulse steady-state H-modes. An example of the longest pulse ELMy H-mode, 20s duration at 2MA with 7-7.5MW additional NBI power, is shown in fig.13. An essential part of this long pulse behaviour is the density and recycling control achieved by the cryopump, evidenced by the steady D_α and volume-averaged density. Figure 13 also shows the relatively modest strike zone temperatures reached with the ~ 100MJ energy conducted to the tiles.

This ELMy H-mode has a confinement enhancement equal to twice the ITER89P L-mode prediction and this is maintained for nearly 50 energy confinement times (τ_E). The current profile has almost completely evolved, as evidenced by the flattening l_i and current moments. The ELMy H-mode period lasts for about 80% of the resistive diffusion time if a scale length of ~ 0.8m (the minor radius) is assumed.

Steady ELMy H-modes have been produced with pulse lengths $\geq 20\ \tau_E$ at currents up to 3MA and input powers up to 11MW. The divertor region in JET-PD L-modes enters routinely into a high recycling state and this is probably maintained in ELMy H-modes which is beneficial in keeping impurities from the target from entering the bulk plasma. The Z_{eff} and carbon impurity profiles in these discharges remain flat throughout the time of the ELMy H-mode period as shown in fig.14 for a 3.0MA/2.8T H-mode lasting 9 seconds. Helium puffing experiments have been performed in these discharges and the helium density profiles also become flat with no sign of accumulation.

The regime has been pushed to higher powers (18-19MW) and densities ($\langle n_e \rangle \sim 9\text{-}10\ 10^{19} m^{-3}$) at plasma currents of 3.5-4.0MA. These discharges have steady ELMy conditions for ~ 4-5 energy confinement times, a limit resulting only from the length of the NBI heating used. An example of a discharge at 4MA is shown in fig.15, where a confinement enhancement relative to

ITER89-P L-mode scaling of 1.9 is maintained for $4.5\tau_E$ at low radiation levels and high purity.

The fusion performance of the steady-state ELMy H-modes in JET-PD is plotted in fig.16 for sample discharges. A best value of $n_D(o)\cdot T_i(o)\cdot\tau_E \sim 2.65$ $10^{20}m^{-3}keV\cdot s$ has been achieved at 4MA/3.4T. This corresponds to a projected $Q_{DT} \sim 0.1$ for a 50:50 D:T plasma mixture. This performance already puts these discharges into the best performance range of previous JET ***non Hot Ion*** H-modes. If density control of these plasmas can be established at lower values, the projected Q_{DT} could be improved by operation at higher temperature.

5.2 Detached plasmas

The development of steady-state plasmas in which the input power is dissipated before reaching the divertor target is a fundamental problem in the research programme leading to a reactor. Most proposals consider the possibility of dissipation by radiation or charge-exchange processes leading to the production of a 'detached' plasma. Previous JET experiments [25] succeeded in establishing detached L-mode plasmas in which nearly all the input power was dissipated by radiation. The production of such radiative divertor plasmas has been attempted in the JET-PD experiment, using the steady-state ELMy H-mode as a basis. The *modus operandi,* described in more detail in [1] and [2], involves strong deuterium gas puffing to raise the density and access the detached divertor regime.

Successful detached plasmas have been produced, but these remain with L-mode confinement. Figure 17 shows the approach to detachment of one such discharge where the ion saturation current detected at the inner and outer strike zones falls to very low levels as the density rises.

The approach to detachment via high density shows a steadily reducing H factor when successive discharges at progressively higher desnsities are compared. Also it is apparent [2] that the character of the ELMs changes as the density increases and core confinement decreases. The ELMs become more 'grassy' and the peak power loading on the tiles increases, probably due to the reduced spreading of the power load by the grassy ELMs.

6. HIGH FUSION YIELD PLASMAS

The production of high fusion yield plasmas formed an important part of the JET programme up to 1992, and culminated in the Preliminary Tritium Experiment (PTE1) in which nearly 2 MW of fusion power was obtained in plasmas with the first significant tritium concentration (11%) [26]. The plasmas used in these experiments were the 'Hot Ion ' (HI) H-modes, heated by NBI. In the 1991-2 campaign, these plasmas were developed to a regime where 'VH-mode' confinement (H factors > 3 with respect to L-mode) was obtained. The new JET-PD configuration has been used in initial experiments to regain this regime.

The results are covered in detail in [3]. Plasmas with high power (16-18 MW) NBI heating have been generated in which the Hot Ion conditions, with central ion temperatures (T_i (0)) above 20 keV and T_i (0) > 2 $\cdot T_e$ (0) , are seen to exist for periods up to ~ 0.75 s. The time history of one such discharge is shown in fig.18. As indicated in section 4, the preparation of slightly peaked target density profiles by careful gas and pumping programming, is essential for the good beam penetration and the achievement of high central parameters and neutron yields. The pumped divertor cryopump has been useful in this respect. The levels of recycling are now similar to those of the 1991-2 VH mode dataset. However the edge density gradient is still higher than in the 1991/2 campaign and this is one of the possible reasons why the VH-mode confinement has not yet been achieved in the new configuration, as it is probable that the edge plasma is not generating the levels of bootstrap current

needed for unconstrained access to the second stable region against ballooning modes which has been identified as a probable signature of the VH mode in JET [15] and in DIIID [27]. Nevertheless, the JET-PD Hot Ion H-modes stand out from the rest of the ELM-free dataset as having enhanced confinement. This is seen for the 2.5 MA dataset in fig.19.

A wide variety of termination scenarios is seen in these HI H-modes, corresponding to the types observed in the old data [15],[26]. These include fast terminations where a sawtooth is coupled to an ELM, and slower terminations where the confinement seems to be lost at the outer part of the plasma first and the limitation of the temperatures moves inwards to the centre. The causes of these terminations are still under investigation.

The DD reaction rate in these plasmas has reached a peak value of 4.5 10^{16} s^{-1}, just over half of the JET record value [26]. This was achieved in a 2.5 MA/ 3.4 T plasma with 17 MW NBI power, the extension to higher currents having not yet been fully exploited as in the previous campaigns. A peak value of fusion triple product ($n_D(0).T_i(0).\tau_E$) ~ 5.6 10^{20} m^{-3}.keV.s has been reached in a separate discharge, representing around 60% of the previous best value, and excellent progress for this stage of the campaign. The fusion triple product values from some of the new HI H-modes is plotted in fig.16, compared to the previous dataset.

7. NON-INDUCTIVE CURRENT DRIVE RESULTS

JET-PD has Non-Inductive Current Drive (NICD) capability in Lower Hybrid (LH) waves, ICRF Fast Waves (by TTMP damping) and Neutral Beams. This complementary system will eventually be used for profile control to enhance the stability of long pulse (> 30s), high β_p discharges. Early studies have concentrated on LHCD [28] although initial work demonstrating the TTMP capability by Fast Waves has also been performed [29]. Current profile control to obtain shear reversal in the current ramp up phase has been achieved using LHCD in conjunction with ICRF (in minority heating mode) at 2 and 3MA [4], [28].

In stand-alone current drive experiments, a maximum of 6MW of LH power has been coupled. 1.8MA driven current has been achieved with 4MW of LHCD power at $\langle n_e \rangle$ = 1.8 $10^{19} m^{-3}$, representing 90% of the total current. The current drive (η_{CD}) efficiency is seen to scale with volume averaged temperature and Z_{eff} in line with previous results from JET [30] and JT-60 [31]. A maximum value of η_{CD} (= $n_e R I_d / P_{LH}$) ~ 0.23 10^{20} $M{\cdot}W^{-1}{\cdot}m^{-2}$ has been achieved at central electron temperatures of 7keV.

8 FUTURE PROGRAMME FOR JET

8.1 Remainder of the 1994-5 campaign

The JET 1994/5 experimental campaign will continue to May 1995. For the remainder of the campaign, the key areas of High Performance Optimisation, Divertor Physics Issues and Tokamak Concept Improvement will continue to be addressed.

By the end of the campaign, it is intended to establish H-mode operation at 5-6MA and Hot Ion H-modes up to 4.5MA. The coupled power should be extended to the 30-40MW level. The Divertor programme is intended to take in radiative divertor work with neon puffing and helium transport using the cryopump with Argon frosting. The ***Long Pulse Steady-State H-modes*** will be developed with recycling control and pushed to higher fusion performance. It is also intended to develop high β_p discharges to resistive steady-state with 40s pulses, and to use negative shear production and profile control to aid stability.

ITER specific studies also figure in the near term programme with work on:

- the effects of variable ripple in the Toroidal Field (TF), the TF configuration being continually varied from the full 32 coil to a 16 coil configuration, to complement previous experiments [32];
- demonstration discharges with ITER non-dimensional parameters eg, ρ^* scaling with steady-state H-modes;
- characterisation of the H-mode power threshold, especially as a function of density; and
- tests of the operation and impurity production with screenless ICRF antennae.

Finally, the JET-PD target will be changed to a beryllium tile set early in 1995 in order that a comparison of the divertor, recycling and high performance behaviour between C and Be targets can be made.

8.2 The JET Programme to 1996 and beyond

An extension of the JET Programme by three years to the end of 1999 is currently being proposed. The proposed extension concentrates on those areas of work, namely, ***Divertor studies and D-T operations***, which are essential for a decision to construct ITER.

The extension would have two objectives:

- to develop a credible divertor concept for ITER; and
- to improve plasma performance and provide D-T operations in an ITER-like configuration.

JET would also contribute significantly to the technologies required for ITER.

8.2.1 The JET Divertor Strategy

The JET divertor strategy is designed to satisfy the divertor requirements of the JET high performance D-T programme; and to provide crucial experiments in support of the development of a credible ITER divertor.

The JET divertor programme is based on three divertor configurations – ***Mark I, Mark IIA and an ITER-specific Mark IIGB*** – which will be introduced sequentially up to the year 1999. These are indicated in fig.20. They should allow a co-ordinated, timely and cost effective investigation of the various options for an ITER divertor.

8.2.2 Deuterium Tritium Experiments DTE1 and DTE2

A first period of D-T operation ***(DTE1)*** is foreseen before the end of 1996. This would demonstrate long pulse fusion power production (Q>1 with more than 10MW for more than one energy replacement time). It would also make important contributions to D-T physics (H-mode threshold, ELM and confinement behaviour, and some RF heating studies) which JET alone can provide in an ITER relevant divertor configuration. An additional technical goal would be to demonstrate the JET Active Gas Handling System processing tritium while supporting a reacting tokamak plasma.

A second period of D-T operation ***(DTE2)*** in 1999, would permit a thorough study of D-T plasmas with substantial α-particle heating. It would also validate, in D-T, improvements in fusion performance achieved in the preceding experimental campaigns.

An overall time plan of the extension is shown in fig.21.

9. CONCLUSIONS

JET has successfully restarted operations in the new Pumped Divertor configuration and many different operating regimes have been featured in experiments.

The excellent power handling capability of the new divertor target combined with the ability to sweep the strike zones has helped the routine production of longer

pulse plasmas with lower carbon impurities than in the prvious campaigns. The divertor is observed to operate routinely in a high recycling regime, and ELMy H-modes are much more prevalent than in the prvious machine. These factors, when coupled with the successful operation and density control facility of the pumped divertor cryopump, have enabled the development of Long pulse ELMy H-modes with steady-state characteristics and good impurity control for periods up to 50 energy confinement times. This regime, of interest to ITER, has been obtained with H factors ~ 1.8 - 2.0 and pushed to fusion trple product values of $n_D(o)\cdot T_i(o)\cdot \tau_E \sim$ 2.65 $10^{20} m^{-3} keV\cdot s$ at 4 MA/ 3.4 T with 18 MW input power for > 4 energy confinement times.

Detached plasmas have been developed from the steady-state ELMy regime but, to date, show only L-mode confinement.

The high recycling conditions in the JET-PD vessel lead to very hollow density profiles when long ELm-free periods are obtained. The studies carried out so far show that the ELMs have the characteristics of ballooning modes. Except in the detached plasmas, the ELMs have the characteristics of giant ELMs.

Hot Ion H-modes have been re-established at 2.5 -3.0 MA, and have produced values of $n_D(o)\cdot T_i(o)\cdot \tau_E \sim 5.6\ 10^{20} m^{-3} keV\cdot s$. This level is comparable to that obtained in the JET Preliminary Tritium Experiment. The discharges show enhanced confinement but the VH-mode regime has not yet been accessed. The discharges show similar termination scenarios to the 1991-2 dataset.

Studies of high β_p have achieved $\beta_p \sim 2$ in ELMy H-modes but without attaining the pVH mode level of confinement. The new experiments have moved the high β_p dataset into a more reactor relevant regime (similar to that foreseen by e.g. SSTR [33]) at high β_N and moderate q(a). The fraction of bootstrap current in these discharges is still rather low however (~ 50%).

An extensive and challenging programme can now be foreseen based on these results and utilising JET-PD in its Mark I, Mark IIA and (possibly) Mark IIGB configurations, in support of ITER,DT physics and Divertor physics strategies in general.

REFERENCES

[1] The JET Team, presented by D J Campbell, these proceedings (paper A-4-I-4).
[2] The JET Team, presented by L D Horton, these proceedings (paper A-4-I-5-1).
[3] The JET Team, presented by P J Lomas, these proceedings (paper A-2-I-4).
[4] The JET Team, presented by C Gormezano, these proceedings (paper A-5-I-3).
[5] N Dolgetta et al, contrib paper 18th Symposium on Fusion Technology (SOFT), Karlsruhe (1994)..
[6] The JET Team, Nuclear Fusion **32**, 187(1992).
[7] D Stork et al, Europhys Conf Abstracts 15C(I), 357(1991).
[8] R Reichle et al, ibid [12], Vol III, 105.
[9] The JET Team, presented by G Janeschitz. Plasma Phys and Contr Nucl Fus Research (1992), Vol 1, 329 (IAEA Vienna, 1993)
[10] D J Campbell et al, Plasma Phys and Contr Fusion **36**(7), A255 (1994).
[11] W Köppendörfer et al, these proceedings (paper A-2-II-1).
[12] The JET Team, presented by R Giannella, these proceedings (paper A-2-III-1).
[13] The DIIID Team, presented by R D Stambaugh, Plasma Phys & Controlled Nuclear Fusion Research (1990), Vol 1, 69 (IAEA Vienna, 1991).
[14] F Ryter et al, ibid [10], A99.
[15] B Balet et al, Nucl Fusion **33**, 1345(1993).
[16] C D Challis et al, Nucl Fus **33** 1097(1993).
[17] D.P.Schissel et al., Europhys Conf Abstracts 17C(I), 103 (1993)
[18] P.N.Yushmanov et al., Nucl Fusion **30**, 1999 (1990)
[19] D P Schissel et al, Nucl Fusion **32**, 73(1991).

[20] S.Ishida et al., ibid [9], vol 1, 219.
[21] D Stork et al, Europhys Conf Abstracts 16C(I), 339 (1992)
[22] T S Taylor et al., ibid [14], 177.
[23] ITER TAC-3 meeting, 1993.
[24] R.D.Stambaugh et al., ibid [10], A249.
[25] S.Clement et al., ibid [21], 239 (1992).
[26] The JET Team, Nucl Fusion **32**, 187 (1992).
[27] C.M.Greenfield et al, ibid [21], 11.
[28] The JET Team, presented by F.X.Söldner, these proceedings (paper A-3-I-2).
[29] The JET Team, presented by F.G.Rimini, these proceedings, (paper A3/5-P-7).
[30] The JET Team, presented by C.Gormezano, ibid [9], vol 1, 587.
[31] O.Naito and the JT-60 Team, Plasma Phys and Contr Fusion **35**, B215 (1993)
[32] The JET Team, presented by B.J.D.Tubbing, ibid [9], vol 1, 429.
[33] M.Kikuchi et al, Nucl Fusion **30**, 343 (1990).

Appendix I

THE JET TEAM

JET Joint Undertaking, Abingdon, Oxon, OX14 3EA, U.K.

J.M. Adams[1], Y. Agarici[3], P. Ageladarakis, B. Alper, H. Altmann, P. Andrew, S.Ali-Arshad, W. Bailey, B.Balet, Y. Baranov[8], P. Barker, R. Barnsley[2], M. Baronian, D.V. Bartlett, A.C. Bell, G. Benali, E. Bertolini, V. Bhatnagar, A.J. Bickley, H. Bindslev, K. Blackler, D. Bond, T. Bonicelli, K. Borras[13], P. Boucquey, M. Brandon, P. Breger, H. Brelen, W.J. Brewerton, T. Brown, M.L. Browne, T. Budd, M. Bures, P. Burton, T. Businaro, H. Buttgereit, C. Caldwell-Nichols, D.J. Campbell, D. Campling, P. Card, F. Cecil[24], G. Celentano, C.D. Challis, A.V. Chankin, D. Chiron, J. Christiansen, P. Chuilon, D. Ciric, R. Claesen, H.E. Clarke, S. Clement, J.P. Coad, D. Collins, S. Colombi, S. Cooper, J.G. Cordey, G. Cottrell, M. Cox[7], P. Crawley, O. Da Costa, R. Cusack, G. D'Antona, N. Davies, S.J. Davies, J.J. Davis, H. de Esch, J. de Haas, E. Deksnis, N, Deliyanakis, A. Dines, S.L. Dmitrenko, J. Dobbing, N. Dolgetta, S.E. Dorling, P.G. Doyle, H. Duquenoy, A. Edwards, J. Ehrenberg, A. Ekedahl[11], T. Elevant[11], J. Ellis, S.K. Erents[7], L.G. Eriksson, H. Falter, A. Fasoli[18], B. Fechner, B. Fischer, G. Fishpool, J. Freiling[15], C. Froger, P. Froissard, K. Fullard, M. Gadeberg, L. Galbiati, M. Garribba, U. Gerstel[13], R. Giannella, A. Gibson, R.D. Gill, R. Goulding[22], A. Gondhalekar, D. Goodall[7], C. Gormezano, N.A. Gottardi, C. Gowers, J. Graham, C. Grisolia[3], H. Guo[23], A. Haigh, C.J. Hancock, P.J. Harbour, N.C. Hawkes[7], N.P. Hawkes[1], J.L. Hemmerich, T. Hender[7], J. Hoekzema, L. Horton, J. How, P.J. Howarth[5], A. Howman, M. Huart, I. Hutchinson[10], T.P. Hughes[4], F. Hurd, C. Ibbott, B. Ingram, M. Irving, S. Ishida[14], J. Jacquinot, H. Jaeckel, J.F. Jaeger, O.N. Jarvis, F. Jensen, M. Johnson, E.M. Jones, L.P.D.F. Jones, T.T.C. Jones, J-F. Junger, F. Junique, A. Kaye, B.E. Keen, M. Keilhacker, W. Kerner, N.G. Kidd, Q.A. King, R. Konig, P. Kupschus, P. Lamalle[26], R. Lässer, J.R. Last, L. Lauro-Taroni, C. Laviron[3], K. Lawson[7], E. Lazzaro[6], M. Lennholm, J. Lingertat[13], A. Loarte, P.J. Lomas, M. Loughlin, C. Lowry, E. Lyadina, A.C. Maas[15], B. Macklin, C.F. Maggi[16], V. Marchese, F. Marcus, J. Mart, D. Martin, T. Martin, G. Matthews, H. McBryan, G. McCormick[13], P.A. McCullen, A. Meigs, F. Milani, J. Mills, R. Monk[25], P. Morgan, G. Murphy, F. Nave[21], G. Newbert, F. Nguyen[3], P. Nielsen, P. Noll, W. Obert, D. O'Brien, E. Oord, R. Ostrom, M. Ottaviani, S. Papastergiou, V.V. Parail, W. Parsons, B. Patel, A. Paynter, A. Peacock, N. Peacock[7], R.J.M. Pearce, G. Pereverzev[13], C. Perry, M.A. Pick, J. Plancoulaine, O. Pogutse, J-P. Poffé, F. Porcelli, L. Porte[19], R. Prentice, P. Prior, S. Puppin, G. Radford[9], T. Raimondi, R. Reichle, S. Richards[12], E. Righi, F. Rimini, A. Rolfe, A. Rookes[12], R.T. Ross, A. Rossi, L. Rossi, R. Russ, G. Sadler, G. Saibene, M. Salisbury[12], G. Sanazzaro, A. Santagiustina, F. Sartori, R. Sartori, R. Saunders, P. Savrukhin, M. Schaffer[17], P. Schild, M. Schmid, B. Schunke, S.M. Scott, S. Sharapov, R.L. Shaw, A. Sibley, R. Simonini, A.C.C. Sips, P. Smeulders, P. Smith, R. Smith, F. Söldner, M. Stamp, P. Stangeby[20], D.F. Start, C.A. Steed, D. Stork, P.E. Stott, P. Stubberfield, D. Summers, H. Summers[19], W. Suverkropp, L. Svensson, T. Szabo, M. Tabellini, J. Tait, A. Tanga, A. Taroni, C. Terella, A. Tesini, P.R. Thomas, E. Thompson, K. Thomsen, B. Tubbing, H. van der Beken, E. van der Goot, G. Vayakis, M. Verrechia, G. Vlases, M. von Hellermann, T. Wade, C. Walker, R. Walton, D. Ward, M.L. Watkins, N. Watkins[1], M.J. Watson, S. Weber, J. Wesson, M. Wheatley, D. Wilson, T. Winkel, R. Wolf, C. Woodward, D. Young, I.D. Young, L. Zannelli, K-D. Zastrow, N. Zornig, G. Zullo, W. Zwingmann.

PERMANENT ADDRESSES

1. UKAEA, Harwell, Didcot, Oxon, UK.
2. University of Leicester, Leicester, UK.
3. CEA, Cadarache, France.
4. University of Essex, Colchester, UK.
5. University of Birmingham, Birmingham, UK.
6. CFP, Milan, Italy.
7. UKAEA Culham Laboratory, Abingdon, Oxon, UK.
8. A.F. Ioffe Institute, St. Petersburg, Russia.
9. Institute of Mathematics, University of Oxford, UK.
10. Massachusetts Institute of Technology, Boston, Mass., USA.
11. Royal Institute of Technology, Stockholm, Sweden.
12. Imperial College, University of London, UK.
13. Max Planck Institut für Plasmaphysik, Garching, Germany.
14. JAERI, Naka Fusion Research Laboratory, Ibaraki, Japan.
15. FOM Instituut voor Plasmafysica, Nieuwegein, The Netherlands.
16. Dipartimento di Fisica, University of Milan, Milano, Italy.
17. General Atomics, San Diego, USA.
18. EPFL, Lausanne, Switzerland.
19. University of Strathclyde, 107 Rottenrow, Glasgow, UK.
20. Institute for Aerospace Studies, University of Toronto, Canada.
21. LNETI, Savacem, Portugal.
22. Oak Ridge National Laboratory, Oak Ridge, Tenn., USA.
23. INRS-Energieet Materiaux, Univ. du Quebec, Canada.
24. Colorado School of Mines, Colorado, USA.
25. Royal Holloway College, University of London, UK.
26. Plasma Physics Laboratory, ERM-KMS, Brussels, Belguim.

At July, 1994

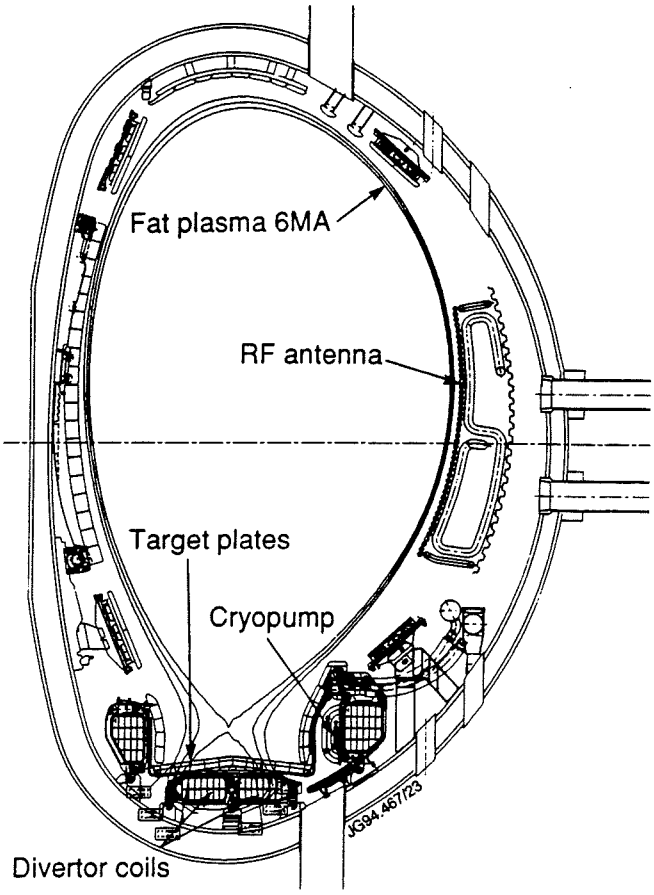

Fig. 1 *Cross section of the JET-PD vessel configuration.*

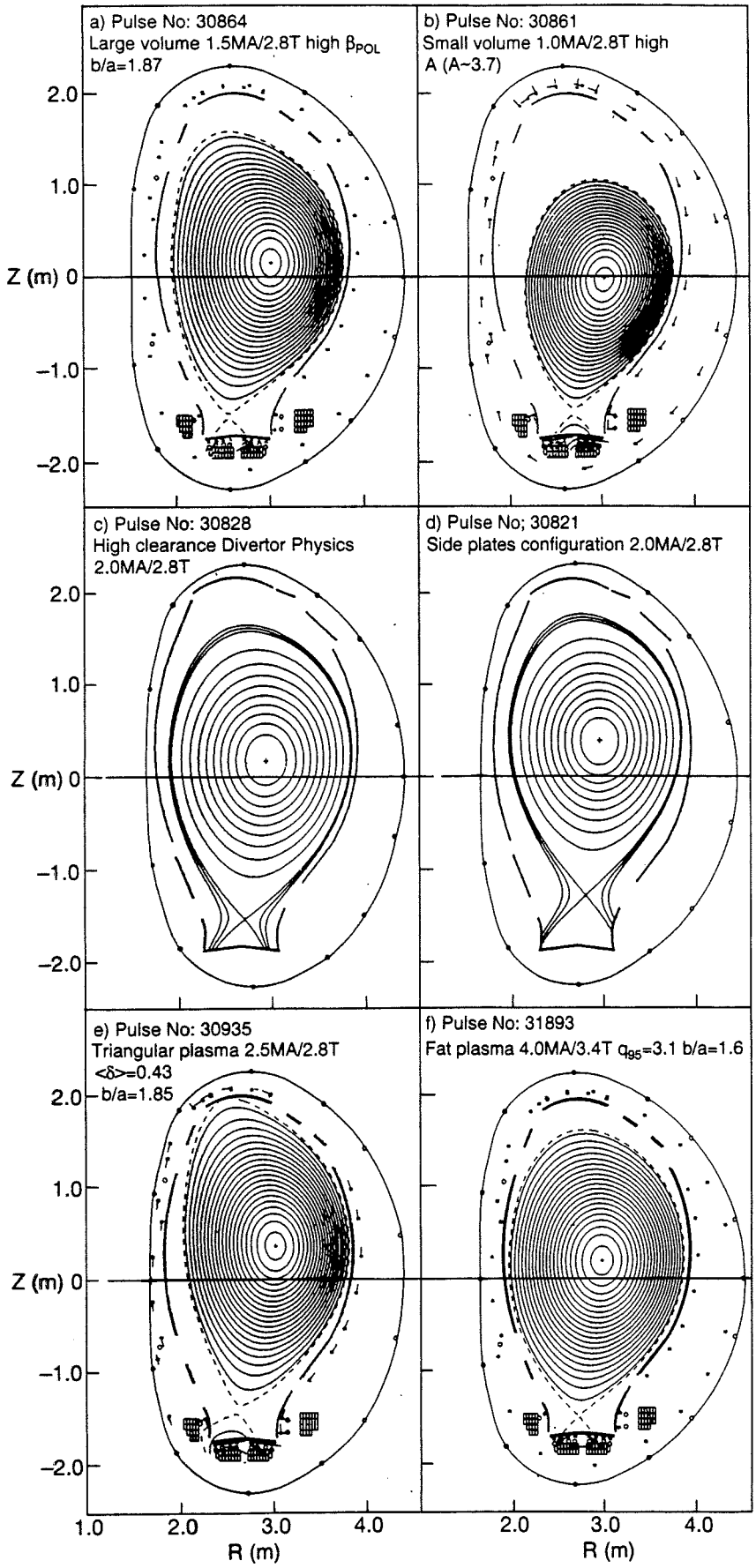

Fig. 2 *Sample equilibria as used in JET-PD experiments.*

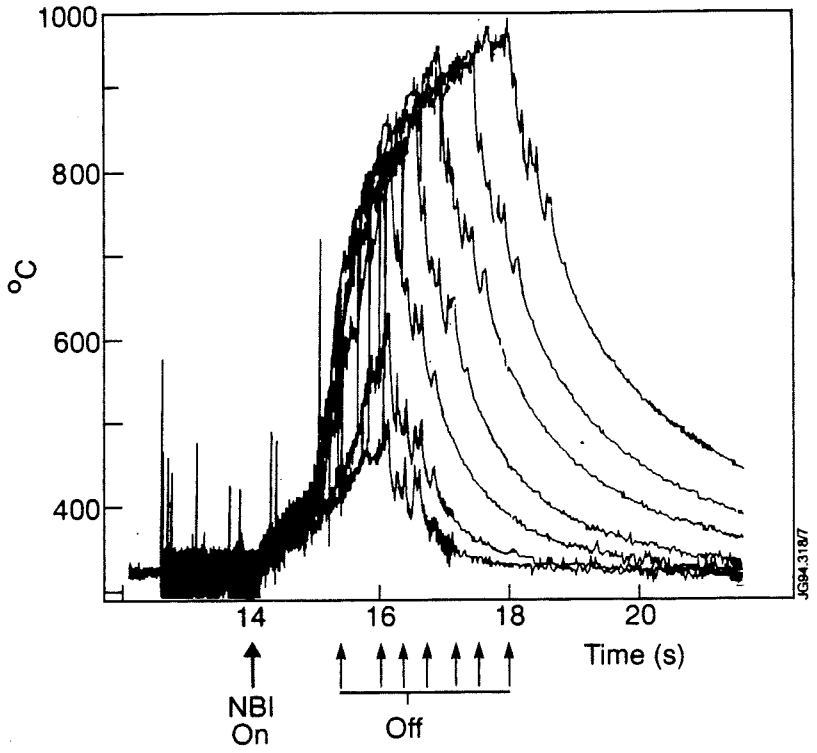

Fig. 3 *Infrared thermographic measurements of the divertor target outer strike zone for successively longer pulses with 14MW NBI heating. The target strike zones were* ***unswept*** *in this case.*

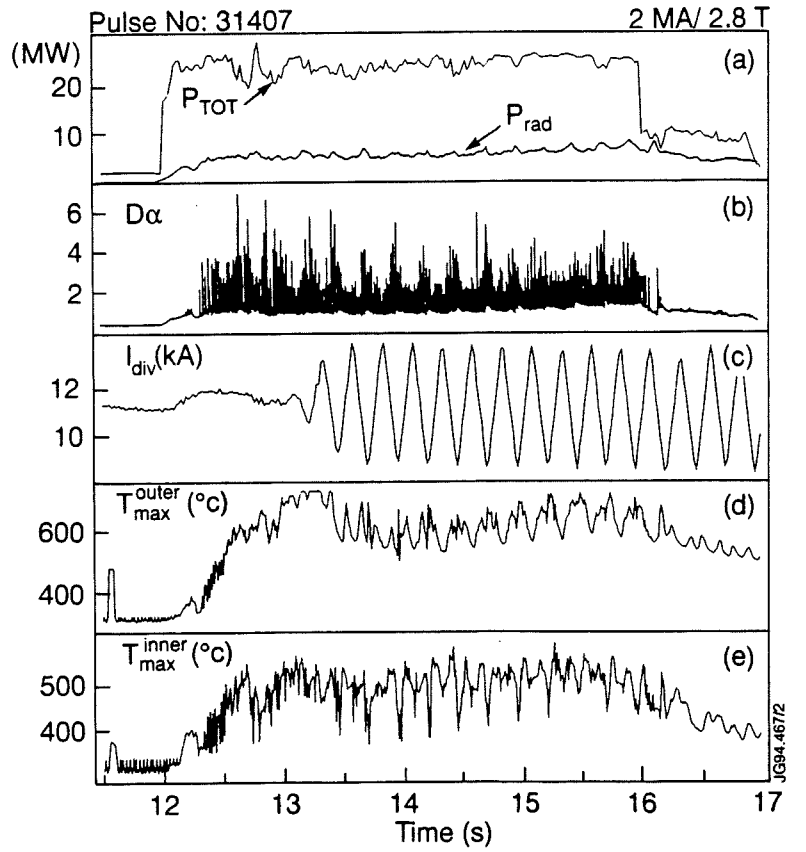

Fig. 4 *Time evolution of discharge and strike zone parameters for a discharge with 25MW of combined heating and divertor sweeping applied at 13s.*

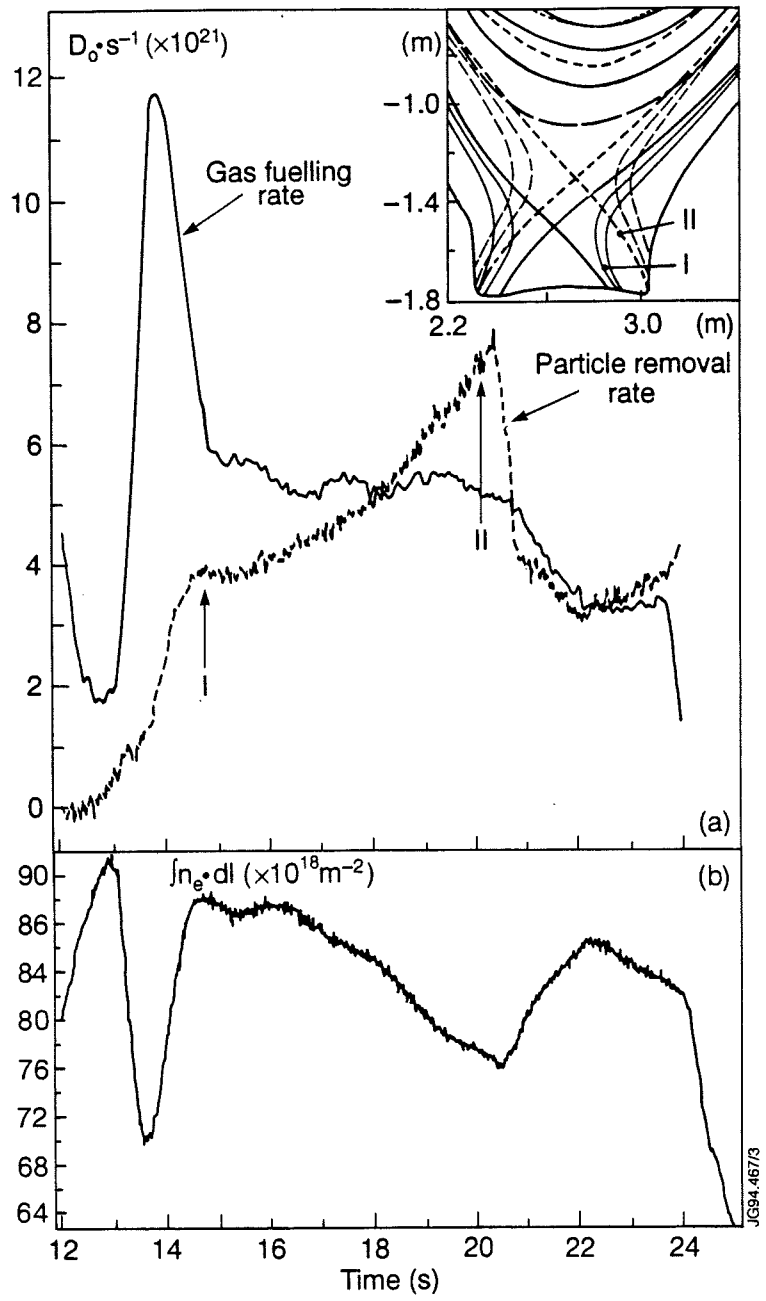

Fig. 5 *Particle removal rate and line density in an OH plasma where the divertor strike zones were swept close to the cryopump entrance (inset). The cryopump was cooled to liquid He temperatures. The improvement in pumping as the discharge moves from equilibrium I to equilibrium II can be clearly seen.*

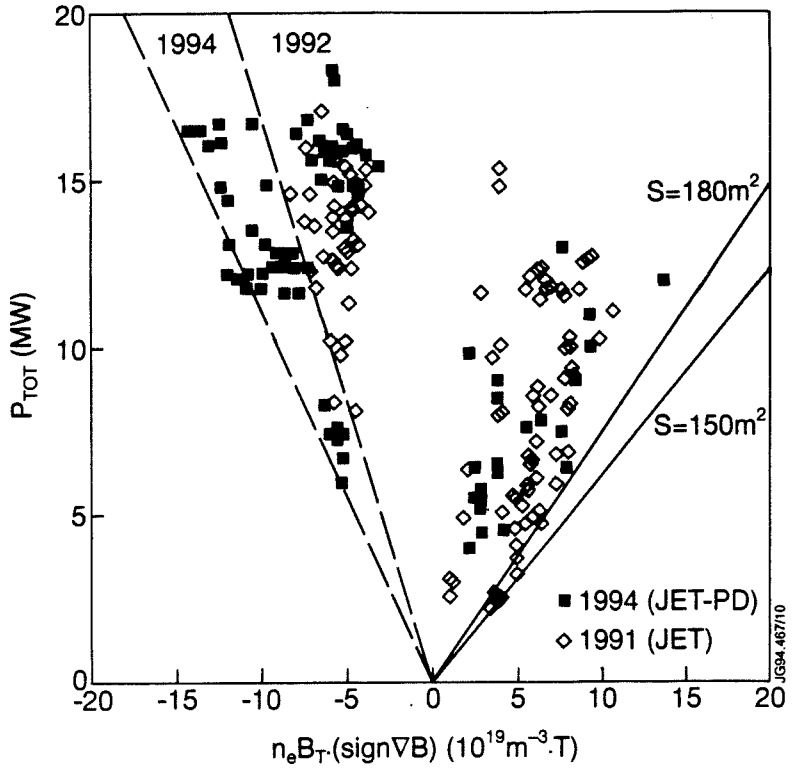

Fig. 6 *Existence diagram for 1994 JET-PD H-modes compared to the 1991/2 data for carbon target, plotted for +ve and –ve ∇B (see text for definition) against total input power in the discharge. The lines for the +ve ∇B data represent the scaling $P_{th} \sim 0.004\ n_e B_T S$ with S (surface area of plasma) values as shown.*

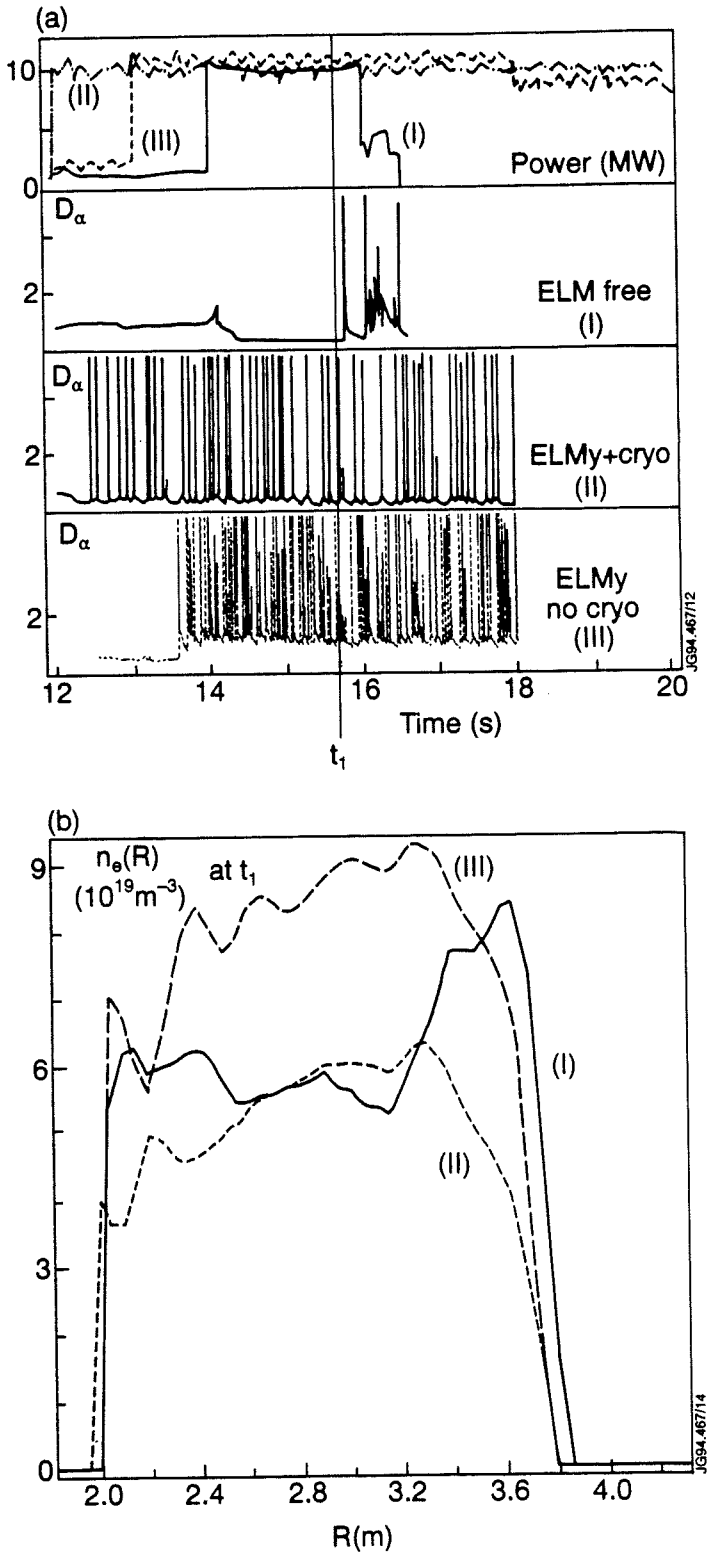

Fig. 7 *(a) Power and D_α traces and (b) Density profiles for three 10MW input 2-2.5MA plasmas. The three plasmas are ELM-free with no cryopump in operation; ELMy with cryopump and without cryopump in operation.*

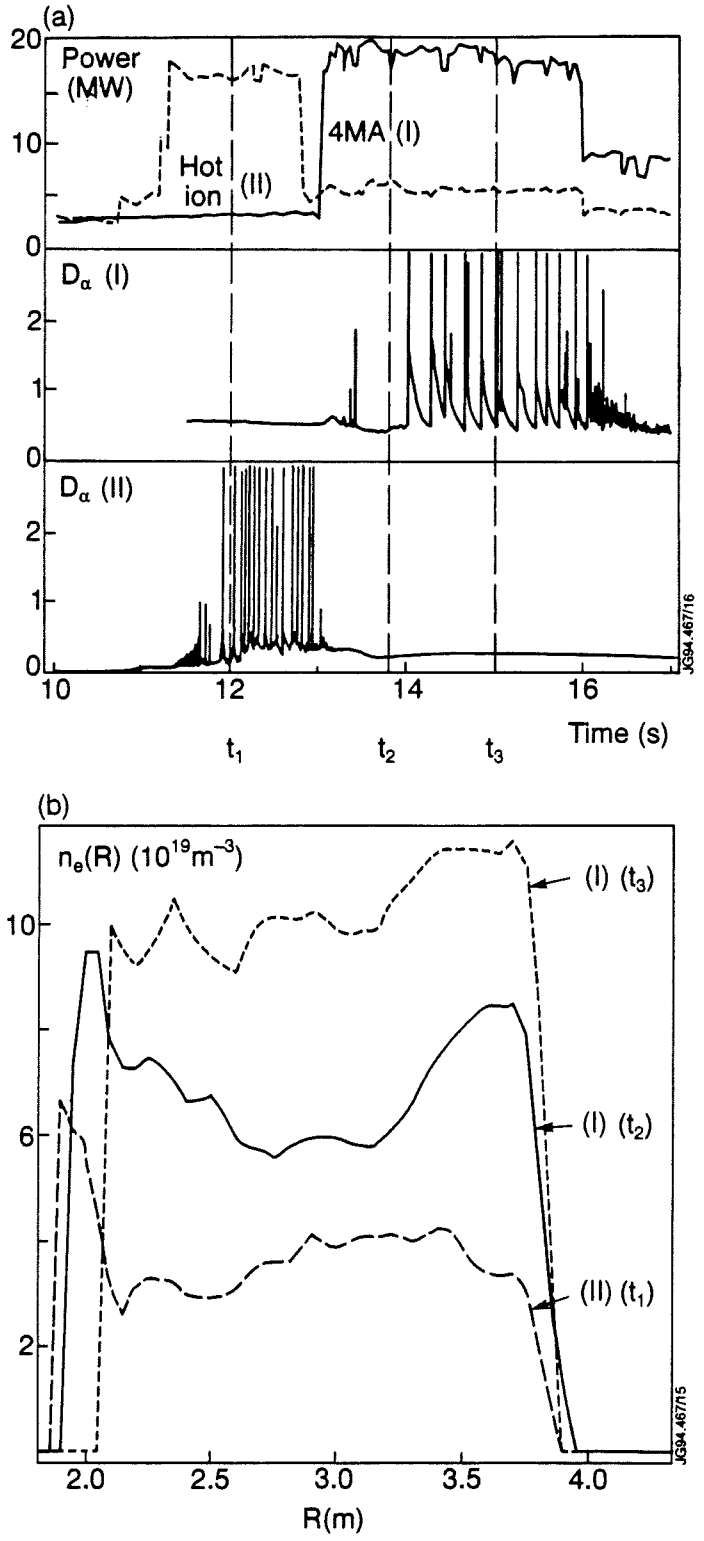

Fig. 8 *(a) Power and D_α traces and (b) Density profiles for a 2.5MA Hot Ion plasma and a 4MA high density plasma with 17-18MW of input power. The cryopump was operational for both discharges.*

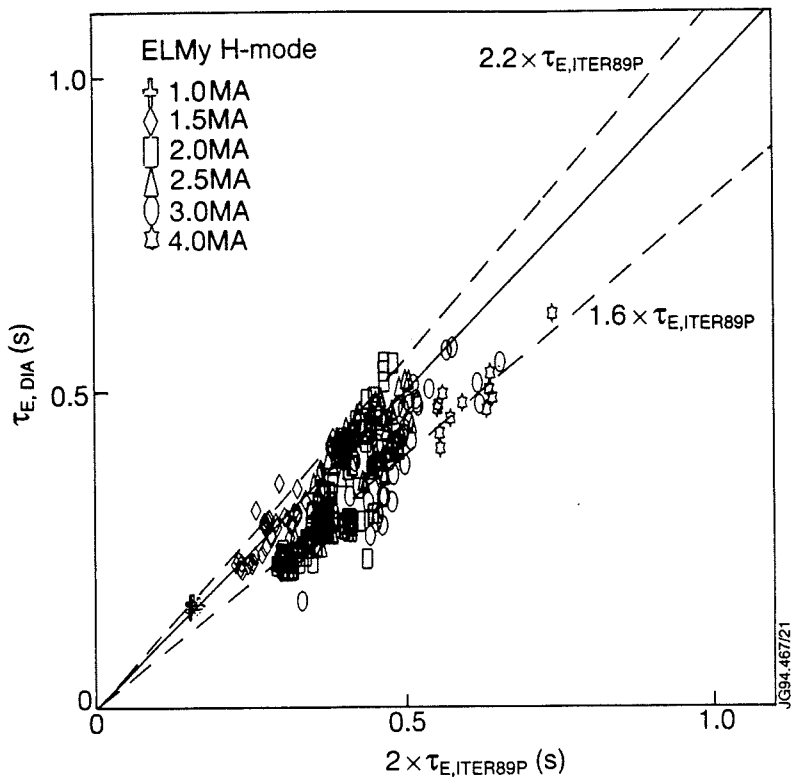

Fig. 9 *Measured diamagnetic energy confinement time ($\tau_{E,DIA}$) for the JET-PD ELMy H-mode dataset plotted against 2x the prediction from the ITER89-P scaling law ($\tau_{E,ITER89P}$). The data selected for the plot are in quasi steady state $dW_{dia}/dt < 0.1P_{in}$.*

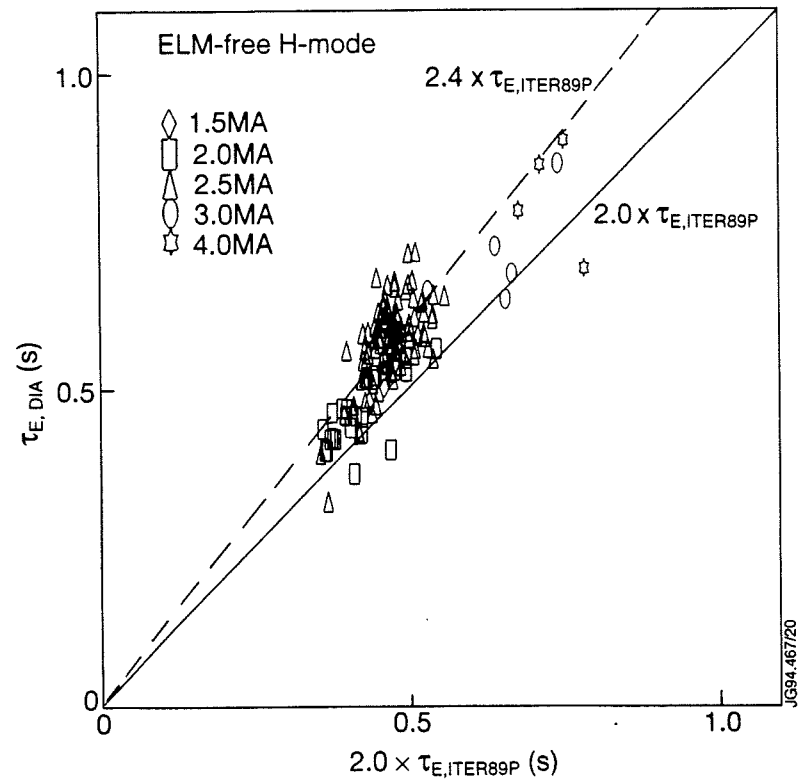

Fig. 10 *As Fig 9 but for ELM-free H-modes with $t_{ELMFREE} > 0.5$ secs. The data selected have $dW_{dia}/dt < 0.4\ P_{in}$.*

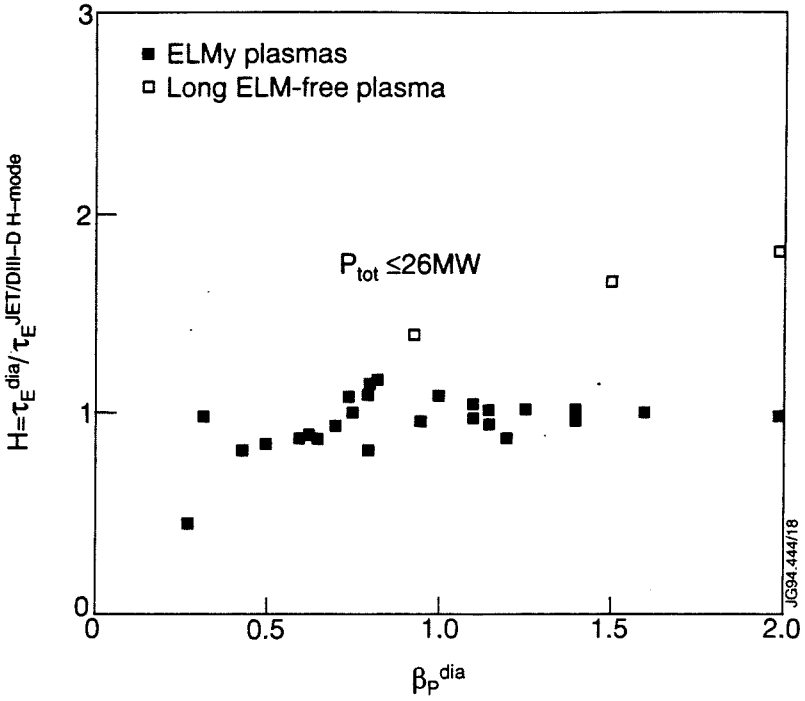

Fig. 11 ***Confinement enhancement*** *relative to JET/DIIID H-mode scaling as a function of* β_p^{dia} *for ELMy JET-PD plasmas and ELM-free plasmas from the JET dataset [16].*

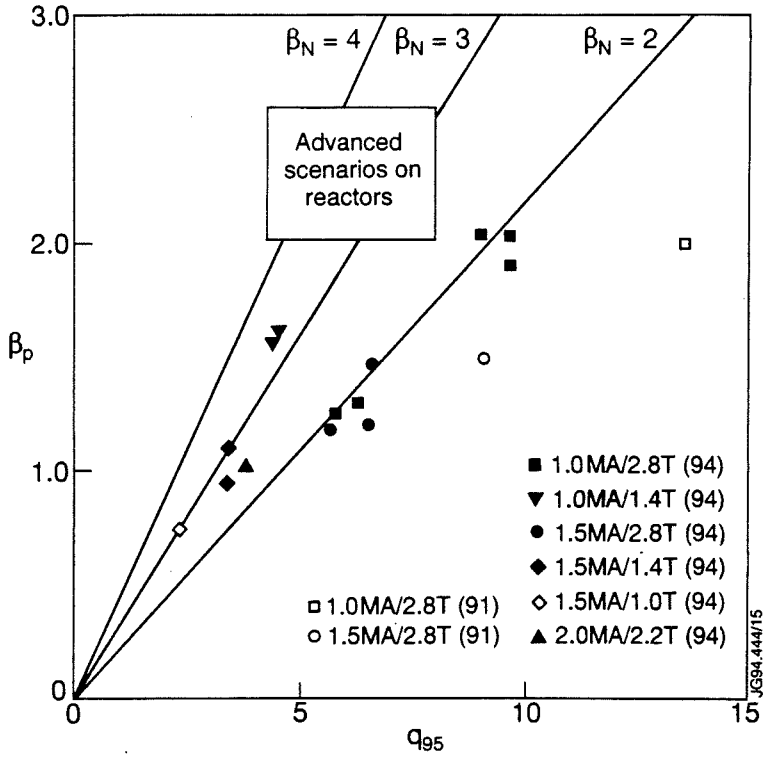

Fig. 12 β_p *vs* q_{95} *region for the JET and JET/PD high* β_p *discharges.*

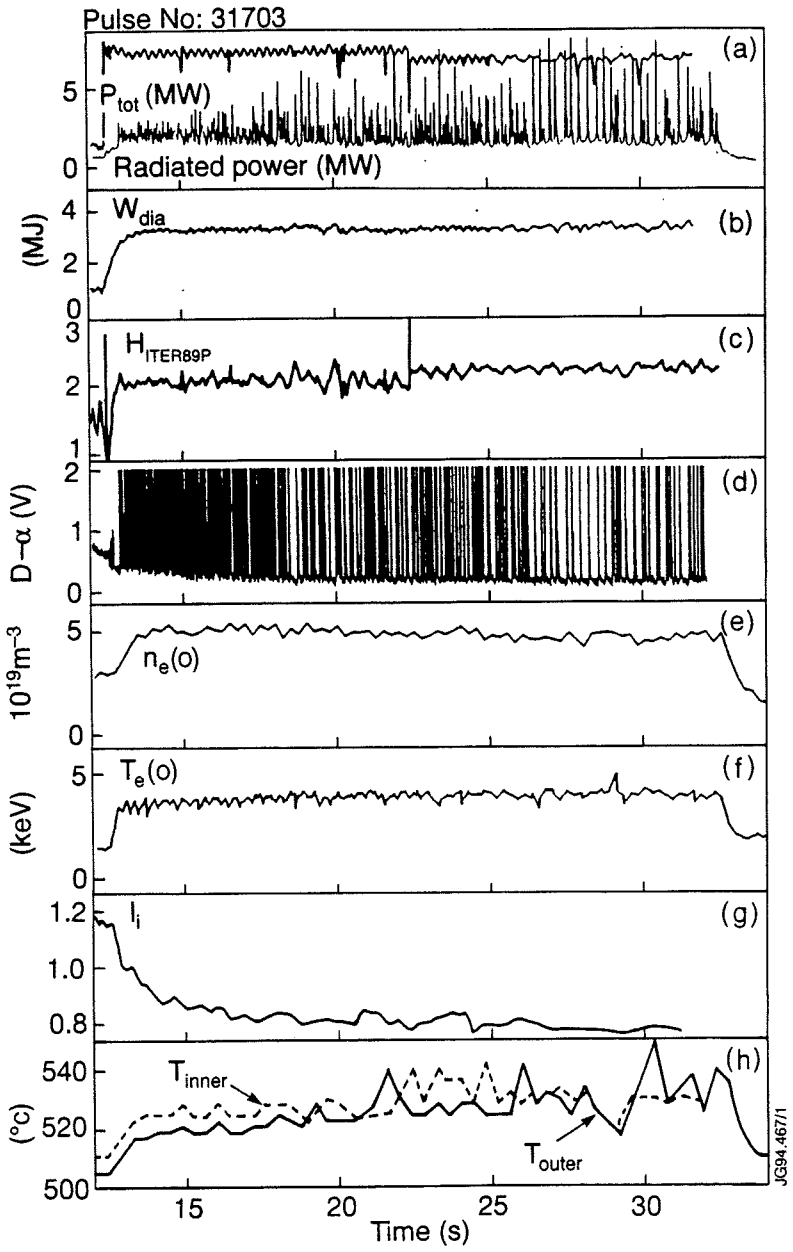

Fig. 13 *20 second ELMy H-mode showing steady-state behaviour.*

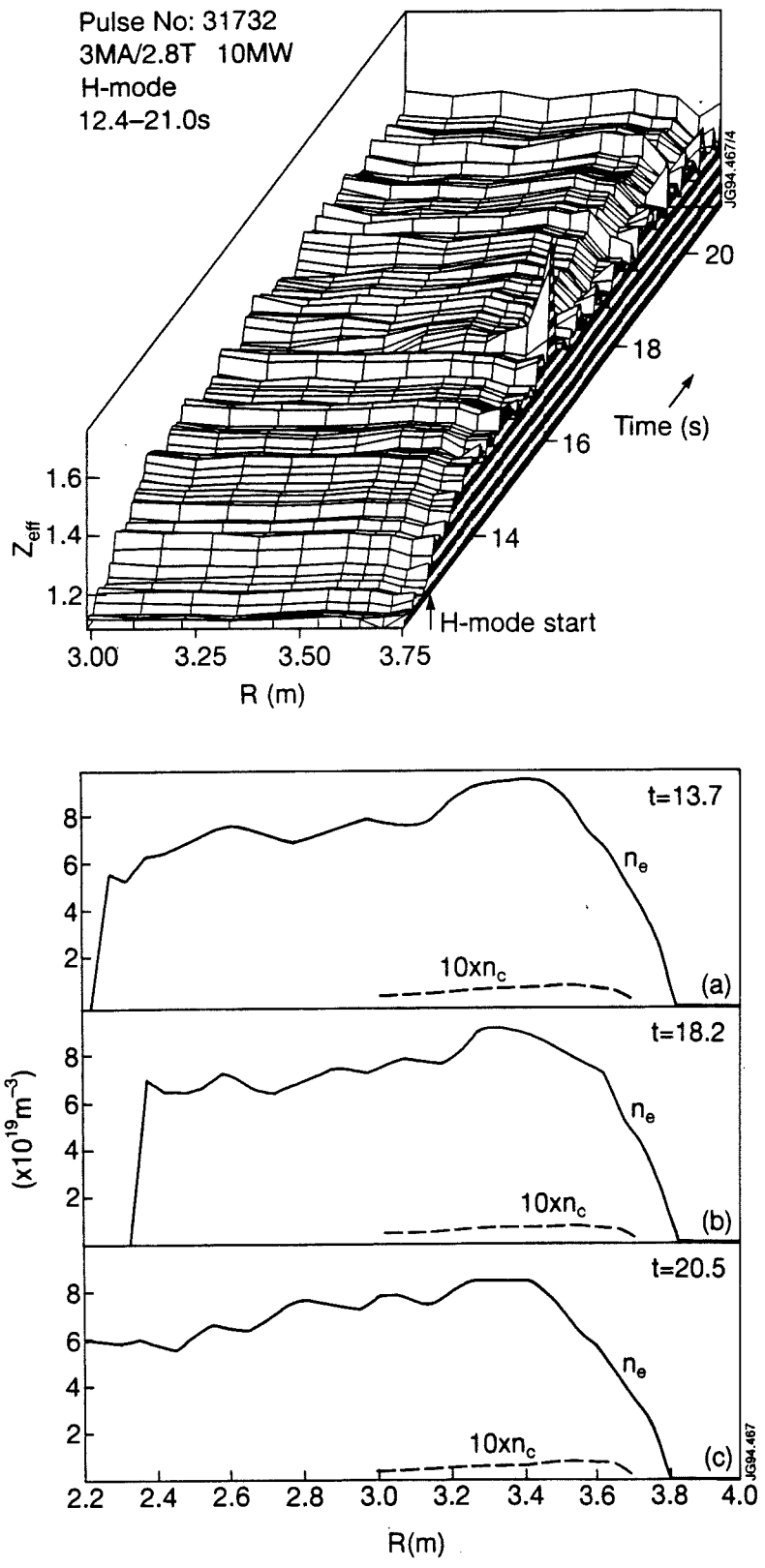

Fig. 14 *Z_{eff}, carbon and electron density profiles as a function of time for a 3MA/2.8T 9s ELMy H-mode with 10MW input power.*

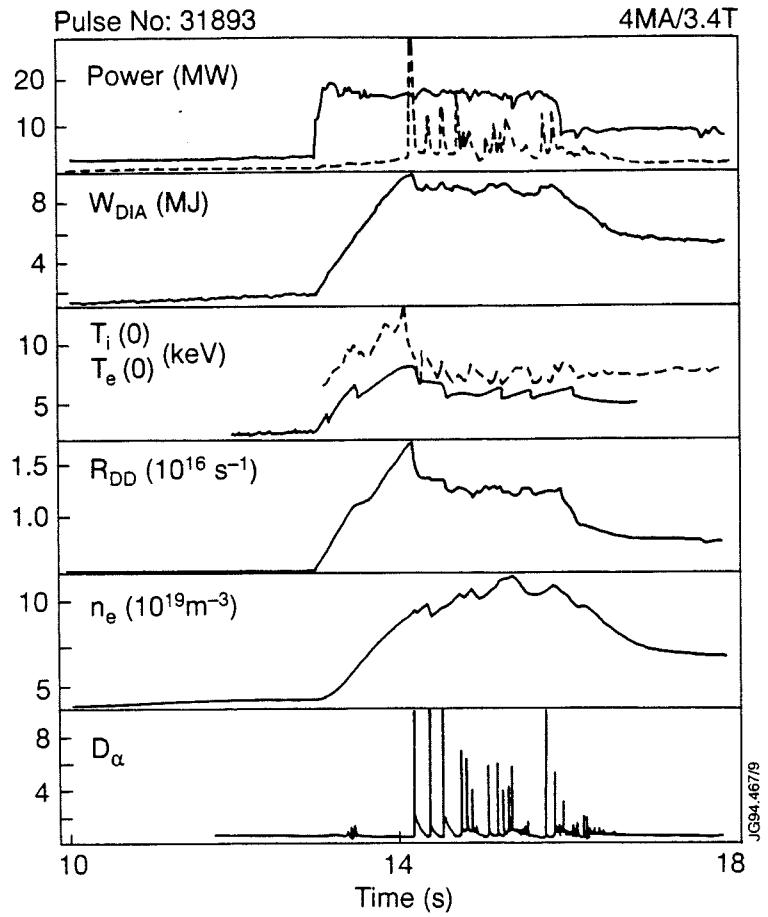

Fig. 15 *Time development of 4MA/3.4T ELMy H-mode at high power.*

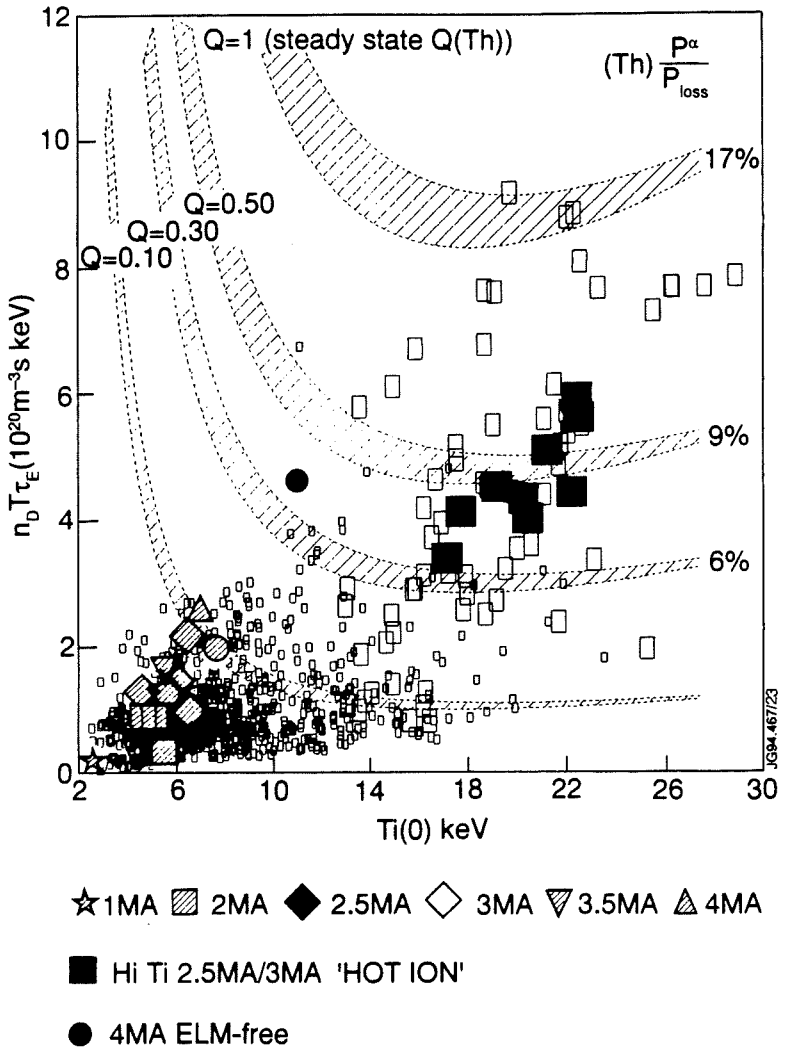

Fig. 16 *Triple fusion product $n_D(o) \cdot T_i(o) \cdot \tau_E$ plotted against central ion temperature ($T_i(o)$ for selected shots from the JET-PD dataset compared to the pre 1992 JET data.*

Key: i) JET-PD Steady-state ($> 4\tau_E$) H-modes

■ 1MA ; ❑ 2MA ; ◆ 2.5MA ◊ 3MA
▲ 3.5MA ; Δ 4MA.

ii) JET-PD Hot Ion H-modes
○ 2.5/3.0MA.

iii) Large filled circles represent JET 1991/2 Hot Ion H-modes.
Small dots represent the remainder of the JET dataset.

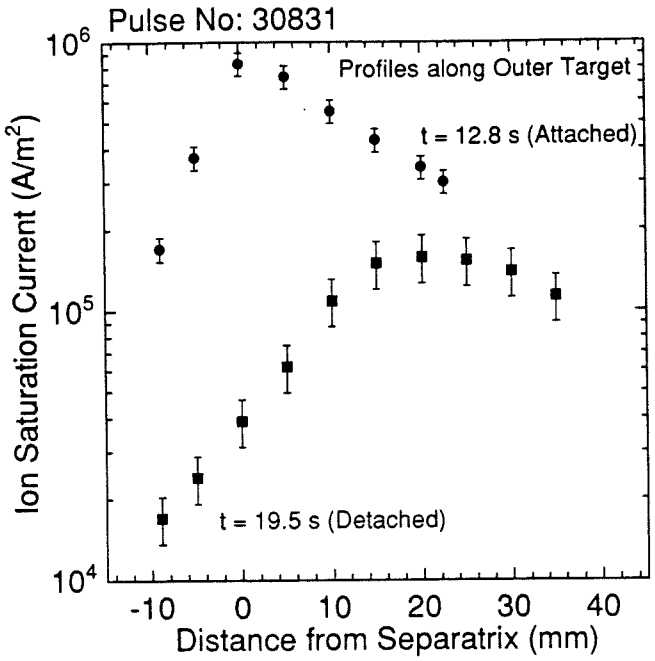

Fig. 17 *Ion saturation current at the outer strike zone at 2 times during a density ramp. The saturation current at 19.5 secs is much lower than at 12.8s in spite of the higher density, indicating a detached plasma has been achieved.*

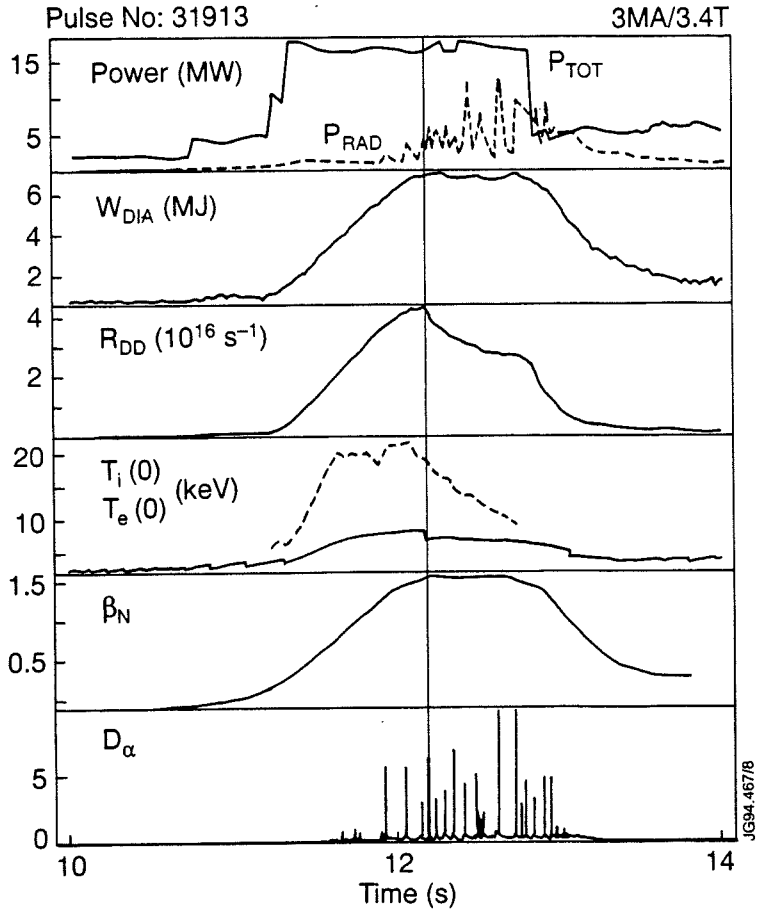

Fig. 18 *Time development of a 3MA/3.4T Hot Ion H-mode in JET-PD.*

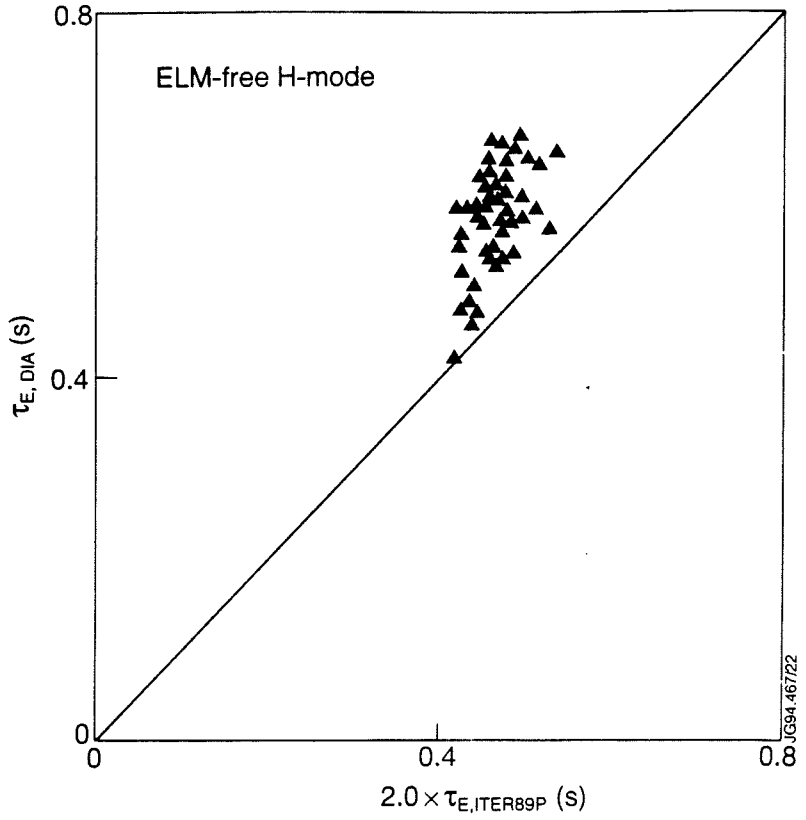

Fig. 19 *Diamagnetic energy confinement time for the 2.5MA Hot Ion H-modes from the 1994 dataset compared to the* $2x\,\tau_{E,ITER81P}$ *value.*

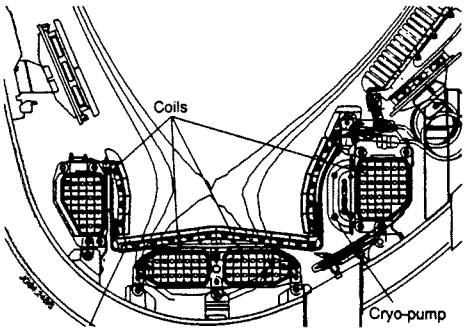

Mark I (1994/95)

- relatively open
- requires sweeping over horizontal targets
- accepts wide range of plasmas
- limited side plate operation
- resilient to ELMs

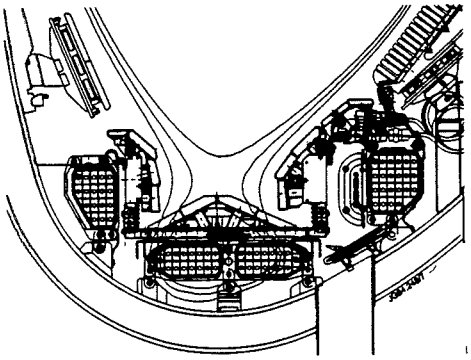

Mark IIA (1995/96)

- more closed moderate slot
- improved static power handling on domed and vertical targets
- improved pumping
- optimised for JET

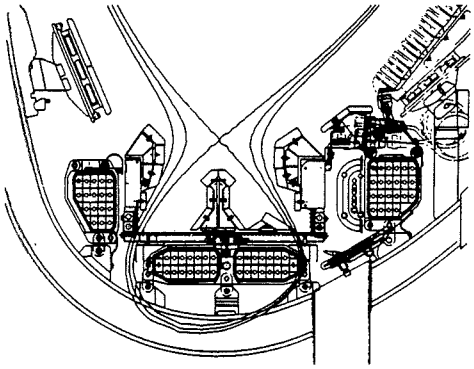

Mark IIGB (1997/98)

- ITER specific Gas Box
- deep divertor with high X-point
- baffle wide enough for ELMs and L-modes but closure adequate for H-modes
- target design not yet finalised
- optimised for ITER?

Fig. 20 JET Divertor configurations.

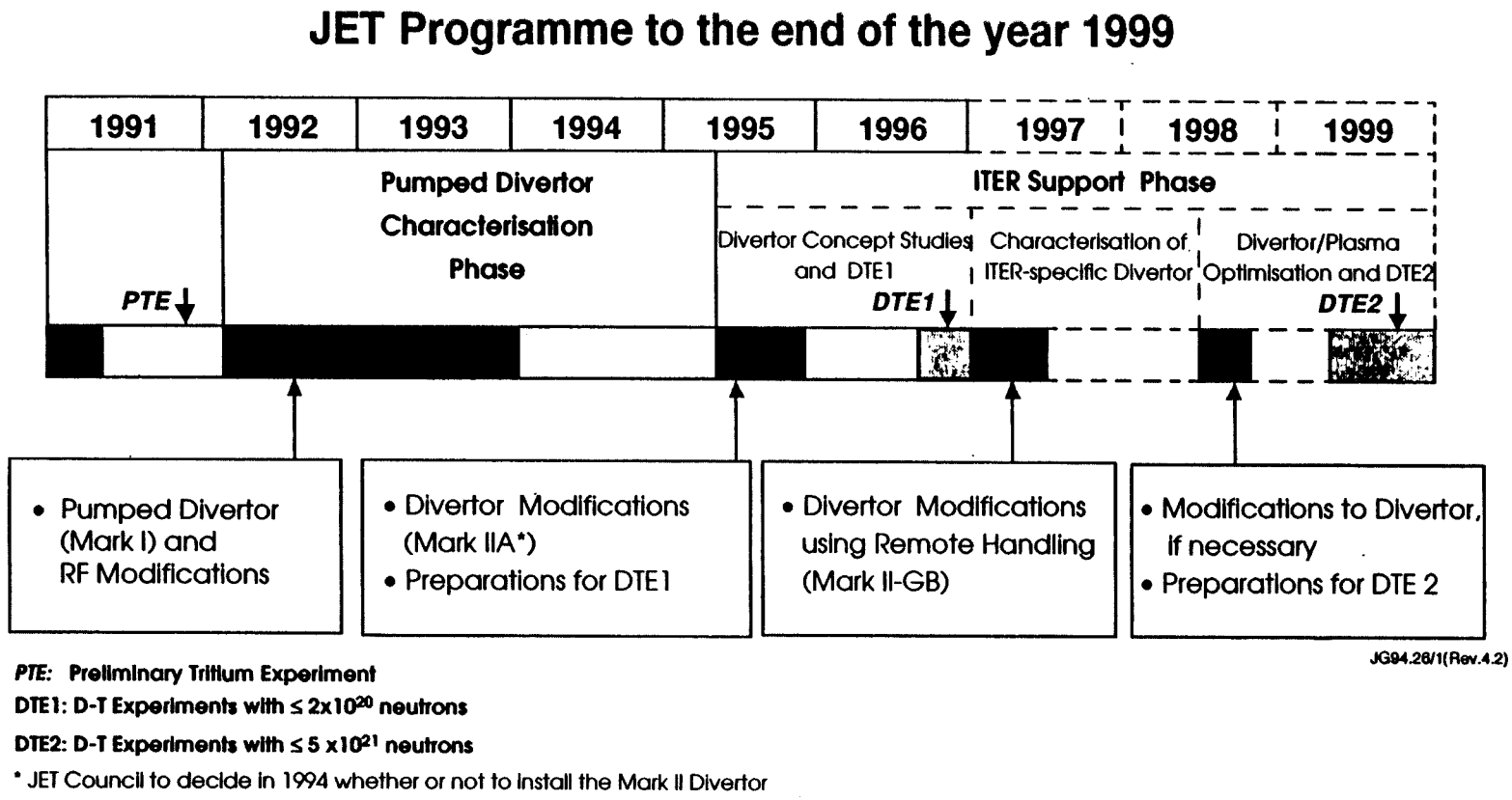

Fig.21 *Time plan for the proposed JET extension.*

Exhaust and Impurity Control Experiments in the JET Pumped Divertor

The JET Team
(presented by D J Campbell)

JET Joint Undertaking, Abingdon, Oxfordshire, OX14 3EA, UK.

EXHAUST AND IMPURITY CONTROL EXPERIMENTS IN THE JET PUMPED DIVERTOR

The JET Team
(Presented by D J Campbell)

JET Joint Undertaking,
Abingdon, Oxfordshire, OX14 3EA,
U.K.

ABSTRACT

The first results of divertor studies in the JET Pumped Divertor are discussed. Plasmas using either the horizontal or vertical plates of the target have been investigated and sweeping of the divertor plasma strike points has been used to increase the wetted area of the target during high power experiments. As a result of careful alignment, the surface of the target has not exceeded 800°C while total plasma input energies of up to 140MJ have been used. Experiments with the divertor cryopump have shown that the most efficient pumping is obtained when the outer strike point is adjacent to the pump. However, pumping efficiency falls by only a factor of 2 as the strike point is moved up to 20cm from the optimum position. Measurements of the SOL and divertor parameters in discharges diverted onto the horizontal or vertical target plates have confirmed certain features predicted by numerical models. Steady-state H-modes with duration of up to 20s and confinement enhancement factors close to twice L-mode scaling have been obtained and have been extended to high density. The approach to detachment, obtained so far only in ohmic and L-mode plasmas, has been studied experimentally and numerically.

1. INTRODUCTION

Following a major upgrade JET now operates with a Pumped Divertor [1] which combines high power handling capability, flexibility of plasma configuration and a cryopump operating at liquid helium temperature. This has equipped JET to address the central problems of the ITER divertor: efficient dissipation of heat exhaust with minimal erosion, control of particle fluxes, including helium, and effective impurity screening. In experiments to date, X-point plasmas with currents of up to 4MA have been established and an extensive characterization of the properties of diverted plasmas has been performed in L and H-modes, with an emphasis on diagnosing plasmas in steady-state conditions. The power handling capability of the target has been demonstrated at total powers of up to 26MW and in steady-state H-modes lasting up to 20s.

Close co-ordination of experimental and theoretical studies of divertor plasmas, to provide validation of numerical codes used in predictive modelling and to guide the evolution of the experimental programme, is a key feature of the JET divertor programme. Here initial comparisons between experimental observations of discharges using horizontal and vertical target plates and the results of simulations are discussed.

2. THE JET PUMPED DIVERTOR

The main features of the new divertor configuration are shown in Fig. 1. Four internal coils allow a wide range of configurations to be established at currents of up to 6MA. Divertor connection length and X-point height can be varied independently. In addition, the divertor strike points can be swept at frequencies above 4Hz and at amplitudes of 10cm to increase the wetted area for heat exhaust. The divertor target consists of narrow, water-cooled inconel beams on which CFC tiles are mounted. Tiles are machined and carefully aligned to

eliminate edge exposure. Slots between the support beams allow neutrals to recirculate and to reach the divertor cryopump [2].

Diagnostics have also been extensively upgraded with many new systems being introduced, particularly for SOL and divertor studies. Principal diagnostics used in these studies include an array of single and triple Langmuir probes, which provide both divertor target and upstream (SOL) plasma parameters; IR and CCD cameras providing observations of target heating and recycling as well as impurity influxes; poloidally resolving visible spectroscopy and bolometry yielding measurements of deuterium and impurity radiation; and ionization gauges, distributed below the divertor target and at the entrance to the cryopump, which determine neutral densities in the divertor.

3. POWER HANDLING STUDIES

Divertor experiments in the original JET device were constrained by the occurrence of the carbon bloom at high power, often as a result of localized heating on exposed tile edges [3]. Considerable care has, therefore, been taken in design and installation of the target tiles to eliminate the exposure of edges. In addition, X-point sweeping distributes the loss power over a larger surface area, reducing the heating rate of the target. In combination with the giant ELM's, which are now a feature of JET H-modes and which distribute power over a wide area of the divertor, sweeping is very effective in establishing essentially steady-state surface temperatures on the target. This is illustrated in Fig. 2, which shows the peak temperature in the outer strike point during a pulse with a total power of 12MW. The target temperature gradually rose over the first 2s of the (unswept) heating phase, reaching ~800C. Following the initiation of sweeping at 16s, as indicated by the 4Hz oscillation in the current of one of the divertor coils, the peak tile temperature fell and oscillated slightly about a steady-state value of ~600C. The sweeping has no deleterious effects on either the ELM behaviour or the plasma energy confinement. In long steady-state H-modes of up to 20s duration, 140MJ has been delivered to the plasma, with >100MJ deposited on the divertor target. The vertical targets have also proved robust in this respect, having sustained 80MJ of injected energy of which 50MJ was deposited on the target.

Asymmetries in the power deposition on inner and outer targets, as observed in previous JET experiments [4], could adversely affect gas target divertor regimes. Therefore, a series of experiments was performed with the ∇B ion drift towards and away from the target to investigate its influence on such asymmetries. In these discharges, the direction of the plasma current was also reversed to maintain a constant magnetic helicity, as required by the inclination of the target tiles, and this necessitated the use of counter-NBI.

The results are illustrated in Fig. 3, in which the ratio of peak temperature on the outer target to that on the inner target (after approximately 4s of additional heating) is plotted as a function of q_{95}. In L-mode plasmas with the ∇B ion drift towards the target it was found that tile heating on the outer target was dominant, but that the degree of asymmetry decreased with increasing q_{95}. With the toroidal field direction reversed, tile heating on the outer target was still dominant, but the degree of asymmetry increased with increasing q_{95}. It was also observed that asymmetries in the D_α emission from the divertor and in the radiation, which were dominated by emission from the inner divertor leg with the ∇B ion drift towards the target, were reversed when the toroidal field was reversed. Thus, it appears the toroidal field reversal mainly affected the density distribution between the two divertor legs [5], a conclusion supported by Langmuir probe data. However, asymmetries in the power flow to the target cannot be simply explained by asymmetries in radiation from the divertor legs and further analysis is in progress to develop a detailed understanding of these experiments.

A power balance analysis of these L-mode plasmas showed that the loss power was completely accounted for by bulk and divertor radiation, convection and

conduction to the divertor target and a significant (~20%) component of atomic recombination at the target. Power accountability in H-mode plasmas is not yet as well documented as ELM's complicate the analysis.

4. EXPLOITATION OF THE DIVERTOR CRYOPUMP

With a measured speed of ~170m^3s^{-1}, the divertor cryopump allows greater control over the plasma density and modification of the particle flows in the divertor and SOL, leading to the possibility of improved impurity control. In addition, the use of argon frosting will permit the study of helium exhaust in reactor-relevant regimes. Initial experiments with the cryopump have investigated the dependence of the pumping efficiency on X-point geometry and the quantitative balance between gas input rate and particle removal rate. The latter is calculated from the measured pressure in front of the pump and its calculated proportionality with particle removal in D gas tests.

Fig. 4 shows the results of an experiment in which the outer strike point of the plasma was moved across the horizontal target and up the vertical plate while the pressure in front of the cryopump was monitored with an ionization gauge. During this scan the plasma density was held constant by gas-puffing. The particle removal rate rose to a maximum of $8\times10^{21}Ds^{-1}$ as the strike point reached the corner of the divertor target, adjacent to a toroidal slot in front of the pump, then fell as the strike point rose up the side-plate. However, the variation in particle removal rate was only a factor of 2 as the strike point scanned over virtually the entire usable surface area of the target, indicating that the radial slots between the target support beams provide an adequate conductance to the cryopump. Moreover, the ratio of removal rate to fuelling rate was found to be independent of the fuelling location.

The low sensitivity of the particle removal rate to strike point position contrasts with the experience in DIII-D [6] and is of great significance to the JET divertor programme, since it permits exploitation of the wide range of configurations for which the divertor was conceived. In addition, it demonstrates the feasibility of using strike point sweeping to redistribute exhaust power while exploiting the benefits of the particle control provided by the pump. This conclusion is supported by observations of density behaviour in steady-state H-modes, which showed a significant reduction in edge plasma density when the cryopump was active, even when the strike point was distant from the cryopump slot.

A quantitative fuelling balance has been performed for a variety of JET plasmas, ranging from ohmic to long steady-state H-modes without gas fuelling and high density L and H-modes. The total gas input in these discharges ranged from 500 to 8000mbl. In the majority of cases, there was a balance to better than 10% between the total gas input and that removed by the pump.

5. INVESTIGATION OF SOL AND DIVERTOR PARAMETERS

A detailed comparison is underway of SOL and divertor parameters in various regimes and plasma configurations in order to develop a greater understanding of the behaviour of the plasma edge, particularly in regimes of interest to ITER such as the gas target divertor, and to benchmark codes used to model divertor behaviour [7]. In particular, it has been predicted that, in plasmas with strike points on the divertor sideplates, the probability of escape for recycling neutrals should be substantially reduced [8], possibly facilitating access to the detached divertor regime. Such plasmas have been established and their edge parameters compared with equivalent plasmas on the horizontal target. Fig. 5 shows equilibria for a pair of discharges at 2MA/2.8T. These cases had similar densities, input and radiated powers, and similar impurity content. Electron temperatures and densities were derived from single and triple Langmuir probe measurements in the divertor target and compared with numerical predictions of the EDGE2D

code [9] which are based on the measured input power, radiated power and a SOL inventory adjusted to match measured divertor densities.

A comparison between the experimentally determined electron temperature and density profiles and the results of modelling for an attached divertor plasma is shown in Fig. 6. One notable result is that even at central plasma densities as low as $4\times10^{19}m^{-3}$ and input powers of 4MW, divertor densities in the region of $1\times10^{20}m^{-3}$ are observed, indicating that the divertor is in a very high recycling regime. This contrasts strongly with observations made in the old JET configuration [10] and suggests that, in spite of its relatively open geometry, the pumped divertor configuration is closed to a far higher degree than the previous JET divertor. The main features of the density profiles predicted by the code are in reasonable agreement with those obtained experimentally. In addition, there is a striking agreement between the code prediction of an inverted temperature profile on the side-plate configuration and that actually observed, suggesting that the behaviour of recycled neutrals is accurately predicted by the code.

The differences in recycling patterns between discharges on the horizontal and vertical targets should lead to a thinner SOL in the latter case. Initial measurements made in L-mode plasmas support this prediction. SOL profiles have been obtained using a reciprocating Langmuir probe near the top of the plasma in equilibria similar to those illustrated in Fig. 5, but with the toroidal field and current directions reversed. Examples of electron density profiles, mapped to the plasma midplane, are shown in Fig. 7. These indicate that, under the same conditions of power and density, the scale length for the density fall off in the vertical plate discharge is approximately half (λ_n=1.6cm) that in the horizontal plate discharge (λ_n=3.1cm).

6. STEADY-STATE REGIMES

Extension of ITER-relevant plasmas to steady-state conditions is a central theme of the JET programme. Two specific regimes have been investigated, steady-state H-modes and detached divertor plasmas. In the new JET configuration, repetitive ELM's occur naturally and this has allowed long pulse, steady-state H-modes to be established. Experiments have been conducted with plasma currents in the range 2-3MA (q_{95}=3.3-2.9) at total input powers of up to 11MW. At the lower current 20s H-modes (Fig. 8) have been produced, while 9s H-modes have been obtained at 3MA. In all cases the H-mode duration was restricted by that of the additional heating. It is particularly significant that, as shown in the figure, the surface temperature of the target does not exceed 550°C. Thus it appears likely that this regime will be limited only by technical constraints, such as bulk heating of the target tiles or limitations of the poloidal and toroidal circuits.

In the 2MA/2.1T case shown in Fig. 8 fuelling was provided by NBI heating only and the cryopump was used. Comparative discharges with and without the cryopump showed that the use of the pump reduced plasma edge density and plasma average density (by ~10%) and improved confinement (by ~15%). A comparison with earlier JET results on steady-state H-modes is also revealing. Long steady-state H-modes were established in the old JET configuration by gas-puffing into otherwise ELM-free plasmas [9]. In those cases $\overline{Z}_{eff}$ fell to ~2, while the plasma density rose after ~10s as the walls saturated. In addition, energy confinement was ~80% of the JET/ DIII-D H-mode scaling and considerable difficulty was experienced with large amplitude mhd activity. In the present experiments, $\overline{Z}_{eff}$ lay in the range 1-1.5 and, as with all significant bulk plasma parameters, was in steady-state throughout. In addition, even in cases in which additional gas-puffing was used to increase the plasma density, there was no evidence of saturation of the pumping. Stored energy in the case shown is equal to that predicted by the JET/ DIII-D H-mode scaling and for all discharges in which the cryopump was used was within 10% of this value.

Maintaining steady-state plasmas in which most of the input power is dissipated by radiation or charge exchange processes in the divertor is a central problem in

current fusion research. Previous experiments on JET [12] succeeded in establishing 'detached' L-mode plasmas in which virtually all of the input power was lost by radiation. Maintaining this regime in steady-state in combination with enhanced confinement is a major aim of JET divertor experiments. Results of an initial experiment are shown in Fig. 9. This illustrates the evolution of an L-mode discharge at 2MA/2.8T with 5.5MW of input power in which deuterium puffing was used to access the 'detached' divertor regime. Operationally this phase is defined to occur when the ion saturation current, I_{sat}, to the target falls as the bulk plasma density increases, indicating that the plasma is detaching. This process occurs initially in the vicinity of the separatrix as the plasma approaches the density limit in JET [13]. We have, therefore, implemented a feedback loop in which the ion saturation current from a Langmuir probe close to the separatrix is used to control the gas fuelling rate and, eventually, to bring the plasma into a steady-state condition. This process is shown in the lower panel of the figure, where the reference waveform and a smoothed version of I_{sat} used to control the deuterium puffing rate are compared. As the bulk plasma density and radiated power rise, I_{sat} falls, gradually reaching the level of the reference waveform, at which point the feedback system holds the plasma in steady-state. The physics of these plasmas is discussed in detail in an accompanying paper [7].

7. SUMMARY

Initial operation with the JET Pumped Divertor has established that it provides a flexible and powerful device for the investigation of key issues relevant to the development of the ITER divertor. A wide range of plasma configurations has been developed with X-point connection lengths of up to 10m. Careful alignment of the divertor target has resulted in excellent power handling capability, which is augmented by the beneficial effects of sweeping and ELM's. Further reduction in the power loading of the target is associated with the existence of a high recycling divertor and access to detached divertor regimes. Experiments with the divertor cryopump have shown that it provides effective particle exhaust over much of the divertor target area and there have clearly been beneficial effects on the performance of steady-state H-modes. Comparisons of discharges using the horizontal and vertical targets have confirmed some aspects of divertor models, although much further experimentation is required to exploit the possible benefits of side-plate operation. The new capabilities of the Pumped Divertor have allowed us to establish steady-state plasmas in regimes of interest to ITER, such as ELMy H-modes and detached divertor plasmas and the study of these regimes will be pursued vigorously in the current experimental campaign. A key goal is to establish the viability of combining the improved confinement of the steady-state H-mode with the beneficial effects in power handling and target erosion of the detached divertor.

ACKNOWLEDGEMENTS

The results presented here are a tribute to the work of those who designed, constructed and installed the Pumped Divertor. It is a pleasure to thank the members of the Divertor Task Force and Topic Group who contributed to the execution of the experimental programme and the analysis of the results: P Andrew, A Bickley, A Chankin, S Clement, S J Davies, J Ehrenberg, S K Erents, M Garribba, H Y Guo, P Harbour, L Horton, J Lingertat, A Loarte, C G Lowry, K McCormick, C Maggi, G F Matthews, C Mayaux, R Monk, D O Brien, W Obert, R Reichle, G Saibene, M Schaffer, M Stamp, D Start, D Stork, A Taroni, E Thompson and G C Vlases.

REFERENCES

[1] The JET Team (presented by P.-H. Rebut), 'Recent JET Results and Future Prospects , Plasma Physics and Controlled Nuclear Fusion Research 1990 (Proc. 13th Int. Conf. Washington, 1990) Vol. 1, IAEA, Vienna (1991) 27.

[2] Obert, W., et al, 'JET Pumped Divertor Cryopump , Fusion Technology 1990 (Proc. 16th Symposium London 1990) Vol. 1, North-Holland, Amsterdam (1991) 488.

[3] Stork, D., et al, 'Control of Carbon Blooms and the Subsequent Effects on the H to L Mode Transition in JET X-Point Plasmas , Controlled Fusion and Plasma Heating (Proc. 18th Euro. Conf. Berlin) Vol. I (1991) 357.

[4] Reichle, R., et al, 'Power Loading and Radiation Distribution at the X-Point Target for Normal and Reversed Toroidal Field , ibid Vol. III (1991) 105.

[5] Chankin, A. V., et al, 'The Effect of B_T Reversal on the Asymmetries between the Strike Zones in Single Null Divertor Discharges: Experiment and Theories , Plasma Phys. and Contr. Fusion **36** (1994) 1853.

[6] Mahdavi, M. A., et al, 'Active Density Control in DIII-D H-Mode Plasmas , Controlled Fusion and Plasma Physics (Proc. 20th Euro. Conf. Lisbon 1993) Vol. II (1993) 647.

[7] The JET Team (presented by L. Horton), 'Modelling and Measurements of JET Divertor Plasmas , paper IAEA-CN-60/A-4-I-5 this conference.

[8] The JET Team (presented by G. C. Vlases), 'Divertor Physics at JET: Experimental Results and Modelling , Plasma Physics and Controlled Nuclear Fusion Research 1992 (Proc. 14th Int. Conf. Würzburg, 1992) Vol. 1, IAEA, Vienna (1993) 287.

[9] Taroni, A., et al, 'The multi-fluid codes EDGE1D and EDGE2D: models and results , Contrib. to Plasma Phys. **32** (1992) 438.

[10] The JET Team (presented by G. Janeschitz), 'Comparison of Plasma Performance with Beryllium and Carbon Divertor Targets in JET , ibid [8] Vol. 1 (1993) 329.

[11] Thomas, P. R., et al, 'Steady State H-Modes in JET , Controlled Fusion and Plasma Physics (Proc. 19th Euro. Conf. Innsbruck 1992) Vol. I (1992) 239.

[12] Clement, S., et al, 'Edge Measurements in the Divertor Region in High Density Discharges at JET , ibid Vol. II (1992) 723.

[13] Campbell, D. J., et al, 'The Density Limit in JET Diverted Plasmas , Controlled Fusion and Plasma Physics (Proc. 21st Euro. Conf. Montpellier 1994) (to be published).

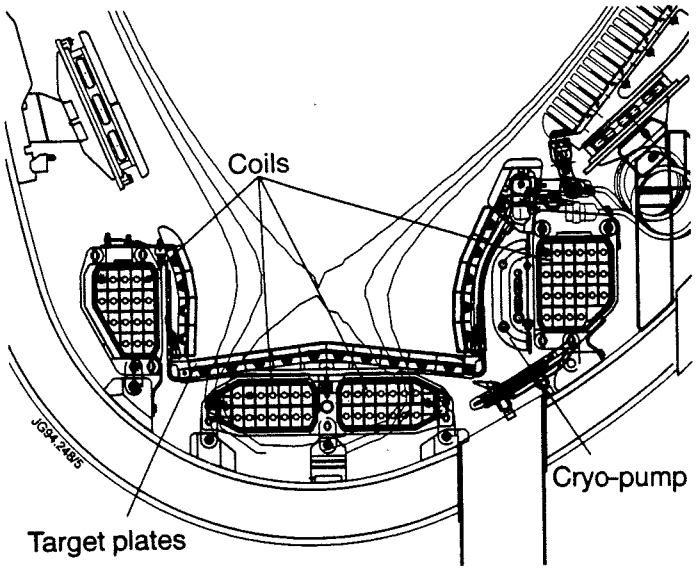

Fig. 1 *Cross-section of the JET Pumped Divertor showing the major components.*

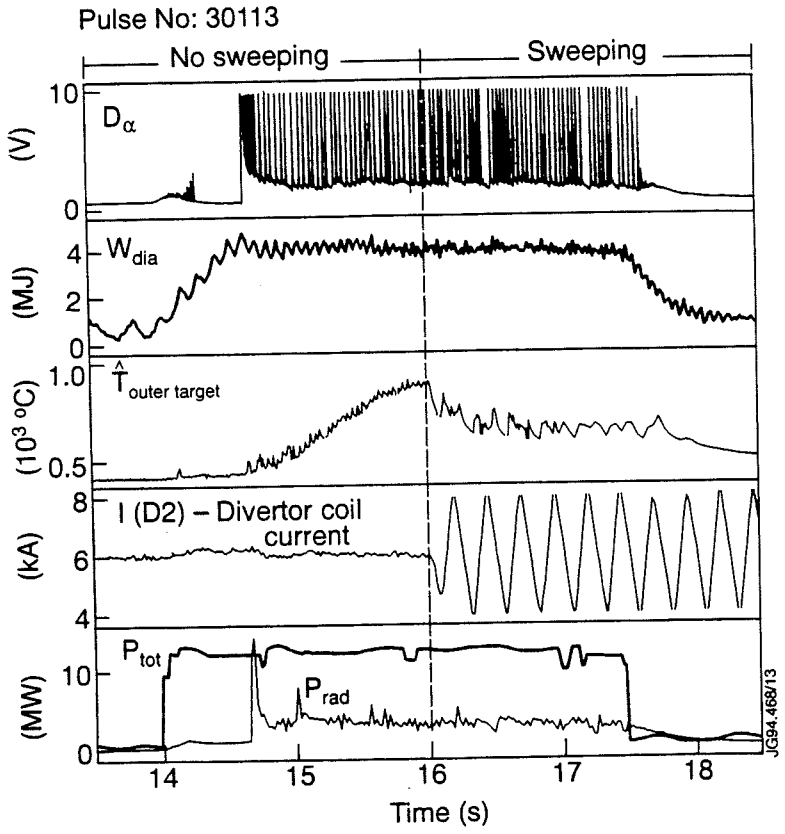

Fig. 2 *An additionally heated pulse in which divertor strike point sweeping was started at 16s. As a result, the peak temperature on the outer target fell from ~800°C and gradually approached a new steady-state value of ~650°C.*

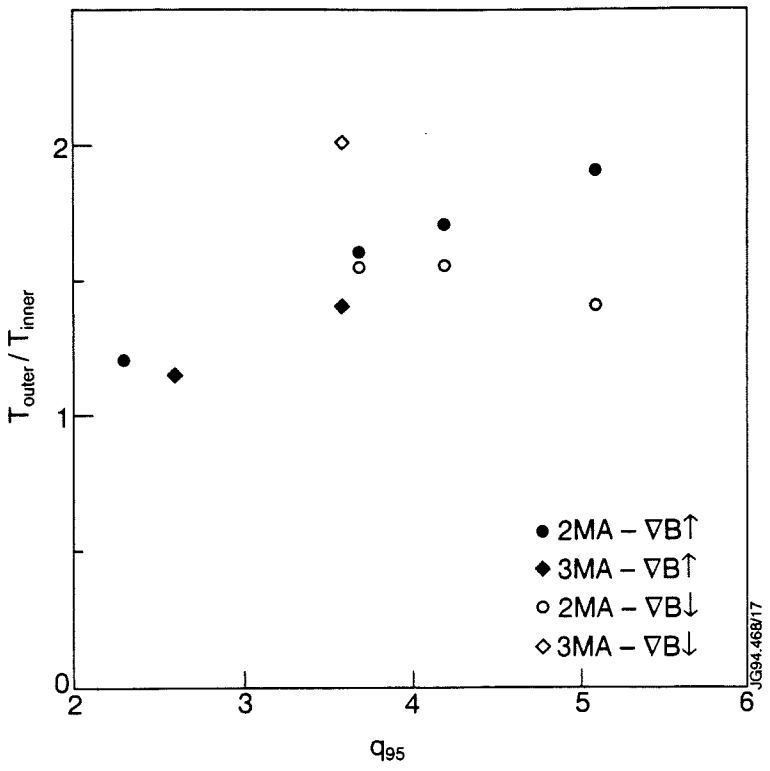

Fig. 3 *Ratio of the measured peak temperature on the outer strike zone to that on the inner strike zone as a function of q_{95} and the direction of the ∇B ion drift for a series of L-mode plasmas.*

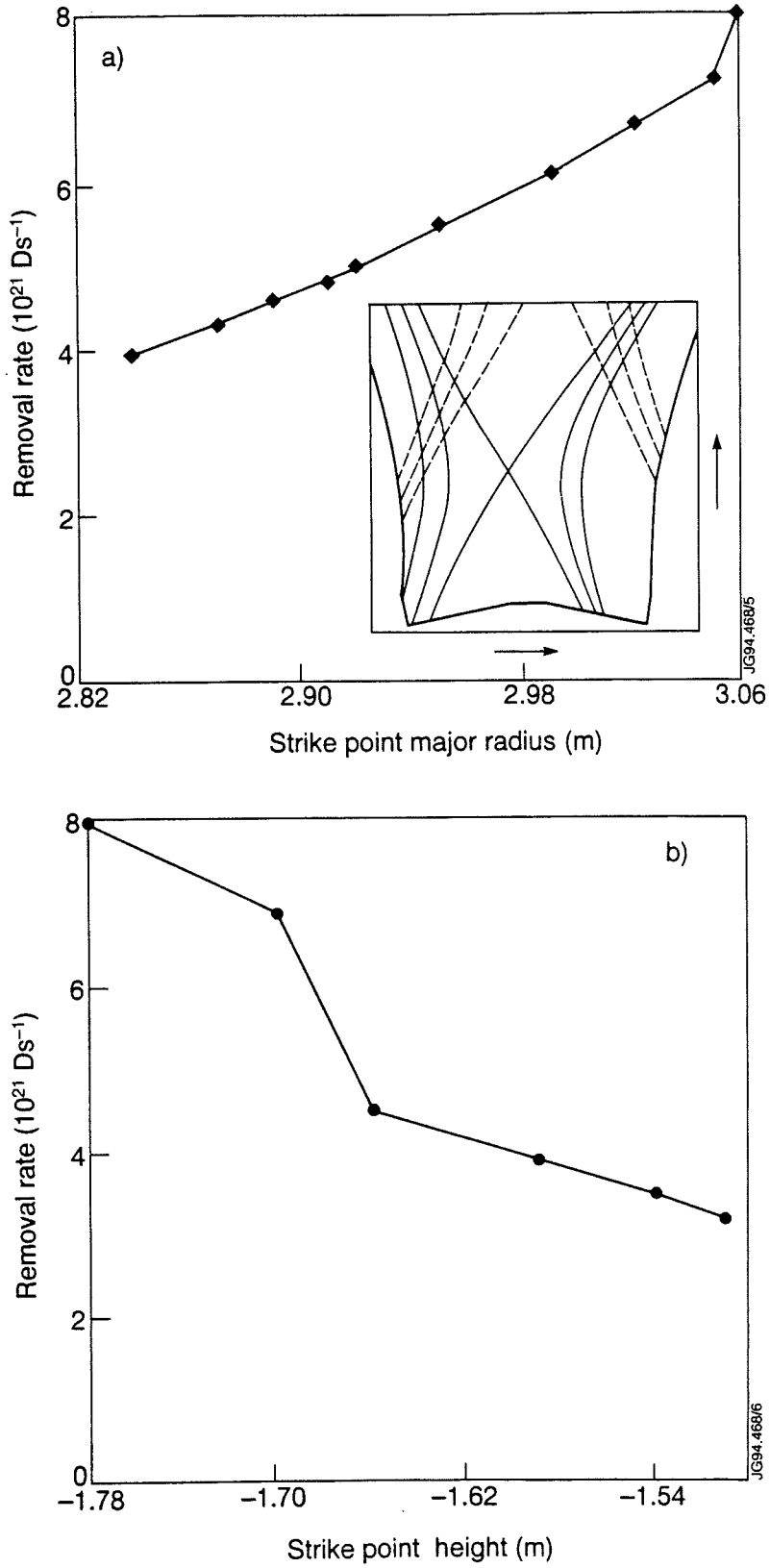

Fig. 4 *The measured particle removal rate as a function of the outer separatrix position for a pulse in which the cryopump was active: a) shows the removal rate as the separatrix moved across the horizontal target plate and b) the removal rate as it moved up the vertical target plate.*

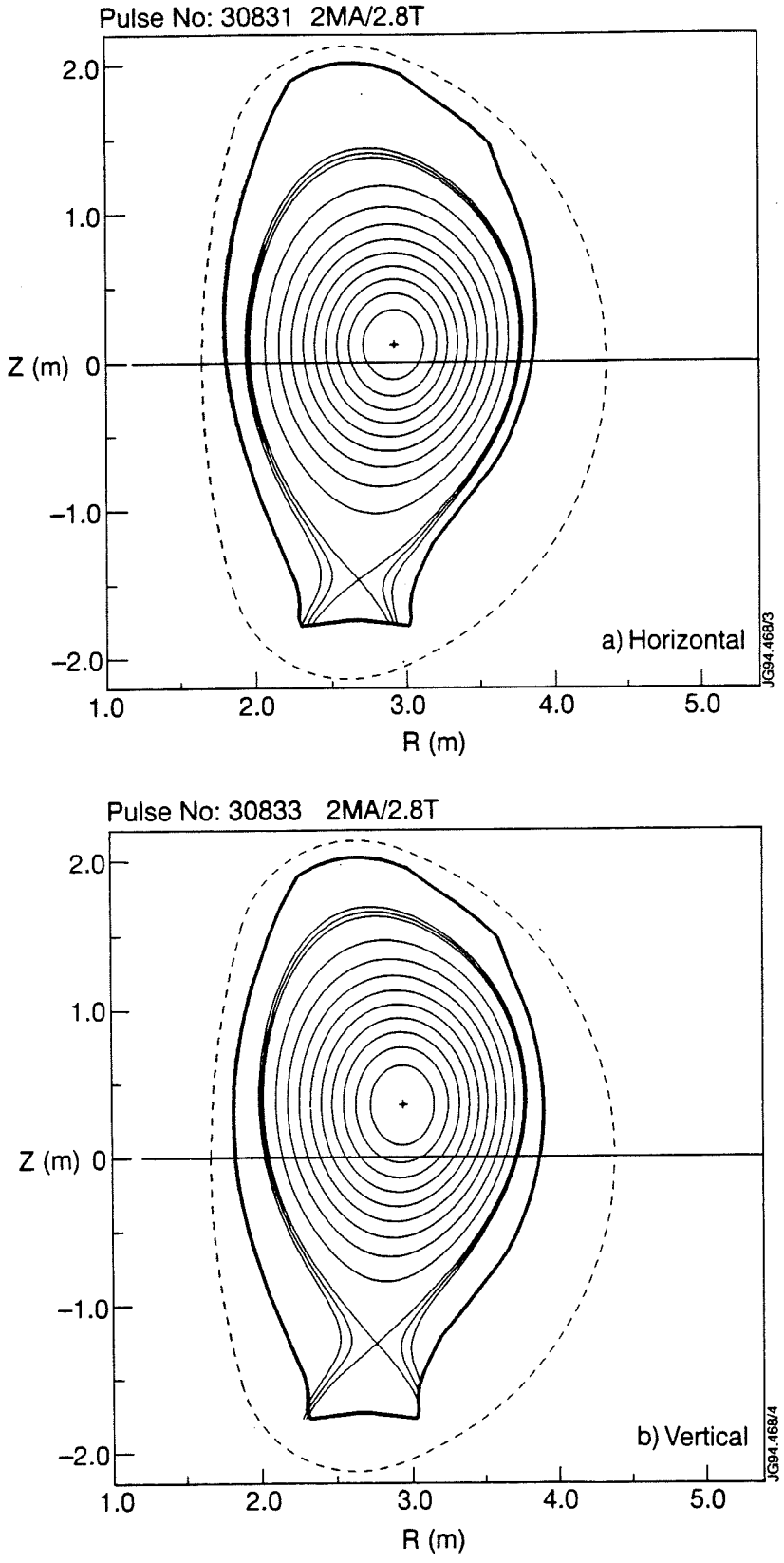

Fig. 5 *a) a horizontal target plate equilibrium. b) a vertical target plate equilibrium.*

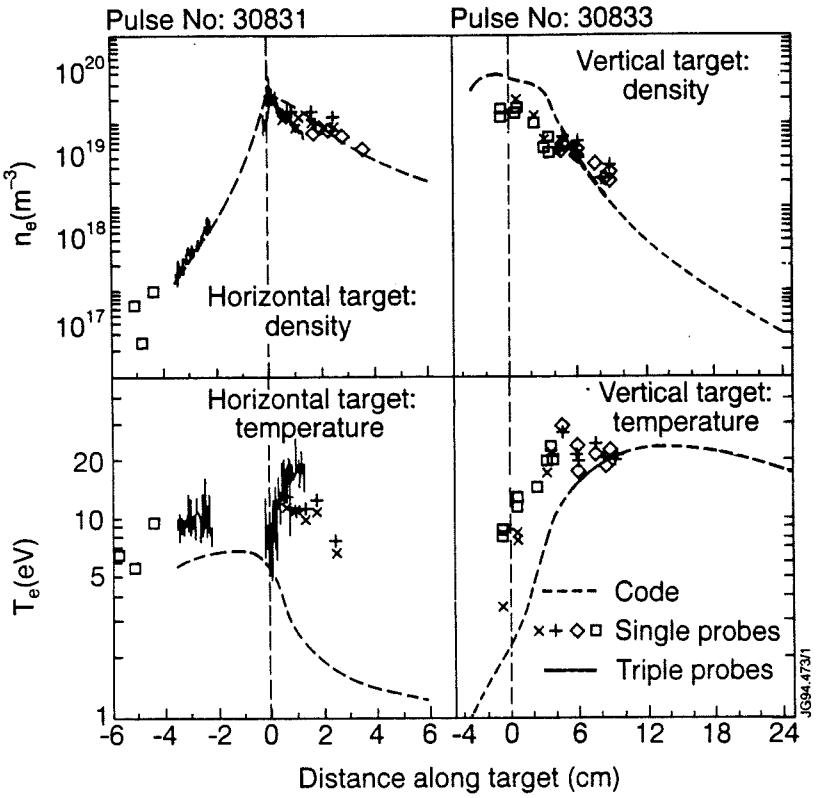

Fig. 6 *A comparison between measured and modelled electron density and temperature profiles at the divertor target for plasmas on the horizontal target, and on the vertical target. The profiles are plotted as a function of radial distance along the target.*

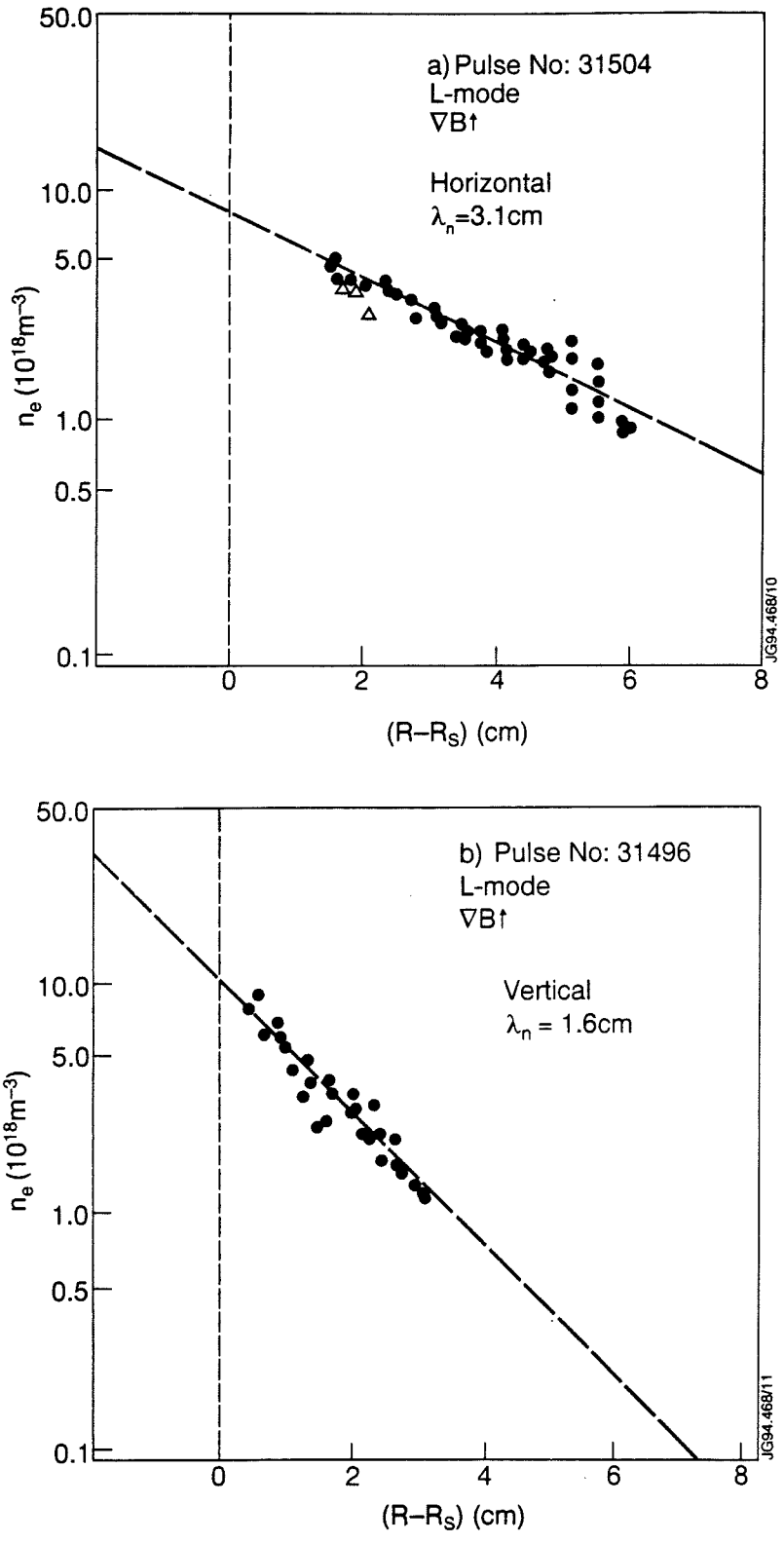

Fig. 7 *A comparison of density fall off lengths for plasmas on the horizontal target, a), and on the vertical target b), mapped to the plasma midplane and plotted as a function of radial distance from the separatrix, R-R_s.*

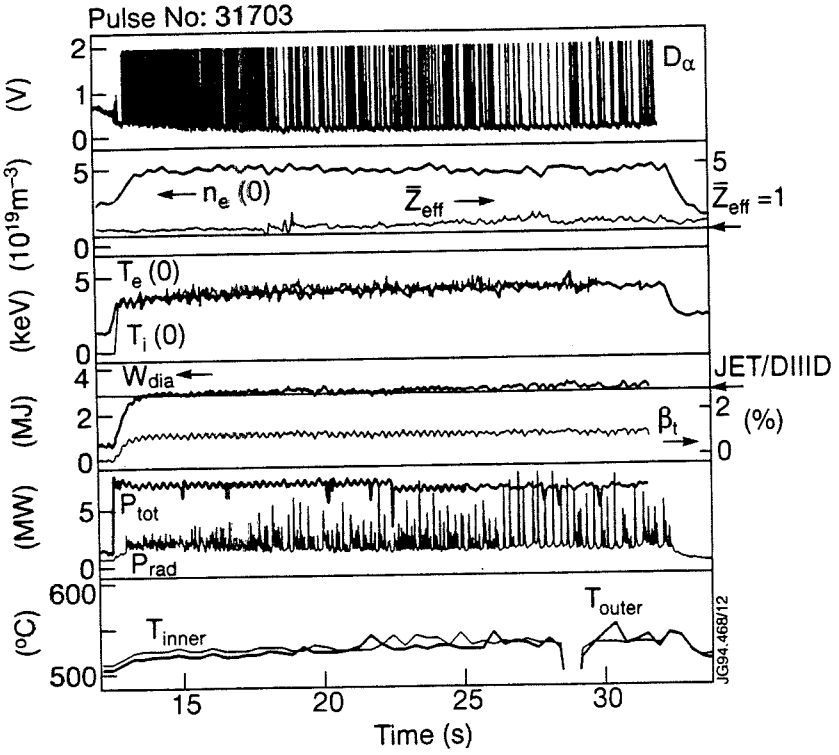

Fig. 8 A 20s steady-state H-mode at 2MA/ 2.1T.

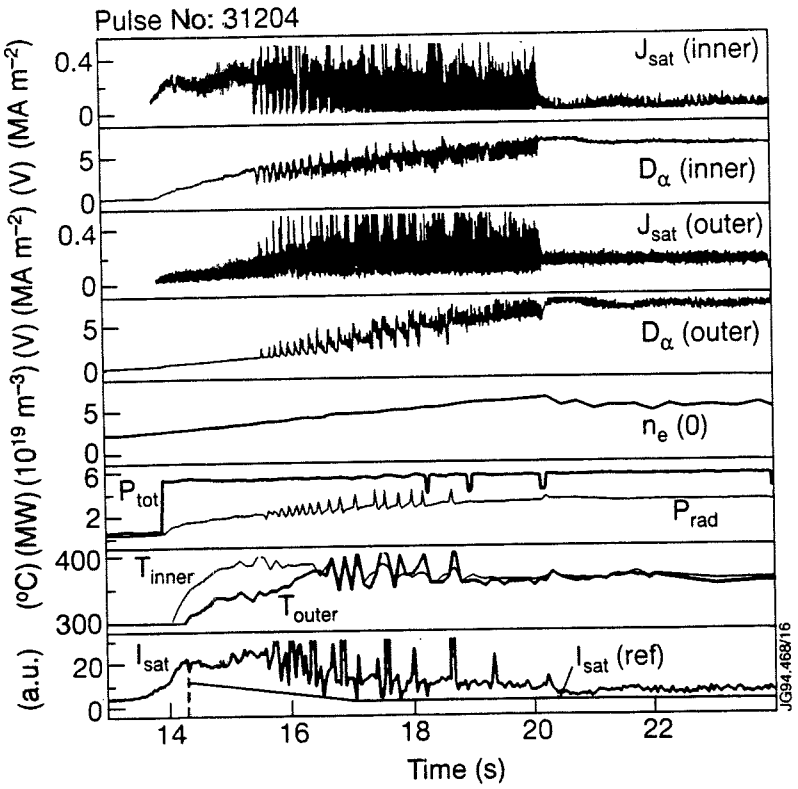

Fig. 9 A detached L-mode plasma at 2MA/ 2.8T in which the approach to detachment was controlled by reducing the ion saturation current measured by a Langmuir probe close to the inner separatrix almost to zero.

Studies of Energy and Particle Transport in JET

The JET Team
(presented by R Giannella)

JET Joint Undertaking, Abingdon, Oxfordshire, OX14 3EA, UK.

STUDIES OF ENERGY AND PARTICLE TRANSPORT IN JET

THE JET TEAM
(Presented by R. Giannella)

JET Joint Undertaking,
Abingdon, Oxfordshire, OX14 3EA
United Kingdom

ABSTRACT

Investigation on H-mode transport has concentrated on pulses where elevated confinement can be achieved. At the time of the L-H transition a prompt transport reduction in the core (as well as at the edge) of the discharge is observed. Poorly performing, higher-Z_{eff} discharges appear to have substantially the same core transport as record achieving pulses. New H-mode power threshold data were acquired in 1994, with ion B drift of both signs, confirming P_{th} to increase with B_t and n_e. The transport of injected impurities indicates that, in L-mode discharges, the outer region of strong anomalous transport more or less coincides with the region of high shear ($s > 1/2$). Analysis of inward propagation of cold pulses supports the hypothesis that, when the edge temperature is perturbed, transport across the discharge suffers a prompt modification.

1. INTRODUCTION

The study of energy and particle transport at JET was mainly devoted, lately, to two basic activities: the further analysis of the database acquired in the experimental campaigns held until 1992 and the comparison of new observations from the present campaign (1994) with those made in the past. For the sake of conciseness the paper is organised in two sections dealing with the high and low confinement respectively. Where possible, reference is made to JET papers, recently published or submitted for publication, that will supply more extensive descriptions of phenomena illustrated here.

2. H-MODE AND ELEVATED CONFINEMENT

Investigation on transport in the H-mode regime has recently concentrated on pulses where elevated energy confinement can be achieved. In **hot-ion pulses**, enhancement factors for the energy confinement time (compared with the JET/DIII-D H-mode scaling) up to 2 are observed. The maximum kinetic energy that can be stored in these plasmas appears limited at a normalised beta $\beta_N \sim 2$ [1] suggesting that the deterioration of transport observed at the highest levels of stored energy may be due to MHD instabilities [2]. This empirical constraint results in a favourable scaling of confinement with the toroidal magnetic field.

Local power balance analysis performed with the TRANSP code on these discharges shows that a marked improvement of transport occurs in the bulk of the plasma immediately after the transition from L- to H-mode. At that time the effective thermal diffusivity χ_{eff} is seen to drop by a factor ~ 3 in the core of the discharge, before the pressure and temperature profiles suffer locally any significant modification, and then to remain at the new reduced level as the stored energy increases by a factor ~ 4 until a sudden termination occurs which often leads to a carbon bloom making recovery impossible [3]. JET pulses run in the new experimental campaign with higher Z_{eff}, broader **density profiles** and different edge fuelling rate appear to have, over the whole radial range where the local energy transport analysis is reliable ($\rho \approx 0.2 - 0.75$), the same χ_{eff} as higher performance pulses performed in the previous campaign (fig. 1).

High β_p discharges [4,5] are another well-known example of high confinement at JET. Global confinement time is shown in fig. 2 for one such pulse to exceed by ~ 75% times the ITER93H-P scaling in the phase following the end of the ELMs. The dimensionless physical parameters of this discharge are quite different from other confinement regimes, e.g. the safety factor q is 4 times higher and the normalised ion gyroradius ρ_i^* is 2 times smaller than in typical hot-ion H-modes. One of the highest JET values of β_p (~ 2.1) and the largest bootstrap fraction of f_{BS}~ 70 % were achieved in the ELM-free phase. The estimated experimental errors on energy content and on the bootstrap current are rather large (± 20%) due to relatively large uncertainties on measured profiles near the plasma edge and to the lack of space resolved information on the ion temperature. A heuristic transport model [6] that aims to account for the effects of the short- and long-scale turbulence as well as of neoclassical mechanisms has been applied to simulate this pulse using the transport code JETTO. The same model has also been successfully applied for the description of transport in a variety of L-modes as well as a number of H-modes including hot-ion H-modes [7]. The same numerical coefficients used in [7] for ELMy and ELM-free phase have been used for the corresponding phases in this simulation. The time evolution of the energy content is reproduced within the experimental uncertainty. The bootstrap current is also computed predictively by the code and agrees, within error bars, with the experimental value of the non-inductively driven current (fig.2).

Pellet enhanced performance (PEP) **discharges** [8] also attain enhanced energy confinement both in L- and H-mode, due to an improvement of the thermal diffusivity in the plasma centre. In that region several unusual conditions are produced during the PEP phase, including high densities, high pressure gradients and negative magnetic shear. This makes it difficult to validate different possible theoretical explanations for the observed improved performance, such as those related to access to the second stability region or stabilisation of ion temperature gradient driven modes [9].

In PEP pulses, depending on the degree of peaking of the n_e and T_e profiles, the shape of the q profile and the amplitude of MHD activity, strong accumulation of light impurities in the plasma centre can occur, occasionally leading to severe depletion of the main plasma ions ($n_D/n_e \leq 30$ %) on the magnetic axis [10]. Impurity accumulation appears however to have only marginal influence on the abrupt collapse of the PEP configuration. The phenomena observed are consistent with the effect of neoclassical forces associated to the logarithmic derivative of the deuterium ion density $\nabla n_D / n_D$ and of the ion temperature $\nabla T_i / T_i$. In these pulses the light impurities are in the plateau collisional regime and both forces are strong and inward-directed. In contrast, no accumulation of light impurities is observed in the hot-ion pulses mentioned previously, that also have strong pressure gradients in the plasma core, but where those impurities are in the banana regime. Indeed for those pulses hollow carbon density profiles appear to develop. This is also in agreement with the neoclassical theories that for collisionalities lower than unity predict a screening effect associated with the $\nabla T_i / T_i$ force.

New **H-mode power threshold** data over a range of toroidal field and density values have been obtained in the present (1994) JET experimental campaign, with the ion *grad B* drift (IGBD) directed both towards (positive) and away (negative) from the target plates. An earlier, partial analysis of these data [11] revealed a weak positive dependence of the threshold on plasma current, X-point position and distance of the limiter from the last closed flux surface. A more recent analysis has shown that with both positive and negative IGBD the power threshold P_{th} scales linearly with the toroidal magnetic field B_t, although it seems to be slightly higher than that of the older data. A very recent experiment, carefully prepared to verify the dependence of P_{th} with the plasma density and carried out with positive IGBD in the line average density range $2.5 < n_e\,(10^{19}\,m^{-3}) < 4$, has also shown that P_{th} decreases when n_e is lowered (fig. 3). Further dedicated experiments are planned to verify the scaling of P_{th} with n_e at higher densities

and to investigate whether there is a minimum threshold power at lower density below which P_{th} might start to increase for decreasing n_e [12].

Dependence of the threshold on $n_e B_t$ for discharges in the present campaign carried out ***with positive IGBD***, NBI heating and carbon-fibre-composite (CFC) target plates is very close to that found in the previous JET campaign (1991-92) with IGBD of the same sign (on pulses mainly performed with the same heating and another type of CFC plates) and to the scaling proposed by the H-mode Database Working Group [13].***With negative IGBD*** the observed thresholds are twice as high for all the 1994 discharges (all run with counter-injection NBI) and the NBI heated ones of 1991-92 (co-injection). It should be noted, however, that significantly lower thresholds were found in the former campaign with ICRF heating and beryllium dump plates [11].

3. L-MODE AND OHMIC CONFINEMENT

The time scale over which modifications occur across the plasma column at the time of the L-H transition [14], is interpreted as the evidence that non local mechanisms are inherent in the L-mode transport processes. The time evolution of the electron temperature T_e, for example, indicates an almost immediate reduction of the thermal conductivity, following the drop in the D_α signals, over a wide radial domain in the outer layers of the discharge. The affected region only excludes a central core about the magnetic axis, where no appreciable change in the behaviour of T_e is detected. The speed of propagation, from the separatrix inward, of the temperature modulation is seen to be 160 m/s or larger. A similar speed of propagation is also deduced for the drop in the **density fluctuation** level at the plasma edge as **measured by** O-mode **reflectometry**. Recent analysis of data obtained with this technique has shown that a strong reduction in fluctuation power (by up to a factor of 20 in a frequency range extending up to 100 KHz) occurs in a 15 to 25 cm thick radial region next to the separatrix. The sharpest drop in the fluctuation corresponds to the region of the profile where the density gradient is highest.

For the pulses analysed so far, the inner edge of the radial interval where the thermal conductivity drops coincides approximately with the radial position where $q = 1$. The same approximate coincidence is often observed [15], in L-mode or ohmic regime, for inner edge of the region of **high diffusivity for trace impurities** in experiments performed using the laser-ablation injection technique. The analysis of these experiments has now been extended to a wider set of discharges nearly exploring the whole practical ranges of plasma current, magnetic field, density and additional power and including a few cases with evolving current profiles [16]. It appears that a central region of slow transport is always present, even when there is no $q = 1$ resonance in the discharge. Its size, however, is highly variable depending on the shape of the current profile.

The boundary between the slow and fast impurity transport regions is experimentally identified by analysing the radial profiles of the perturbation to the soft X-ray emissivity induced by the injected impurities (fig. 4). After an initial phase of fast propagation in the outer region of the plasma, the inward progression of the maxima in those profiles is strongly slowed down as they reach an intermediate radial position that varies for pulses with different q profiles. Such a position appears to be regularly in very close proximity with the flux surface where the magnetic shear ($s \equiv \rho/q \cdot dq/d\rho$) is equal to 0.5. Within that surface the diffusion of impurities is always moderate, even when the electron temperature gradient is high. The observed shapes and variation trend of the profiles of D_{imp}, the impurity diffusion coefficient, suggest a strong dependence, at intermediate radii, of transport on s and possibly the existence of a threshold condition on that parameter that governs the transition from low to high anomalous transport across the plasma column. These findings appear not inconsistent with theoretical predictions based on the analysis of toroidal

coupling of adjacent resonant modes [17] or on the radial distribution of those modes in the discharge [18].

The local values of the D_{imp} in the core region and up to radial positions of about $\rho = 0.6$ is now measured using a recently developed iterative technique [19]. It shows that at the different radial positions the local transport is dominated by diffusion and that the local transport parameters remain the same during several successive quiescent phases between sawtooth crashes, until the injected impurities are lost from the discharge. The measured values of D_{imp} in the plasma core (always between 0.1 m^2/s and 0.3 m^2/s) are generally higher, by a factor of 2 to 10, than the neoclassical predictions. They also do not appear to undergo the strong variation with the magnetic field predicted by the neoclassical theories. In the outer fast-transport region, the effective average level of the impurity diffusion coefficient D_{imp} is seen to increase linearly with ∇T_e (or with T_e), but no appreciable dependence on the plasma density is found when the electron temperature profile is kept constant.

The radiation produced by the injected impurities induces a **cold pulse,** propagating from the plasma periphery inwards, which can be used to analyse the electron energy transport. A prompt change of the T_e time derivative $\dot{T}_e$ is observed over a very wide radial range (fig. 5). This is consistent with the hypothesis that a sudden modification of the electron thermal diffusivity χ_e is occurring practically at once over that radial interval. While at intermediate minor radii ($\rho \approx 0.6$ to $\rho \approx 0.8$) the rapidity of the response to the edge perturbation is seen to decrease moving inwards, further in ($\rho < 0.6$) $\dot{T}_e$ does not vary appreciably with radius. This is also in agreement with the above hypothesis because the rapidity of the perturbation $\tilde{T}_e$ due to diffusive propagation is expected to decrease moving away from the source of the perturbation [20] as observed in the first region; further away and below a certain level the cold wave is mainly consisting of the transient response to the sudden modification of χ_e and its radial variation is much smaller. This is also seen in the radial plots of the Fourier amplitude $A(\omega,\rho)$ and phase $\phi(\omega,\rho)$ of the Fourier transformed temperature perturbation $\tilde{T}_e(\omega,\rho)$ (fig. 6). In the inner region $A(\omega,\rho)$ and $\phi(\omega,\rho)$ do not vary appreciably with the radius while in the intermediate one the normal diffusive behaviour is observed.

ACKNOWLEDGEMENTS

Grateful Acknowledgment is due to B. Balet, D. Campbell, C.D. Challis, A. Cherubini, J.G. Cordey, R. De Angelis, M. Erba, G. Gorini, C. Gormezano, L. Lauro-Taroni, P. Lomas, G. Magyar, P. Mantica, M. Mattioli, D.G. Muir, J. O' Rourke, V. Parail, L. Porte, E. Righi, A. Rookes, D. Start, P.M. Stubberfield, A. Taroni, K. Thomsen, G. Vayakis for the preparation and analysis of data presented here.

REFERENCES

[1] STORK, D., et al., Plasma Phys. Control. Fus.**36** (1994) A23.
[2] DELIYANAKIS, N., et al. Plasma Phys. Control. Fus. **36** (1994) 1159.
[3] BALET, B., et al. Nucl Fus. **33** (1993) 1345.
[4] CHALLIS, C.D., et al. Nucl. Fus. **33** (1993) 1097.
[5] The JET Team (presented by C. Gormezano) paper A-5-I-3 this Conference.
[6] ERBA, M. et al. to be published by Plasma Phys and Contr. Fus. (1994).
[7] PARAIL, V.V., et al. paper A-2-II-3 this Conference.
[8] SMEULDERS, P., et al. to be published by Nucl. Fus. 1994.
[9] BALET, B., et al. in "Local Transport Studies in Fusion Plasmas" edited by Proc. of Worksh. at Varenna Callen, J.D., Gorini, G., Sindoni, E. Eds. SIF, Bologna 1993 p. 81.
[10] LAURO-TARONI, L., et al. to be published in Controlled Fusion and Plasma Physics (Proc. Conf. Montpellier, 1994) European Physical Society.

[11] START, D.F.H., et al. to be published in Controlled Fusion and Plasma Physics (Proc. Conf. Montpellier, 1994) European Physical Society.
[12] The ASDEX Team, Nucl. Fus. **29** (1989) 1959.
[13] RYTER, F., and the H-mode Database Working Group, Proc. 19th EPS Conference on Controlled Fusion and Plasma Physics, Lisbon (1992), Vol. 17c, part 1, p.15.
[14] CORDEY, J.G., et al. submitted to Nucl. Fus. 1994.
[15] PASINI, D., et al. Nucl. Fus. **30** (1990) 2049.
[16] GIANNELLA, R., et al. to be published by Nucl. Fus. 1994.
[17] ROMANELLI, F., ZONCA, F., Phys. Fluids B **5** (1993) 4081.
[18] BEKLEMISHEV, A.D., HORTON, W., Phys. Fluids B **4** (1992) 200.
[19] GIANNELLA, R., LAURO-TARONI, L. to be published in Controlled Fusion and Plasma Physics (Proc. Conf. Montpellier, 1994) European Physical Society.
[20] MANTICA, P., et al. Nucl. Fus. **32** (1992) 2203.

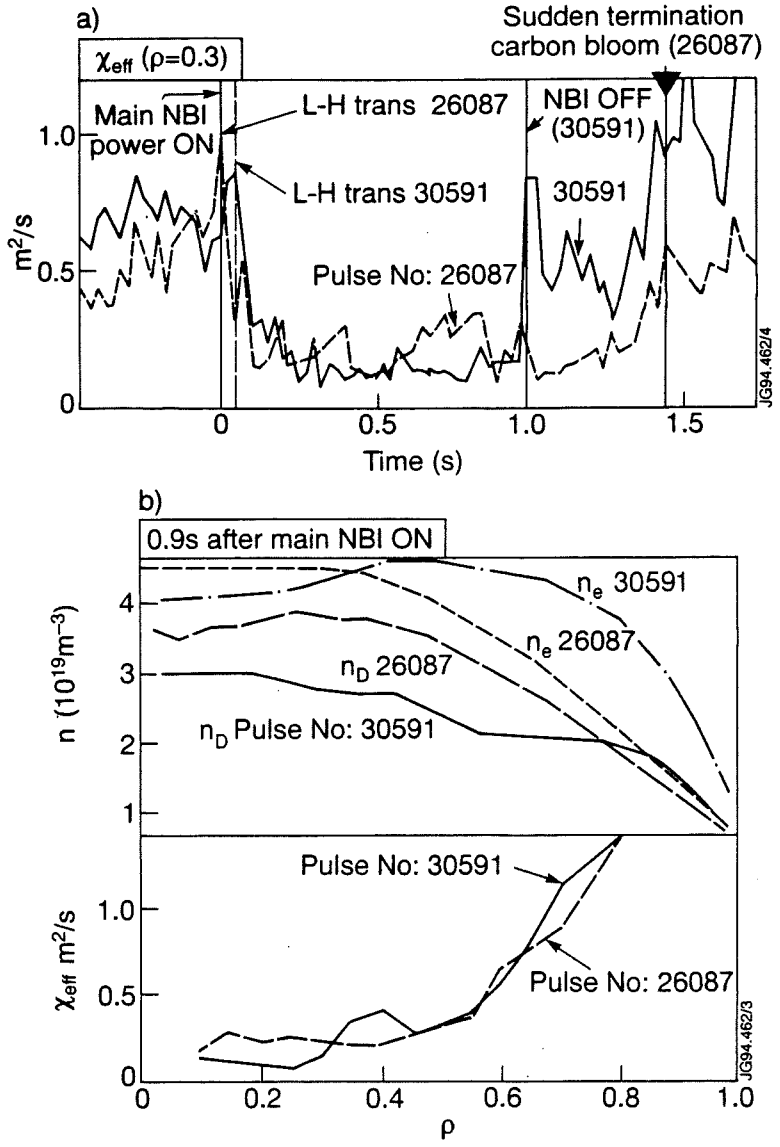

Fig.1 *Time evolution of $\chi_{eff}(\rho = 0.3)$ for two hot-ion JET discharges. Time is measured starting from the application of the main neutral beam power (a). Electron and deuteron density profiles during the ELM-free phases for for the above discharges; also shown are the profiles of χ_{eff} during the ELM-free phase (b).*

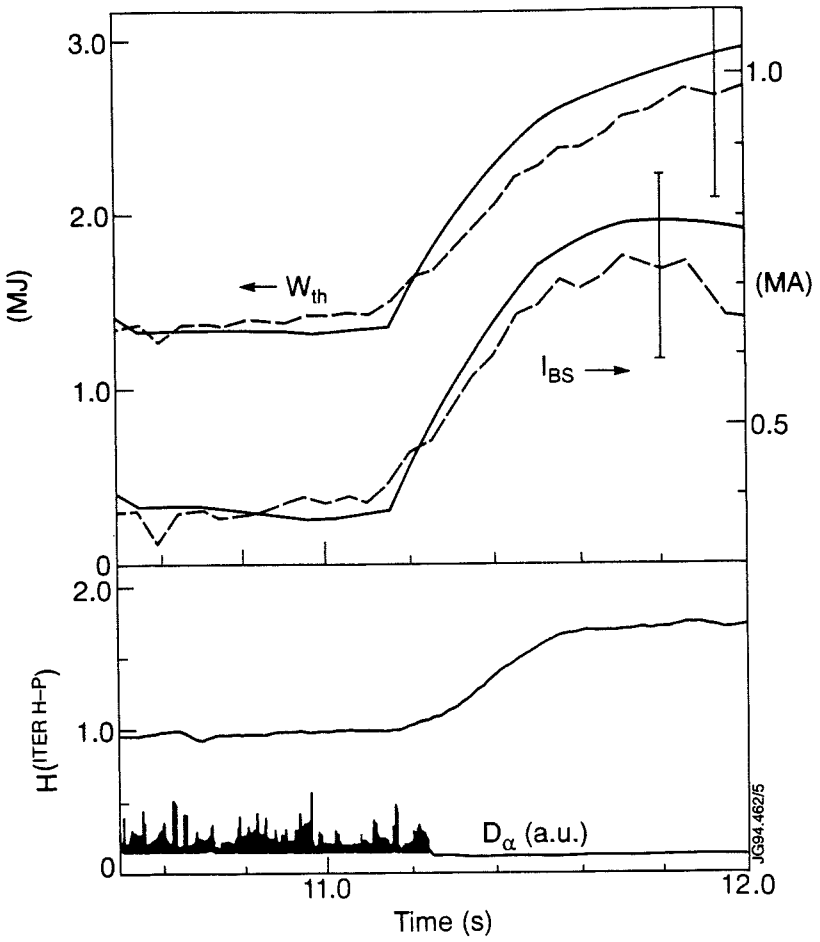

Fig.2 *Time evolution of thermal energy W_{th}, and bootstrap current I_{BS}, in a high β_p discharge (JET pulse 25264) as deduced from the experimental data (dashed lines) and from the simulation performed using the transport model proposed by Taroni, Erba and Parail (see paper A-2-II-3, this Conference). Also shown are the enhancement H(ITERH-P) of the energy confinement time over the ITER93H-P scaling and the D_α signal.*

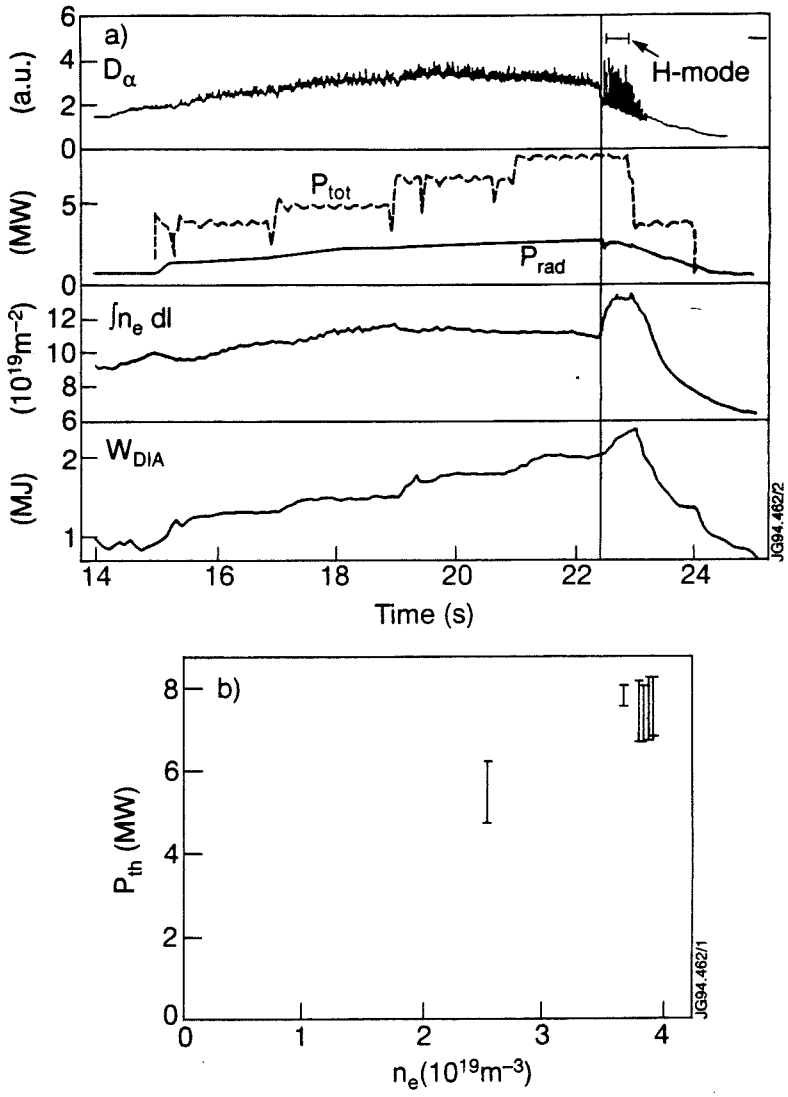

Fig.3 *Time evolution of D_α light, total heating power, total radiated power, line integrated electron density and stored energy from the diamagnetic loop for JET pulse 31596 (B_T = 2.4 T, I_p = 2 MA). In the last phase of the discharge, at t ~ 22.4 s, the transition to H-mode occurs when the line average electron density, that was slowly decreasing, reaches the value of $3.65x10^{19}m^{-3}$ (a). Power threshold versus line average electron density in a set of discharges run at B_T = 2.4 T, I_p = 2 MA with ion B drift directed towards from the target plates (b).*

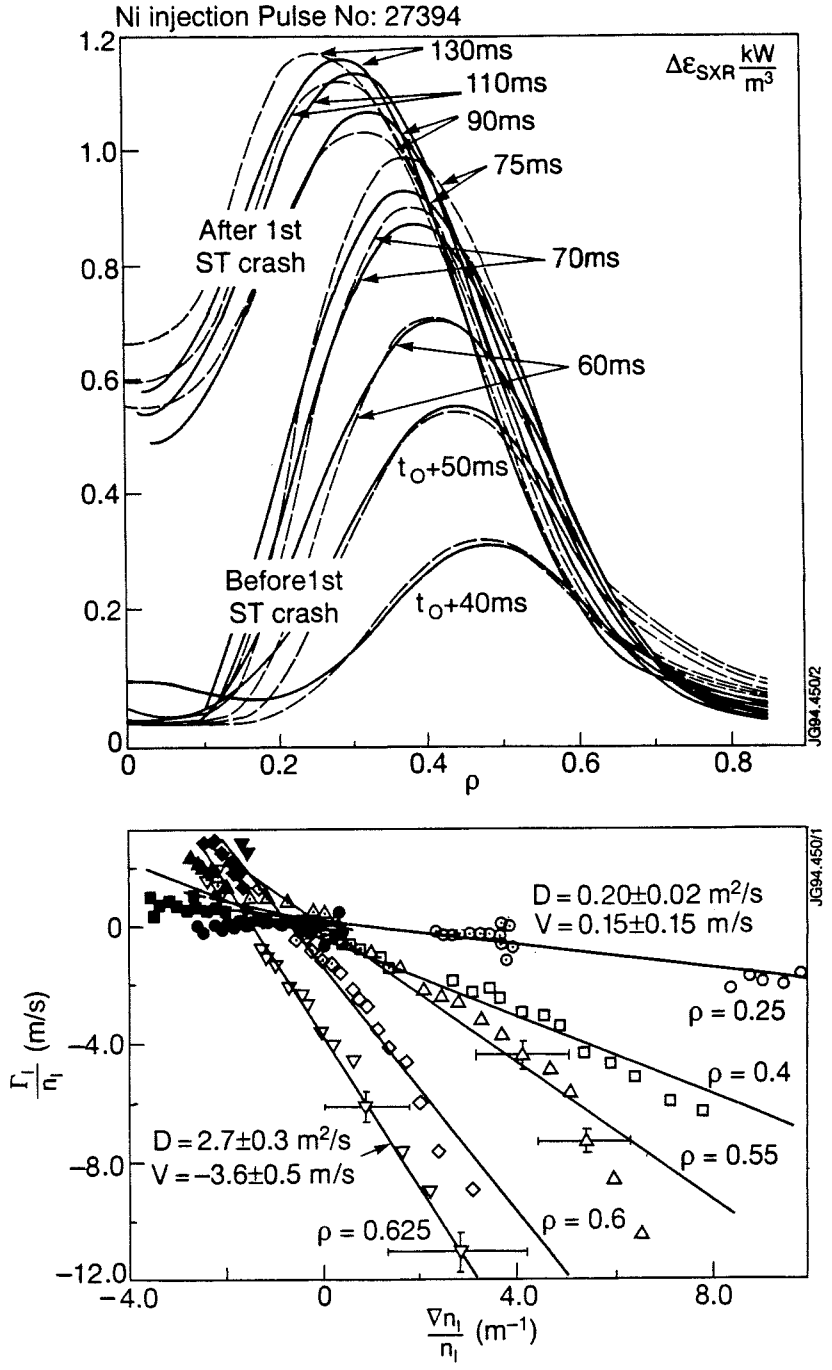

Fig.4 *Measured (solid lines) and simulated (dashed lines) radial profiles of the perturbation to the soft X-ray emissivity $\Delta\varepsilon_{SXR}$ induced by the injection of Ni. Data refer to consecutive quiescent phases between sawtooth crashes (a). Local measurements of the transport parameters are obtained from linear regressions of the normalized Ni fluxes Γ_I/n_I versus the normalized Ni density gradients $\nabla n_I/n_I$. The data points are from the first three quiescent phases between sawtooth crashes (respectively empty, dotted and filled shapes); the different shapes refer to different radial posistions. The Ni density profiles $n_I(\rho,t)$ are deduced from $\Delta\varepsilon_{SXR}(\rho,t)$ using the iterative technique illustrated in ref. [19] (b).*

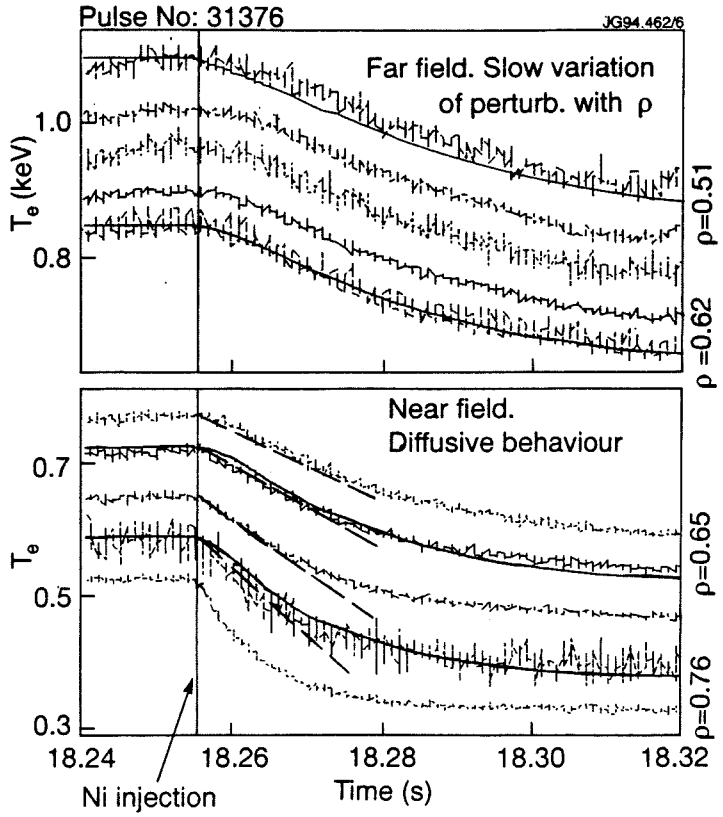

Fig.5 *Time evolution of the electron temperature at different radii following injection of Ni in one ohmic discharge. The solid lines are from the simulation of the phenomenon using the transport model of ref. 7 and a perturbation of the electron thermal diffusivity* $\Delta\chi_e(\rho,t) = \chi_e(\rho,t_0)\xi H(t-t_0)\xi exp(-t/0.15\,s)$.

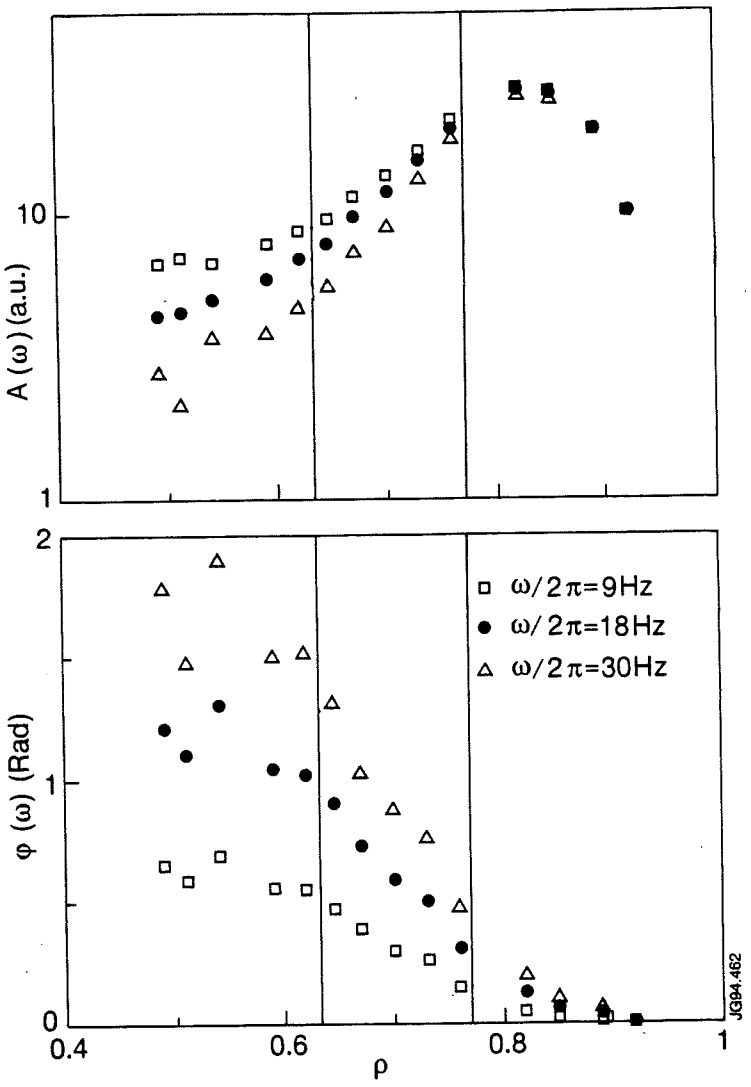

Fig.6 *Amplitude A(ω) and phase φ(ω) of the Fourier transformed temperature perturbation induced by laser blow-off injection of Ni in the discharge illustrated in fig. 5. At values of the normalised minor radius above ρ = 0.77 the propagation is affected by the modulation of the radiated power induced by the injected impurity; within that radius, the influence of the radiated power on the radial profiles of A and φ is negligible. For 0.63 < ρ < 0.77 those profiles are consistent with a diffusive propagation characterized by a value of the incremental electron thermal diffusivity χ_e^{inc} 2.5 m^2/s For ρ < 0.63 the propagation is much faster and consistent with the expected transient response of the plasma to a sudden modification of χ_e.*

Development of Advanced Tokamak Scenarios based on High Bootstrap Currents in JET

The JET Team
(presented by C Gormezano)

JET Joint Undertaking, Abingdon, Oxfordshire, OX14 3EA, UK.

DEVELOPMENT OF ADVANCED TOKAMAK SCENARIOS BASED ON HIGH BOOTSTRAP CURRENTS IN JET.

The JET Team
(presented by C Gormezano)

JET Joint Undertaking,
Abingdon, Oxon, OX14 3EA, U.K.

ABSTRACT

High bootstrap current experiments with the bootstrap fraction ($I_{bootstrap}/I_{plasma}$) up to 0.7 at 1 MA and 0.5 at 1.5 MA were previously achieved in JET in plasmas with high q(a), high triangularity and high confinement (H≥3). During initial operation with the new JET pumped divertor, the domain of parameters has been extended to cover reactor relevant domains such as low q(a) and high β_n; up to β_n =3. High beta poloidal plasmas (necessary for the achievement of high bootstrap fractions) with β_p up to 1 for 2MA plasmas and with β_p up to 2 for 1MA plasmas have been achieved. β_p = 1.5 and β_n = 3 have been obtained simultaneously over several seconds at q_{95} = 4.5. The confinement of these plasmas is lower than in the previous campaign but these discharges display "quasi steady state" characteristics. In order to improve the confinement of these discharges, several parameters have been varied such as plasma volume, triangularity and β_p itself showing no significant benefit. Configurations using non-inductive current drive to produce stable, higher confinement plasmas are being developed. A "deep" shear reversal configuration has been established and initial data are presented.

1. INTRODUCTION

A large proportion of the plasma current in a steady state reactor [1] will probably have to be provided by the neoclassical bootstrap effect. This "advanced tokamak" scenario results in challenging requirements for both plasma confinement and stability. In previous JET experiments [2] a bootstrap fraction of 0.7 has been obtained in plasmas with high confinement compared to the usual L-mode and H-mode scalings. However, these discharges, although sustained for ≈2 seconds, were not stable and collapsed with a large ELM. The cause of the collapse has not yet been unambiguously identified. Theory predicts that high bootstrap fraction discharges will tend to be prone to a large number of MHD instabilities on the current diffusion time scale, the more dangerous being the infernal modes due to the hollow current profile and the external kink modes due to the large current density in the plasma periphery. It is also predicted that several of these instabilities can be avoided if the current profile and/or pressure profiles are optimised. JET is developing "advanced tokamak" scenarios aiming at achieving high β_p plasmas in reactor relevant conditions in quasi steady state conditions using JET high power heating systems and using current profile control techniques to produce MHD stable configurations and possibly to improve confinement.

2. HIGH BETA EXPERIMENTS

The new JET pumped divertor configuration has several features which are noticeably different from the old JET configuration as discussed in [3]. For instance, the plasma volume and q(a) are lower for similar plasma current and magnetic field. During initial JET experiments in the new configuration, the recycling appears to be high and long ELM free periods with high confinement (VH-mode) have not yet been achieved, but the power handling capability of the divertor tiles is higher.

2.1 Beta poloidal values

The performance of the new JET configuration has some consequences on the magnitude of the current bootstrap which depends directly upon the confinement for a given power. Higher power is necessary to obtain a similar β_p as achieved previously, 26MW to achieve $\beta_p = 2.1$ at 1MA and 23MW for $\beta_p = 1.45$ at 1.5MA instead of the previously required 10MW in ELM-free condition. In the new configuration, the high β_p discharges are no longer transient and reach "quasi steady state" conditions as shown in fig.1: with a combined power of 20MW (ICRH plus NBI) for several seconds, β_p stays at a value of 0.8 at $I_p = 2$MA while the confinement time is 0.9 times the JET-DIIID H-mode scaling.

2.2 Confinement

Some ELM free discharges lasting more than one second have been achieved in double null configuration as shown in fig.2. These discharges have a higher β_p than single null discharges, but the ELM-free period is much reduced when power exceeds 15MW and the benefit of this type of configuration seems to be eroded by the re-occurrence of ELMs. It is also to be noted in fig.2 that the lower confinement normally observed in reversed ∇B configuration for counter NBI injection is partially restored when combined ICRH NBI heating is used in this configuration.

Other attempts to try to increase the confinement of these high β_p discharges have been made. For instance, the volume and the aspect ratio of the plasma have been varied respectively from $80m^3$ to $55m^3$ and from 3.7 to 3.1. The ELM free phase disappears with small volume plasmas, but during the ELMy phase, the confinement is observed to be similar, with H factor between 1.8 and 2, for both configurations as shown in fig.3. This is quite remarkable given the large change in the plasma configuration.

It should also be noted, as shown in fig.4, that the confinement does not increase with β_p for ELMy plasmas although some parameters such as ℓ_i, T_e, collisionality, etc. were also changed.

2.3 Beta normalised values

β_n values of 3 have been obtained together with β_p values of 1.5 and H = 2 (see note*) for $I_p = 1$MA B_T - 1.4T plasmas as shown in fig.5. For discharges with $I_p = 1.5$MA and $B_T = 1$T, high β_n values are also achieved but a degradation is observed at high power compared to plasmas at 1.4T. A stability analysis has shown that at 1.4T the plasma is completely stable to ballooning modes. If the same pressure profiles were achieved at 1T, the plasma would then have become unstable. In practice the pressure gradients are reduced in the 1T plasma so that the analysis again indicates stability against ballooning modes. It is therefore possible that the lower achieved β_n at high power is linked to the effect of ballooning modes on the pressure profile.

3. SHEAR REVERSAL EXPERIMENTS

It is probable that very high bootstrap experiments need some form of plasma profile control to remain mhd stable. Extrapolation of previous high bootstrap current plasmas in JET to steady state using the TRANSP code has shown that steady state would be reached in 20 to 30sec. but that the resulting current profile would be unstable to ballooning modes. Other analyses [4] have shown that "deep" shear reversal with high central q values and q minimum above 2.5 have

to be achieved to prevent instabilities due to infernal modes. Simulations [5] have shown the possibility of producing such configurations at JET.

In JET, an attempt has been made to obtain such a "deep" shear reversal configuration by injecting LHCD and ICRF early in the discharge to "freeze" the current profile at the required shape. An X-point plasma is produced and ICRH and LHCD are used together during the ramp-up phase to maintain the broad profiles with the high q(o) which normally occur during this phase. The time history of such a plasma is shown in fig.6. The ramp up rate of the current is 0.75MA/sec. LHCD and ICRF are injected less than 1 second after the breakdown when the plasma current is only 300 kA The temperature goes up to 6 keV during this phase. In the absence of specific diagnostics, the q profiles are deduced from magnetic reconstruction. Analysis has shown that shear reversal is produced at 42s and persists in the current flat top with q(o) values from 4 and 5 and minimum q values of about 3. ℓ_i remains very low, at about 0.5, and confinement time is about 0.8 times the JET-DIIID H-mode scaling. But the stored energy is larger than the stored energy observed in discharges with similar power and current and ℓ_i in the range 0.7-0.8. Further experiments are required to assess the benefit of these profiles.

4. CONCLUSIONS

The previous JET high bootstrap current experiments were performed within a limited parameter range: medium power (10 MW of ICRF), relatively low β_n values (1.5), high q(a) (~10) and high triangularity. The new JET configuration allows a significant enlargement of the parameter domain: variation of q(a), and triangularity, combined ICRF and Neutral Beam Heating. This is shown in fig. 7 where β_p is plotted versus q_{95}. The achieved parameters are now much closer to the advanced scenario domain. For instance, β_p of 1.5 together with $\beta_n = 3$ and H = 2 have been achieved in quasi steady state. High β_p plasmas obtained during the initial operation in the JET pumped divertor configuration have a lower confinement than during the previous campaign when only transient conditions were achieved. Confinement does not increase with β_p in ELMy plasmas. Deep shear reversal configurations have been established. Further experiments are required to assess the benefit of these configurations and to exploit the JET non inductive current drive capabilities. With the heating systems installed on JET, a target domain with $\beta_p \geq 2$, $\beta_n \sim 3$ and $H \geq 2$ appears to be achievable at 1MA. The confinement has to be slightly improved to enter this domain at $I_p = 1.5$MA, and significantly improved for larger plasma currents. Current profile control will mainly be used to improve the confinement.

* H factor refers to ITER 89-P L-mode scaling law.

REFERENCES

[1] P-H Rebut , D Boucher, C Gormezano, B E Keen, M L Watkins, Plasma Phys. & Cont. Fusion, 35 (1993) A1.

[2] C D Challis et al., Nuclear Fusion 33, 8 (1993), 1097.

[3] The JET Team presented by D Stork, this conference.

[4] G T A Huysmans, H De Blank, W O Kerner, J P Goedbloed, M F F Nave, Proc. of the Conf. on Plasma Physics, Innsbruck (1992) 72.

[5] F X Söldner, to be presented at 21st Europ. Conf. on Controlled Fusion & Plasma Physics, Montpellier, (1994)

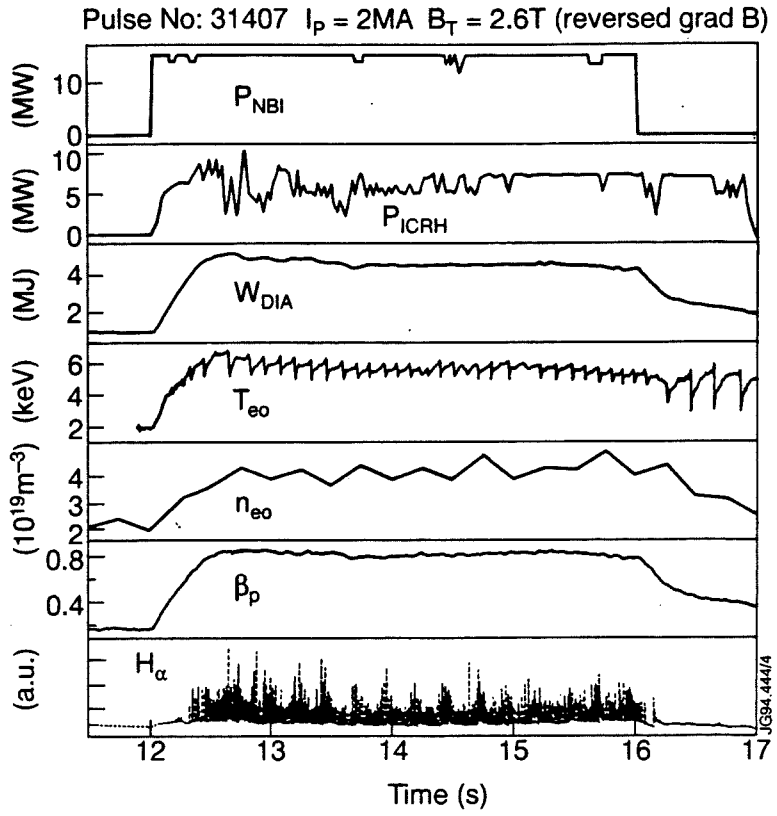

Fig.1 *Time history of a "quasi" steady state discharge*

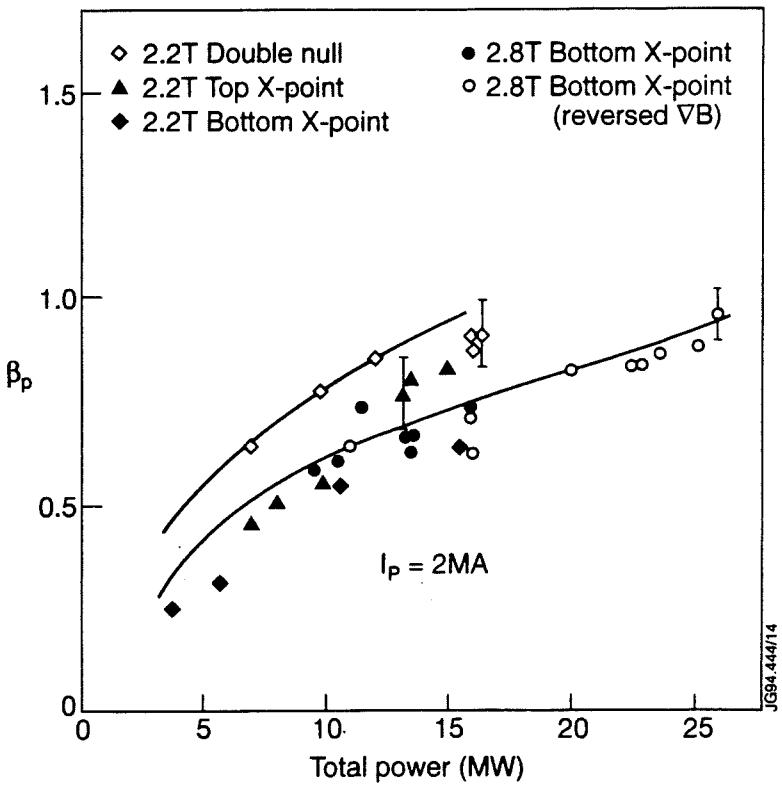

Fig.2 *Beta poloidal dependence with power at I_p = 2MA*

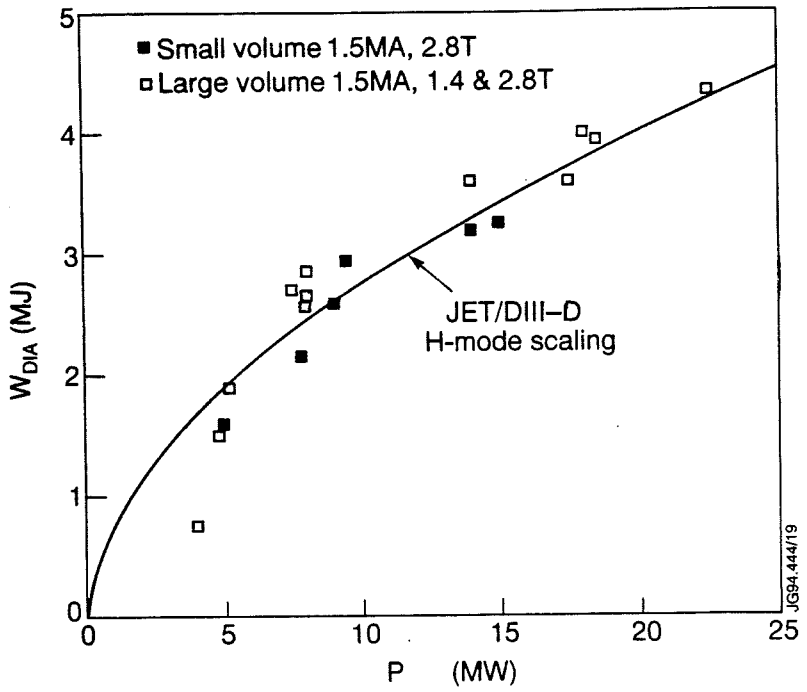

Fig.3 *Stored energy (diamagnetic loop) versus total power for small ($55m^3$) and large volume ($80m^3$) plasmas*

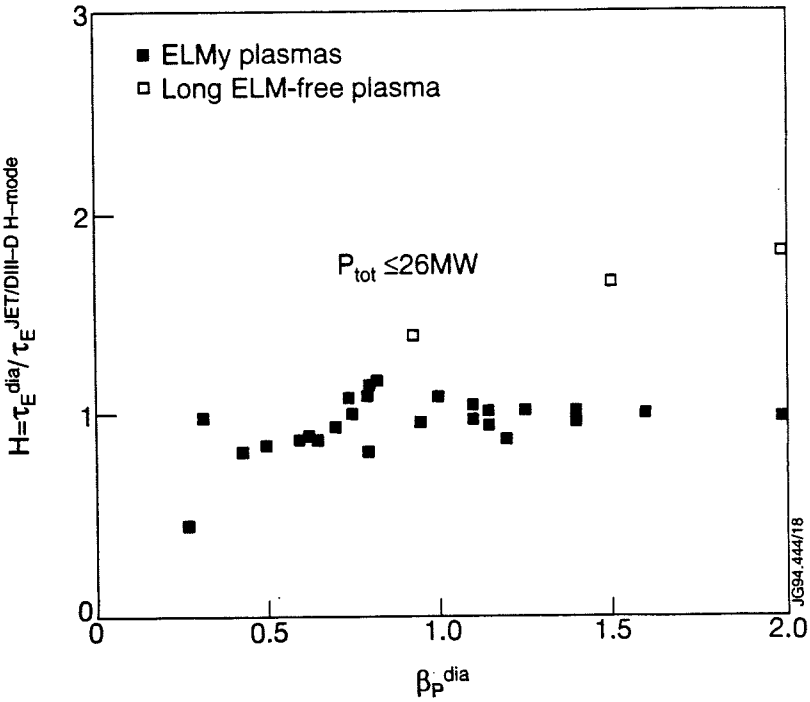

Fig.4 *Confinement time versus β_p. Both data are from diamagnetic loop.*

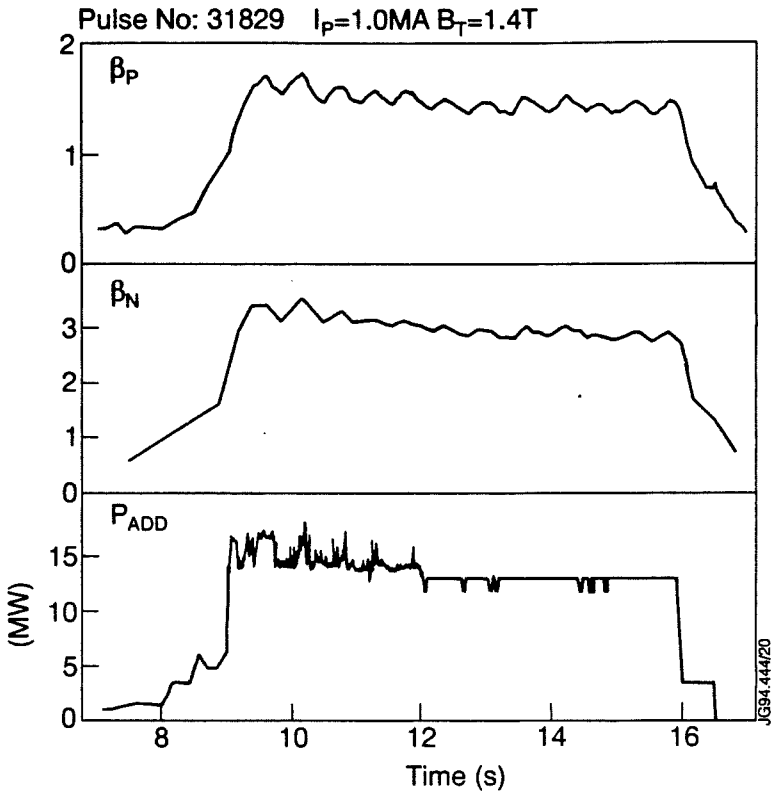

Fig.5 *Time history of a high β_n pulse. Energy confinement time corresponds to JET-DIIID H-mode scaling.*

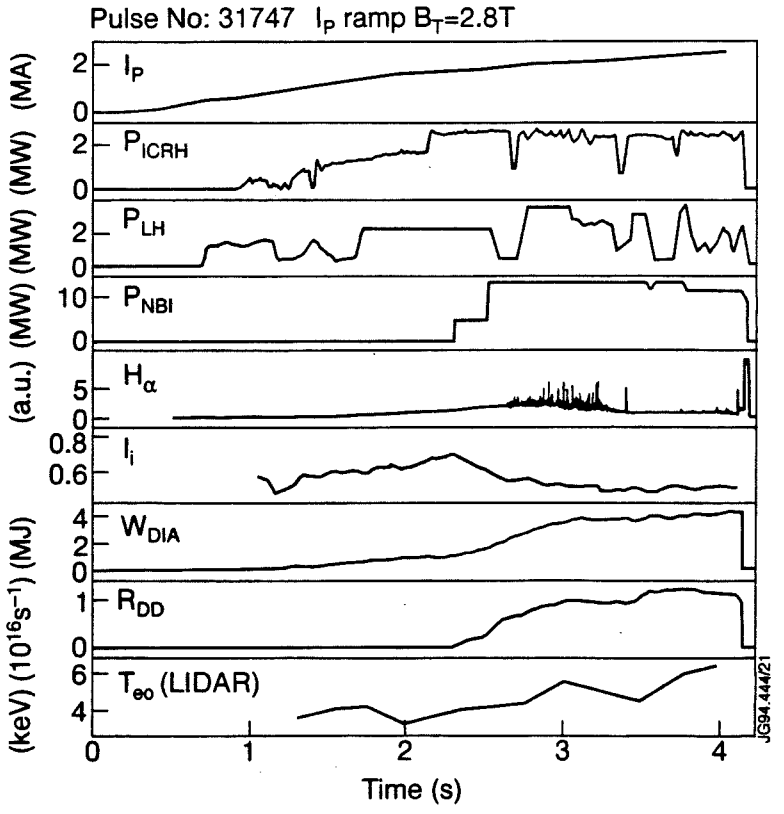

Fig.6 *Time history of a shear reversal configuration plasma discharge.*

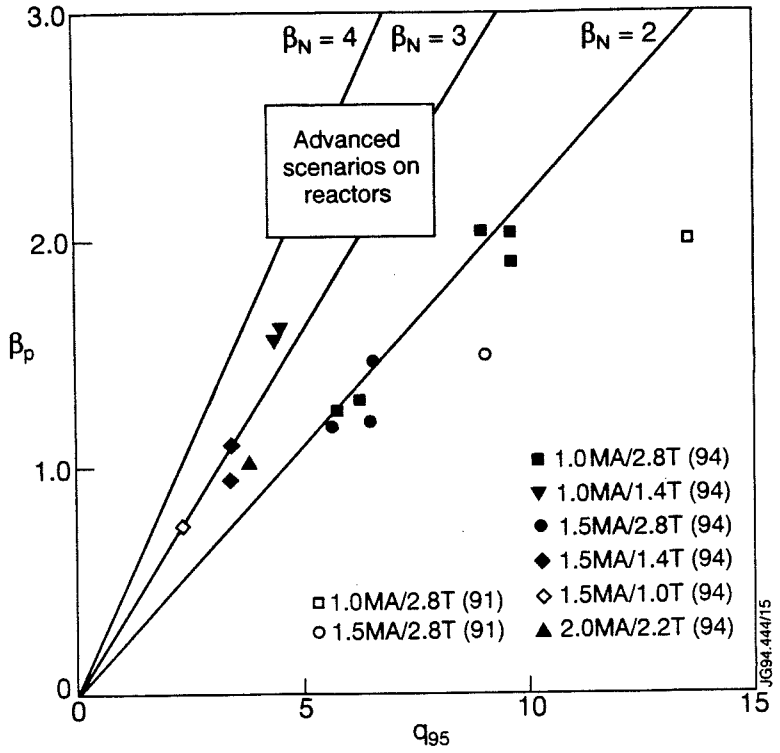

Fig.7 Beta poloidal versus q_{95}.

Modelling and Measurements of JET Divertor Plasmas

The JET Team
(presented by L D Horton)

JET Joint Undertaking, Abingdon, Oxfordshire, OX14 3EA, UK.

MODELLING AND MEASUREMENTS OF JET DIVERTOR PLASMAS

The JET Team
(Presented by L.D. Horton)

JET Joint Undertaking
Abingdon, Oxon, OX14 3EA, U.K.

ABSTRACT

The new JET Mark I divertor operates at higher densities and lower temperatures for a given upstream SOL density than the previous divertor geometry. At these high divertor densities the ion saturation current to the divertor target plates is seen to decrease with increasing core plasma density, thus providing an operational definition of a detached plasma as well as a convenient control input for stable operation in the detached state. The global parameters of these high density discharges have been successfully modelled with the JET edge transport codes. In order to reproduce the experimentally observed SOL profiles, it is necessary to add an inward pinch to the model. Detailed profile measurements of the divertor radiation show an area of high density and radiation in the core plasma just above the X point which is not reproduced in the model. H-mode confinement degrades at high densities until a transition back to the L-mode occurs. The highest density H-modes have low ion saturation current between ELMs, but the peak particle and power loss to the target plates become dominated by the ELMs and increase as the density increases.

1. INTRODUCTION

The new JET Mark I divertor operates successfully in a wide range of geometries and plasma parameters [1]. In particular, it has been possible to achieve high density divertor discharges which have very low particle, momentum, and energy flows to the divertor target plates. These plasmas have been achieved in both steady state and density ramp experiments. When the core plasma density is ramped towards the density limit, the ion saturation current flowing to Langmuir probes in the divertor target tiles is seen to first increase and then decrease. This drop in current has become our operational definition of a detached plasma.

In Ohmic and L-mode plasmas there is a clear sequence of events as the density in the plasma core is increased. An example of the time history of an Ohmic density ramp pulse is shown in Fig. 1. At a certain core density the ion saturation current to the target peaks (~3×10^{19} m^{-3} for Ohmic plasmas) and then begins to fall gradually. At 5×10^{19} m^{-3} there is sudden drop in current to the inner divertor plate, and an increase in radiation from the X point region. The density limit is reached when a MARFE forms on the inner wall.

In H-mode plasmas the situation is complicated by ELMs. As the core density is increased the ELM frequency also increases. The ion saturation current to the target between ELMs is low and drops, at least on the inner target. The density limit in H-mode plasmas is set by the H-to-L transition, which is followed by a loss of density from the core. Because of the ELMs it is difficult to analyse the target probe data and the quality of detachment which can be achieved below this limit is still unclear.

The available operating space for detached divertor plasmas is shown in Fig. 2 as a function of input power and line-averaged plasma density. Using both preprogrammed gas fuelling and with a feedback system controling on an ion saturation current measurement, it has been possible to operate JET with stable, detached divertor plasmas very close to the density limit.

Significant progress has been made in modelling detached plasmas. It is now possible to reproduce qualitatively the features seen at the divertor target plates. For

the modelling presented here, the two dimensional fluid transport code EDGE2D [2] has been run with an analytic formula for the impurity radiation loss [3] and the impurity distribution then found by using the impurity Monte Carlo transport code DIVIMP [4] on the pure background plasma generated by EDGE2D. With the new set of diagnostics available on JET, it is now possible to better validate these models.

Examples in this paper will be solely for divertor plasmas on the lower, horizontal target plates. Interesting differences exist between such plasmas and those on the vertical plates [1]. These will be reported in detail in a later paper.

2. IMPURITY SOURCES IN HIGH DENSITY DISCHARGES

At high core density the plasma temperature in front of the divertor target plates becomes so low that there is essentially no source of carbon from physical sputtering. However, when physical sputtering is the only source of carbon in the model, the experimental values of carbon influx and radiated power are not reproduced [5]. A good example of this is provided by our modelling of a 2.8 T, 2 MA Ohmic plasma. The measured input power to the scrape-off layer (SOL) is 1.2 MW, with 0.6 MW of power radiated in the SOL and divertor, and 0.2 MW conducted and convected to the divertor target plates. When the code is run with physical sputtering alone, the total SOL plus divertor radiation is predicted to be 0.2 MW, essentially all from deuterium with <0.01 MW from carbon. Because the carbon influx is seen to decrease with the ion saturation current, a constant yield better matches experiment rather than a constant additional source of carbon. A yield of 0.2% is found to reproduce the measured influx and at the same time to match the total radiated power as measured by the bolometers. While this greatly exceeds the yield from physical sputtering it is also a factor of 10 or more less than what one would expect from chemical sputtering.

Significantly, bolometer measurements of detached plasmas show that the region of peak radiation is above the X point and in the core plasma. In Fig. 3 the lines-of-sight of a few of the in-vessel bolometers are overlaid on the magnetic geometry of the divertor region. The views which are marked in thick, solid lines increase as the divertor detaches, while those marked with dashed lines decrease. This region of high radiation corresponds to a region of very high density, considerably higher than the densities typically measured on the target plates in detached plasmas. The bremsstrahlung radiation seen by the infrared camera which views the divertor from the top of the machine is compared to results of the model in Fig. 4. The two peaks in the modelled emission result from two high density regions in the SOL on either side of the X point (Fig. 5). The experiment shows only one such region, located near the X point. This discrepancy may be due to the inconsistent treatment of impurities in these simulations or to limitations caused by the restricted region of the core plasma covered by the numerical grid.

3. TARGET PARAMETERS IN A DETACHED PLASMA

The pulse modelled here is a 2.8 T, 2 MA L-mode discharge on the horizontal target plates with 6 MW of input power. Throughout the pulse, the density was increased until the divertor plasma detached and, finally, the plasma disrupted. Profiles of electron density and temperature along the outer divertor target are plotted in Figs. 6 and 7 for two times during the discharge. At the first time, the divertor plasma has a high density (1.2×10^{20} m^{-3}) and is still attached to the target. By the second time the plasma is detached and the power to the target plates is 0.4 MW, down from 4 MW in the attached case.

Unlike the case of the Ohmic plasma described above, the model does not produce a detached plasma when the measured radiation loss from the SOL (~2 MW) is used to calculate the quantity of impurity radiation to apply with the analytic formula. Detached solutions can be found when 4 MW of impurity radiated power is used. The calculated target profiles are compared to experiment in Figs. 6 and 7. The

model can be seen to underpredict the temperature at the target and overpredict the measured density. This is typical for our simulations of detached plasmas, and is thought to be outside the (large) error bars of the experimental measurements. It is thought that this problem may be due to insufficiencies in the atomic and, especially, the molecular physics in the model. At present, elastic scattering of ions with molecules is not included as a momentum loss mechanism in the code.

4. SOL PROFILES IN HIGH DENSITY DISCHARGES

Experimentally, the width of the SOL is seen to increase as the core plasma density increases. The density fall-off lengths are compared in Fig. 8 for a medium density Ohmic plasma and, later in the same discharge, a detached divertor plasma. In high density discharges, the model overpredicts this observed broadening, even producing non-monotonic density profiles (Fig. 9). Profiles much better matched to experiment can be produced by adding a pinch term to the perpendicular transport. The second model profile in Fig. 9 was obtained with a pinch velocity of 6 m/s. This is similar to the size of the pinch used previously near the edge of the core plasma in impurity transport experiments [6].

5. COMPATIBILITY OF H-MODE CONFINEMENT WITH DETACHED DIVERTOR PLASMAS

With the divertor cryopump activated, it has been possible to produce long pulse, high quality H-mode plasmas whose duration are limited only by the available duration of high power heating [1]. The peak surface temperature of the divertor tiles comes quickly into equilibrium at a value lower than that found in lower power L-mode shots. This is due to the large spreading of power deposition by the ELMs, which can be seen on probes over the entire divertor. When the density of these discharges is increased the ELM frequency also increases and the core confinement decreases (Fig. 10). At a certain density ($\sim 9 \times 10^{19}$ m^{-3} at 9 MW), the discharge makes a transition back to L-mode. At the highest density compatible with H-mode operation, the ion saturation current to the target plates is low between the ELMs but remains at a high level during the ELMs. The peak temperature on the target plate increases with increasing density, probably due to reduced speading of the power load by the high frequency, grassy ELMs.

6. CONCLUSIONS

The JET Mark I divertor geometry has allowed access to higher density, lower temperature divertor plasmas for comparable core plasma densities. At the highest densities, stable operation with low particle flows to the divertor target plates is possible. The global features of these plasmas can be reproduced with the present model. Considerable progress has been made in modelling plasmas with large pressure and density drops along open field lines. The model requires a source of carbon in addition to the normal physical sputtering mechanism in order to match experiment. The details of the profiles of density and radiated power as predicted by the model are still not in agreement with experiment. Calculations using the full multi-species impurity equations and including a larger area of the core plasma are required. The comparison of predicted and measured density profiles in the SOL has led to the inclusion of a pinch term in the particle transport in the model. The situation with high density H-mode plasmas is less satisfactory. The core confinement is seen to decrease with increasing density leading eventually to a transition back to the L-mode. Peak power loading on the target plates in H-mode discharges is dominated by ELM behaviour and is seen to increase with increasing density, in contrast to L-mode detached plasmas.

REFERENCES

[1] THE JET TEAM, IAEA-CN-60/A-4-I-4, these proceedings.
[2] TARONI, A., *et al.*, Contrib. Plasma Phys. **32** (1992) 438.
[3] NEUHAUSER, J., SCHNEIDER, W., WUNDERLICH, R., Nucl. Fusion **26** (1986) 1679.
[4] STANGEBY, P.C., ELDER, J.D., J. Nucl. Mater. **196-198** (1992) 258.
[5] SIMONINI, R., *et al.*, to be published in the proceedings of the 21st EPS Conf. on Contr. Fusion and Plasma Phys.
[6] PASINI, D., *et al.*, Nucl. Fusion **30** (1990) 2049.

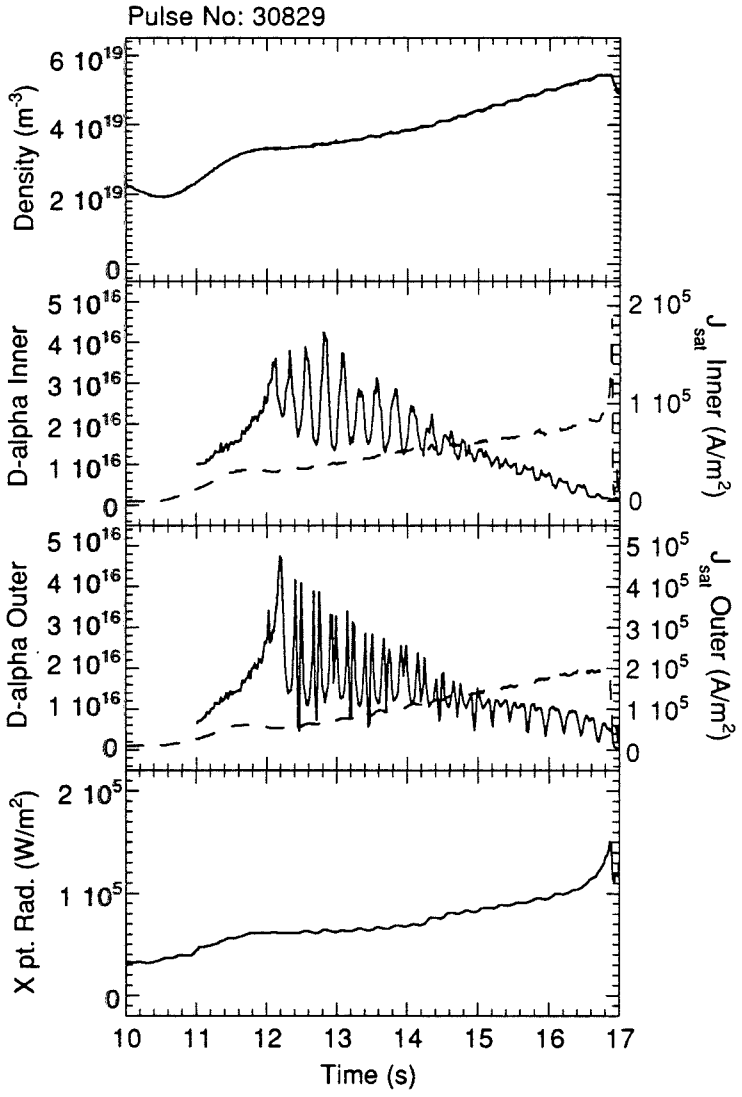

Fig.1 *Time traces of an Ohmic density ramp experiment: (a) the line-averaged plasma density, (b) D_α radiation from the inner divertor leg (dashed curve) and the ion saturation current flowing to a Langmuir probe in the inner divertor target plate (solid curve), (c) D_α radiation from the outer divertor leg (dashed curve) and the ion saturation current flowing to a Langmuir probe in the outer divertor target plate (solid curve), and (d) the radiated power integrated along a sight line which passes through the X point. The currents oscillate because the plasma is being swept across the target from 12 s to the end of the shot.*

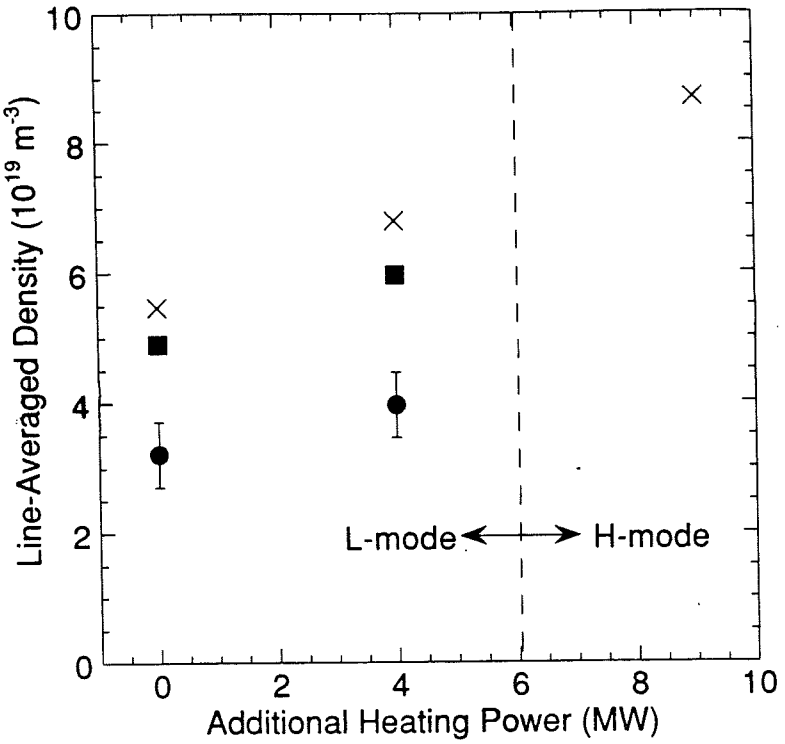

Fig. 2 *The operational space for high density plasmas in JET. The crosses are the density limit. In Ohmic and L-mode discharges this is the density at which a MARFE moves up the inner wall. In H-mode discharges the density limit is set by an H-to-L transition, which is followed by a reduction in the core density. The circles mark the density at which the ion saturation current to the divertor target plates peaks. The squares mark the density at which there is a sudden decrease in this current to the inner divertor.*

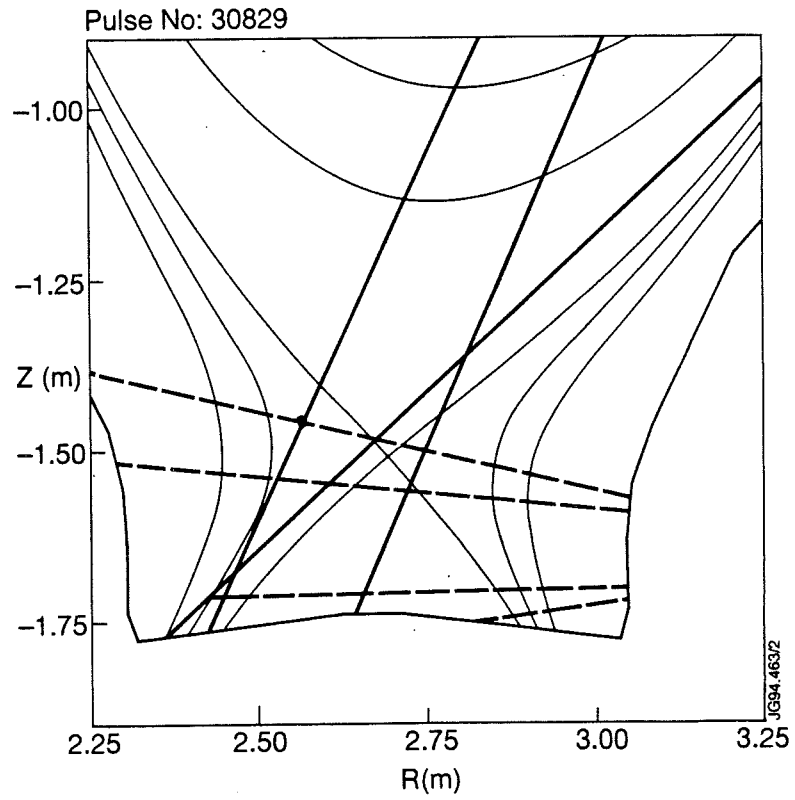

Fig.3 *Geometry of several bolometer views overlaid on the plasma geometry of JET pulse 30829. The views marked with a solid line increase as the divertor detaches while those marked with a dashed line decrease.*

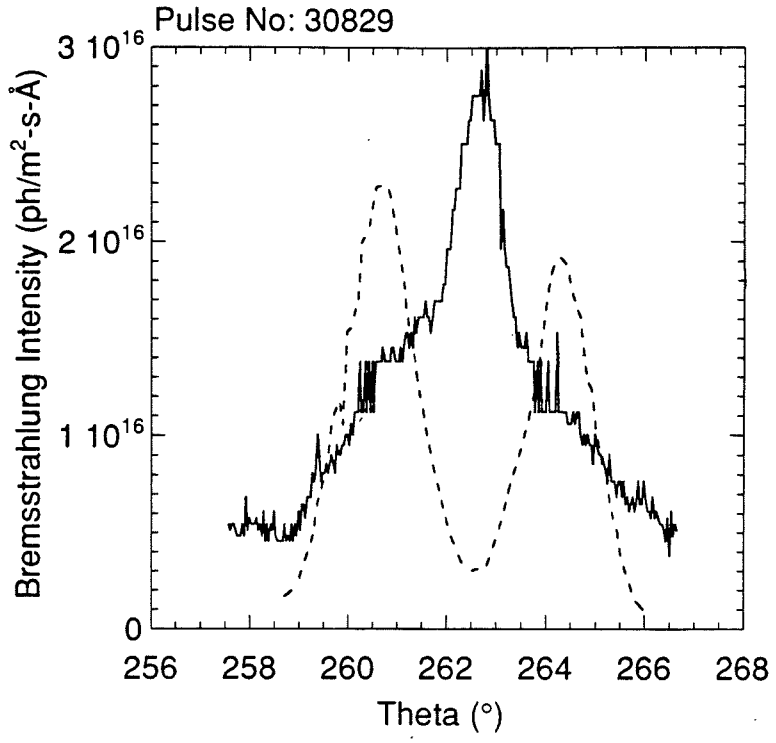

Fig.4 *The profile of bremsstrahlung radiation seen from the top of JET looking down at the divertor. The solid curve is the experimentally measured profile for an ohmic detached plasma and the dashed curve is the prediction of the fluid code.*

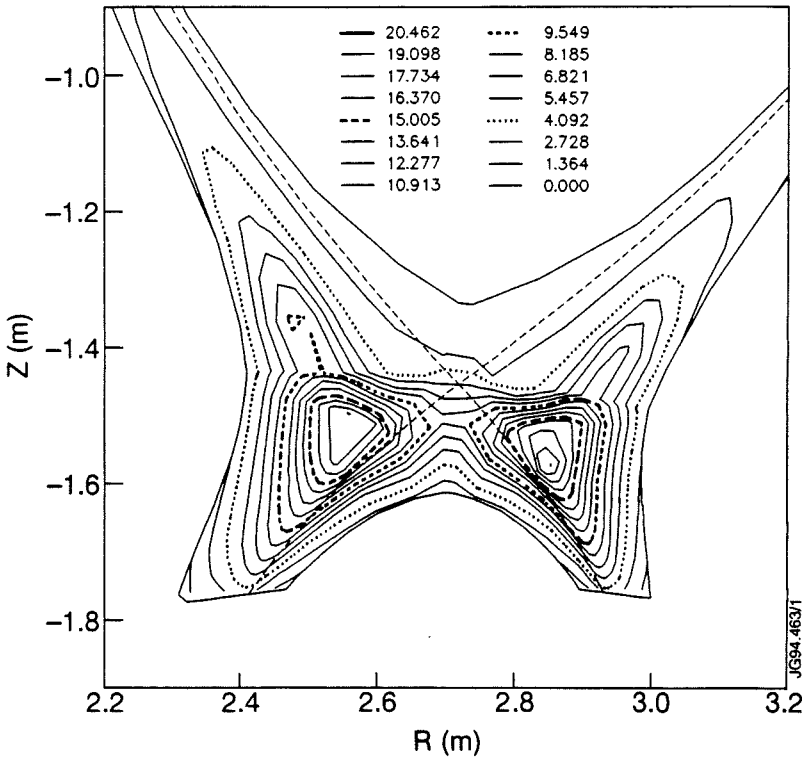

Fig.5 *Modelled contours of constant electron density from the same simulation as Fig. 4. The two peaks in the modelled bremsstrahlung emission can be seen to come from two areas of high density in the SOL on either side of the X point. The densities are in units of 10^{19} m^{-3}.*

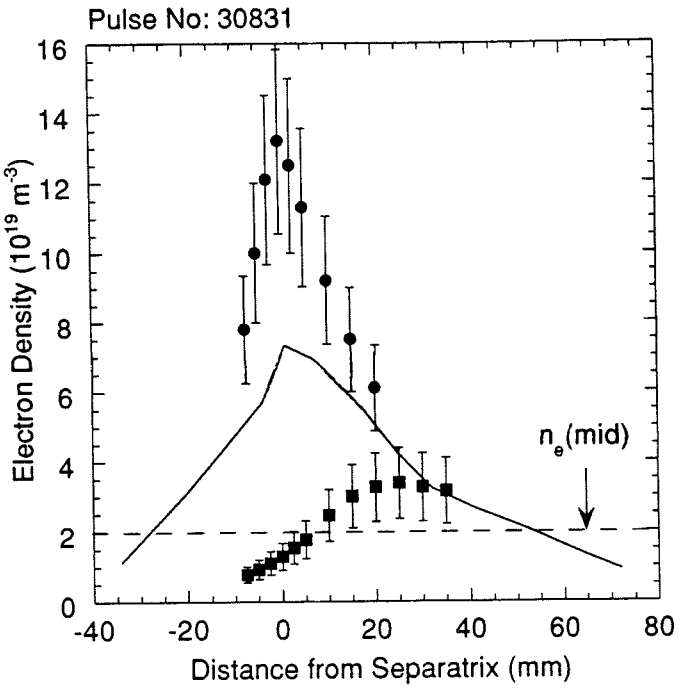

Fig.6 *Divertor target plate electron density profiles for a 6 MW L-mode discharge. The circles are experimental measurements during the attached phase of the discharge. The squares are the measured profile during the detached phase of the shot. The curve is the model prediction for the detached plasma. During the detached phase the midplane separatrix density is ~2x10^{19} m^{-3}.*

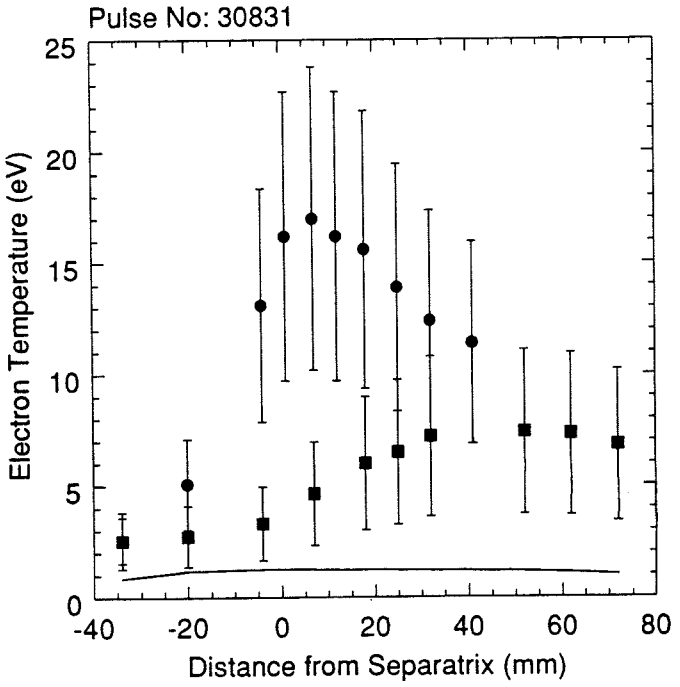

Fig.7 *Divertor target plate electron temperature profiles for a 6 MW L-mode discharge. The circles are experimental measurements during the attached phase of the discharge. The squares are the measured profile during the detached phase of the shot. The curve is the model prediction for the detached plasma.*

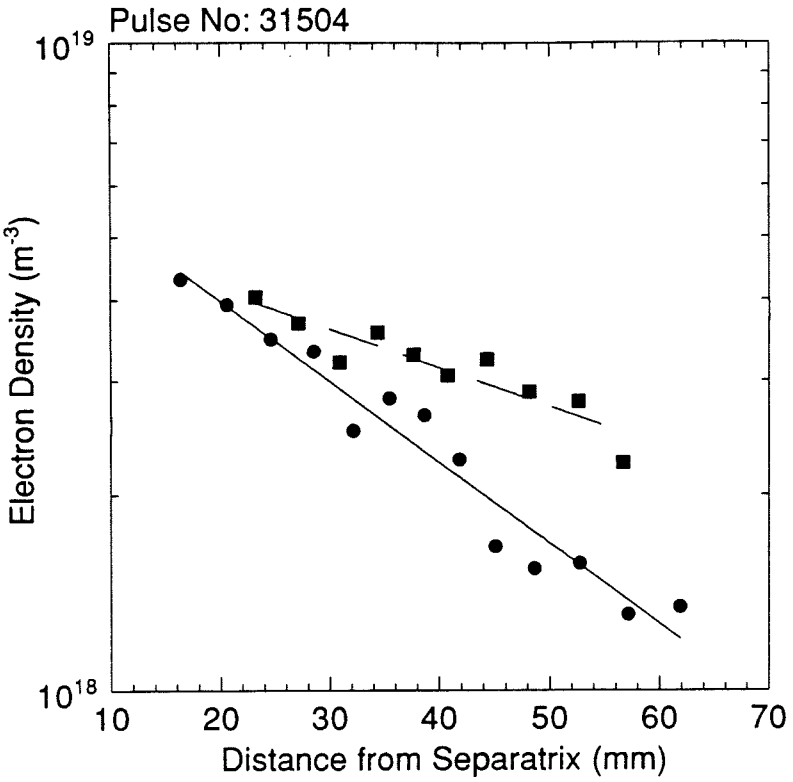

Fig.8 *Profiles of SOL electron density at the outer midplane for a 6 MW L-mode plasma. The circles are measurements for a medium density plasma while the squares correspond to a high density, detached plasma. The lines are exponential fits to the data.*

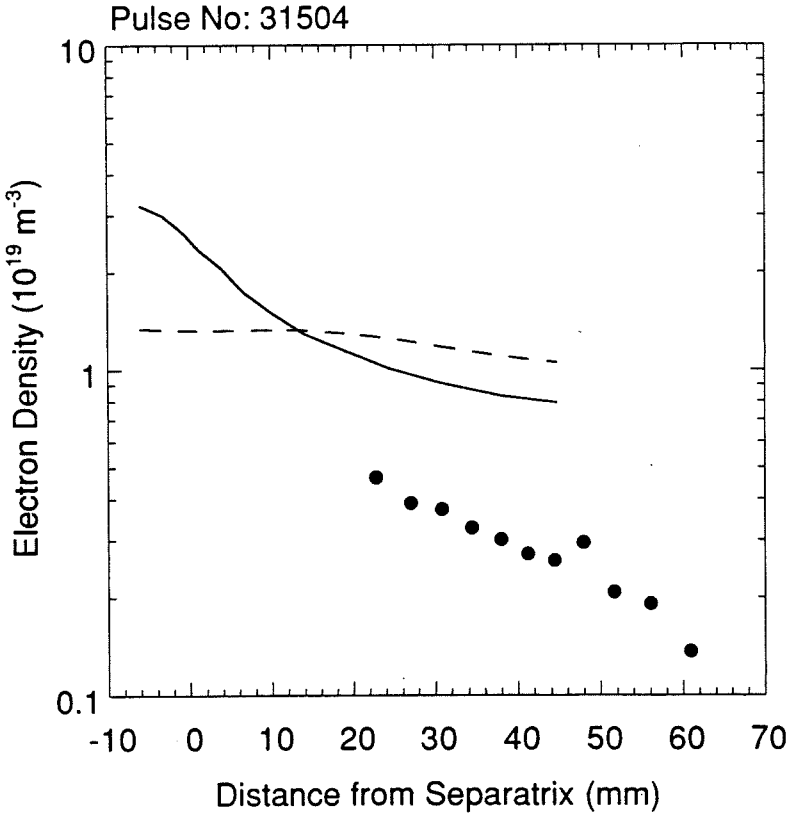

Fig.9 *Profiles of electron density at the outer midplane. The points are an experimental measurement for a 6 MW high density discharge. The dashed curve is the prediction of the fluid model assuming no particle pinch. The solid curve is the model result using an inward pinch of 6 m/s.*

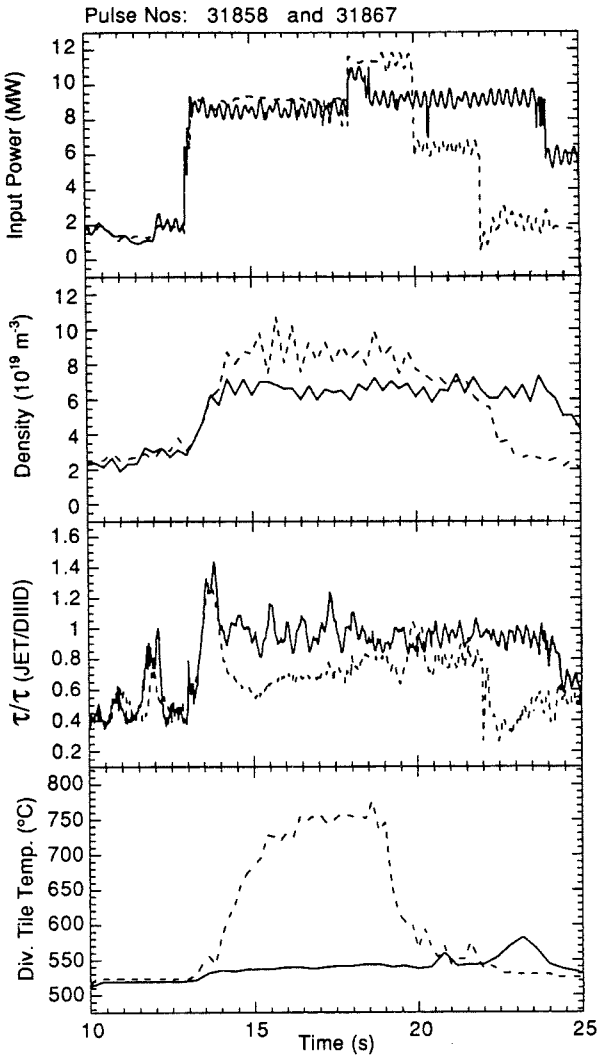

Fig.10 *Comparison of medium density (solid curves) and high density (dashed curves) H-mode discharges. At high density the ELM frequency increases and the core confinement decreases. Peak power loading, which is dominated by ELMs, also increases with increasing density.*

Operation for High Performance in the New JET Configuration

The JET Team
(presented by P J Lomas)

JET Joint Undertaking, Abingdon, Oxfordshire, OX14 3EA, UK.

OPERATION FOR HIGH PERFORMANCE IN THE NEW JET CONFIGURATION

The JET Team
(Presented by P J Lomas)

JET Joint Undertaking
Abingdon, Oxfordshire OX14 3EA, U.K.

ABSTRACT

H-mode operation has been demonstrated in the new JET configuration at plasma currents up to 4MA. Unlike the previous high current H-modes in JET, these plasmas have a clear divertor configuration. Typical H-modes in the old JET were ELM free for several seconds limited by rising density leading to radiative driven transition to L-mode. The recent H-modes are typically ELMy with steady state density, and confinement close to ELM free values. The ELM free period increases with increasing plasma current and triangularity, in double null configurations and with reduced recycling consistent with the predictions of ideal ballooning at the edge. Initially the fusion performance in the new JET was limited by high main chamber recycling, unfavourable density profiles and short ELM free period. Now the fusion performance achieved is in the middle of the range observed previously in the hot ion regime, and clear routes for further optimisation have been identified.

1. INTRODUCTION

JET has recently installed internal divertor coils, a new target plate assembly and a torus cryopump. These installations were designed to permit significantly improved divertor configurations for plasma currents, ultimately, up to 6MA. Bearing in mind the future DT experiments in JET, it is desirable to investigate in the new JET configuration high fusion performance in regimes with steady state potential in addition to regimes with the maximum fusion yield. For this reason, ELMy, ELM free and enhanced H-modes are of interest.

In the following sections a comparison is made between H-mode behaviour in the old and new JET configuration, experiments to elucidate the reasons for differences are described, progress towards high fusion yield in the hot ion H-mode is reviewed, and finally H-modes at the highest plasma current are shown.

2. H-MODE BEHAVIOUR IN THE NEW JET CONFIGURATION

Fig. 1 shows a typical H-mode at 3MA in the new JET configuration at moderate neutral beam power and moderate density. The transition into H-mode occurs at the same power as previously [1], but the initial ELM free period is short (300 ms in this case), and thereafter ELMs are repetitive and density, stored energy and neutron yield become steady. Similar pulses have been extended to show steady state for times up to 20 secs. [2].

The confinement time in such plasmas over a range in current from 1 to 4MA and toroidal field 1 to 3.4T appears to be between 90 and 100% of ELM free H-mode predictions (ITERH93-P). The ELM frequency increases strongly with power and decreases with plasma current in a similar manner to that observed on Asdex and DIIID [2, 3].

These H-modes contrast with the long ELM free behaviour typical of the old JET configuration [1]. In the old results the density and radiated power increase throughout the ELM free period leading to a return to L-mode.

3. PROLONGATION OF ELM FREE PERIOD

There are a number of differences between the old and new JET which might be significant in determining the ELM behaviour including vessel temperature, proportion of bare inconel on the vessel wall, the plasma shape and diverted plasma geometry, the divertor chamber geometry and divertor tile design and cooling and finally the limiter configuration.

Experiments on conditioning schemes, divertor tile heating, X point to target distance, diverted plasma flux expansion, top X point (ie. using the original divertor assembly hot tiles) have shown only small effects on the ELM free period. Plasma scenarios optimised for minimum gas input and the use of the cryopump can reduce the main chamber recycling. Fig. 2 shows that reduction of main chamber recycling can increase the ELM free period to as long as 1 sec. for the "standard" plasma shape. Both double null x point configurations and more triangular configurations can extend the ELM free period to of order 2 secs. at 10MW. A scan of elongation, triangularity and strike point location at constant power plasma current, toroidal field and target density confirms that an increase in triangularity from 0.2 to 0.35 can extend the ELM free period from 0.3 to 2 secs. Fig. 3(a) shows the triangular configuration overlaid on the standard configuration and Fig. 3(b) shows the H-mode behaviour in this triangular case. It can be seen that in addition to the long ELM free period the rising density and increasing radiation are similar to the old JET behaviour and the ELM free period is often limited by a return to L-mode driven by power balance considerations. Interestingly this higher triangularity is similar to the values typical of the old JET configurations.

Reduction of recycling reduces the density gradient at the separatrix and both increasing triangularity and using double null configurations increase edge shear and therefore increase the ideal ballooning limit to pressure gradient at the separatrix. This leads to the hypothesis that the proximity to the ideal limit determines the ELM free period. The theoretical pressure gradient limit due to the ideal ballooning limit has been calculated using EFIT reconstructions of the plasma equilibria. These reconstructions assume zero edge current density, but more limited investigations show that edge current density has negligible effect at the 95% flux surface. The experimental pressure gradients are determined from ECE, reflectometry and LIDAR with spatial resolution varying from 3 to 10cm. Fig. 4(a) examines the relationship between global stored energy and calculated edge limit whereas Fig. 4(b) compares the measured edge profiles with the calculated limits. Taken together, and bearing in mind the caveats described above there is support for the hypothesis that the edge is limited by ideal ballooning, and that therefore the ELM free period is determined by the time to reach this limit.

4. THE HOT ION H-MODE REGIME

Fig. 5(a) shows time traces for an hot ion H-mode in the new JET configuration at 2.5MA. In comparison with the best hot ion with the old configuration at 3MA the ion temperature is similar but electron temperature stored energy and neutron yield are lower. Beryllium gettering and Helium GDC together reduce the mainchamber recycling but only to levels a factor 2 - 5 higher than previously obtained with the old JET. Further reduction in recycling was obtained using first one half of the cryopump, but the use of the full cryopump reduced the recycling to the levels previously obtained in the highest performance pulses. Fig. 6 shows that this reduction in recycling has brought a significant improvement in fusion performance. The reduced recycling reduces the edge

density and allows the neutral beam fuelling to dominate the wall source and therefore develop more peaked density profiles where the beam deposition is more favourable. Note that there is a large scatter in the old results at low recycling, attributed to a variety of phenomena which can terminate the high performance phase [5] including carbon blooms, the early appearance of ELMs and sawteeth. In the new data the carbon bloom is absent as a result of good divertor design but the other phenomena have been observed in the new JET. For example the pulse in Fig. 5(a) is clearly ELM limited, whereas the more triangular configuration of Fig. 5(b) is limited in a more subtle manner (the so called slow termination) and not by ELM or sawtooth. Fig. 7 illustrates the difficulty in understanding such phenomena. Here early in the H-mode the recycling level is low, but 100ms after the sawtooth the rate of rise of stored energy decreases, and at the same time the target temperature increases indicating an increase in loss power from the core. The recycling light (H_α) increases, the magnetic activity changes in character and the edge temperature clamps. It is therefore difficult to separate cause and effect.

The highest performance pulses from the old data exhibit enhanced global confinement (up to 1.8 times elm free H-mode scaling prediction), the so called VH-mode, whereas the new data has global confinement enhancement factors between 1 and 1.4. In both data sets the core transport is essentially the same [6] and therefore any differences must lie in the outer 20% of minor radius. Analysis has suggested [7] that the highest performing pulses in the old JET entered second stability. This would then indicate that the evolution of the edge bootstrap current and edge resistivity are important factors yet to be exploited in the new JET configuration.

5. HIGH CURRENT H-MODES

The highest current H-mode so far demonstrated in the New JET configuration is 4 MA as illustrated in Fig. 8, for moderate target density. The general behaviour is similar to lower current cases such as Fig. 1, but the initial ELM free period is longer and the ELM frequency during the steady state phase is lower. The maximum D-D rate is reached at the first ELM and is comparable to the best hot ion cases at similar recycling. The stored energy approaches 10MJ which is comparable to previous 4MA data at similar loss power, but in this case is maintained steady state by the ELMs. The fusion triple produce $n_D\ T_{i0}\ \tau_E$ reaches $4.9 \times 10^{20} m^{-3}$ keV during the transient ELM free phase and $2.5\ 10^{20} m^{-3} s$ keV during the stationary ELMy phase. The former value is quite promising and offers the prospect of further improvement along the lines already described in the previous section. The Q_{DT} equivalent for the ELMy phase is modest because the density is too high ($10^{20} m^{-3}$) and therefore the temperature is too low for optimum yield, again indicating a clear route for further optimisation.

6. CONCLUSIONS

The new JET configurations shows naturally ELMy H-modes which exhibit steady state character with good confinement demonstrated up to 4MA. The optimisation of this regime to higher plasma current with improved density control appears promising for JET DT experiments. Clearly still higher fusion performance is possible exploiting the hot ion regime, and promises the highest α particle power in the JET DT phase and therefore is most relevant for studies of α particle heating. In this regime the control of core recycling and elm free period has brought improvement in performance to within the range previously obtained. Increase in plasma current in this regime offers immediate prospects of further improvement. The enhanced H-mode confinement (the VH) mode was achieved in the highest performance plasma in the old JET but has, as yet, not been clearly identified in the new configuration. The reduced recycling and improved triangularity recently demonstrated open up exciting prospects for this regime.

ACKNOWLEDGEMENTS

The material presented in this paper represents the efforts of the whole JET Team, but in addition the specific contributions of the members of the High Performance Task Force and others is acknowledged with pleasure - A. Ali-Arshad, M. Bures, J.P. Christiansen, N. Deliyanakis, H. de Esch, G. Fishpool, T. Hender (AEA Fusion) O.N. Jarvis, T.T.C. Jones, R. König, K. Lawson, K. McCormick (Garching), F. Marcus, F. Nave, L. Porte, R. Sartori, P. Smelders, E.J. Strait (GA), B. Schunke, A. Taroni, K. Thomsen and B. Tubbing.

REFERENCES

[1] Keilhacker, M. et al., in Plasma Physics and Controlled Nuclear Fusion Research (Proc. 12th Int. Conf. Nice, 1988), Vol. 1, IAEA, Vienna (1988) 159.
[2] Campbell, D. et al., This Conference IAEA-CN-60/A-4-I-4.
[3] Vollmer, O, et al., Controlled Fusion and Plasma Physics (Proc. 18th Eur. Conf. Berlin, 1991), Vol. 1, European Physical Society (1991) 385.
[4] Zomm H, et al., GA-A21302.
[5] Stork, D, and the JET Team, Plasma Physics and Controlled Fusion, Vol. 36 (7a) p. A23, 1994.
[6] Parail, V, et al., Paper IAEA-CN-60/A-2-II-3 and Giannella, R, et al., Paper IAEA-CN-60/A-2-III-1.
[7] Delyanakis, N., et al., Plasma Phys. Control. Fusion 36 (1994) 1159 and Greenfield, G.M., et al., Plasma Phys., Control. Fusion 35 (1993) B263

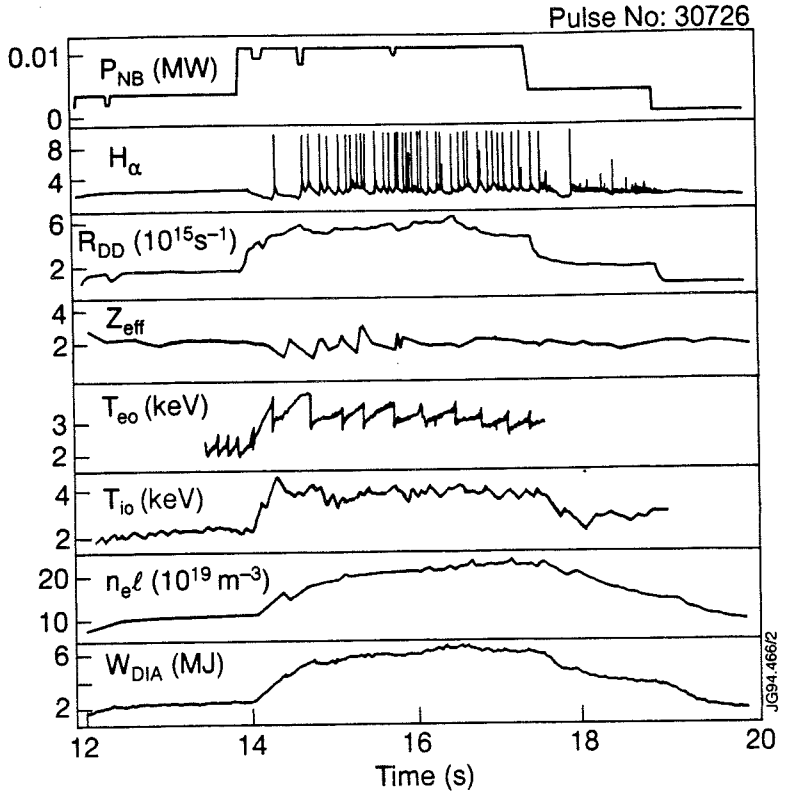

Fig. 1 *Various time traces for a typical H-mode at 3MA in the new JET configuration.*

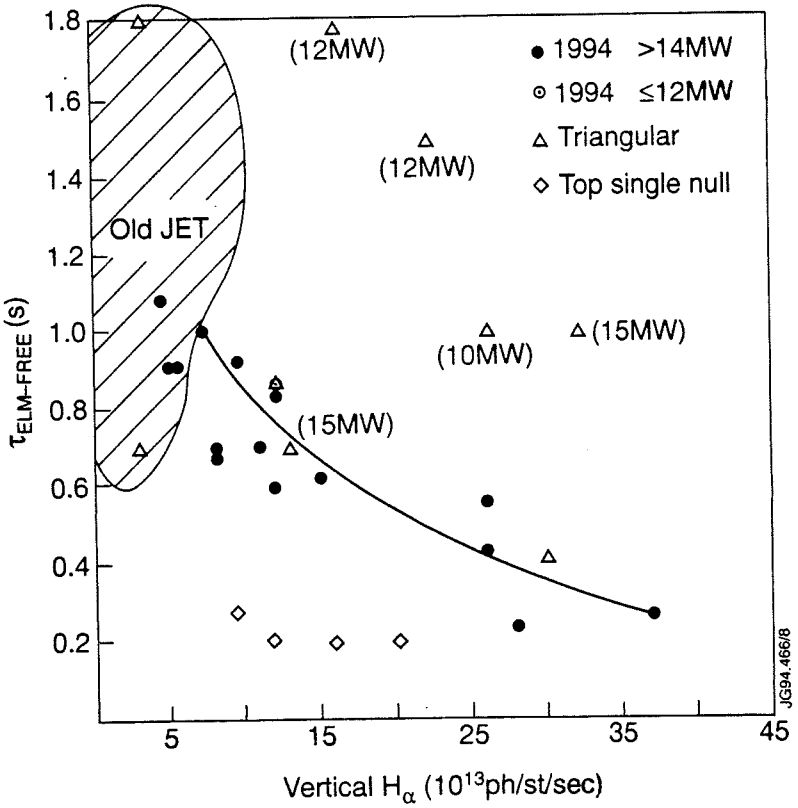

Fig. 2 *ELM-free period plotted against main chamber recycling light for standard fat configurations, triangular configurations and top single null on the original tiles. Where appropriate the ELM free period is counted from the first clear H-mode signature or the start of the high power phase and ends at the first clear giant ELM or ELM associated with neutron yield maximum.*

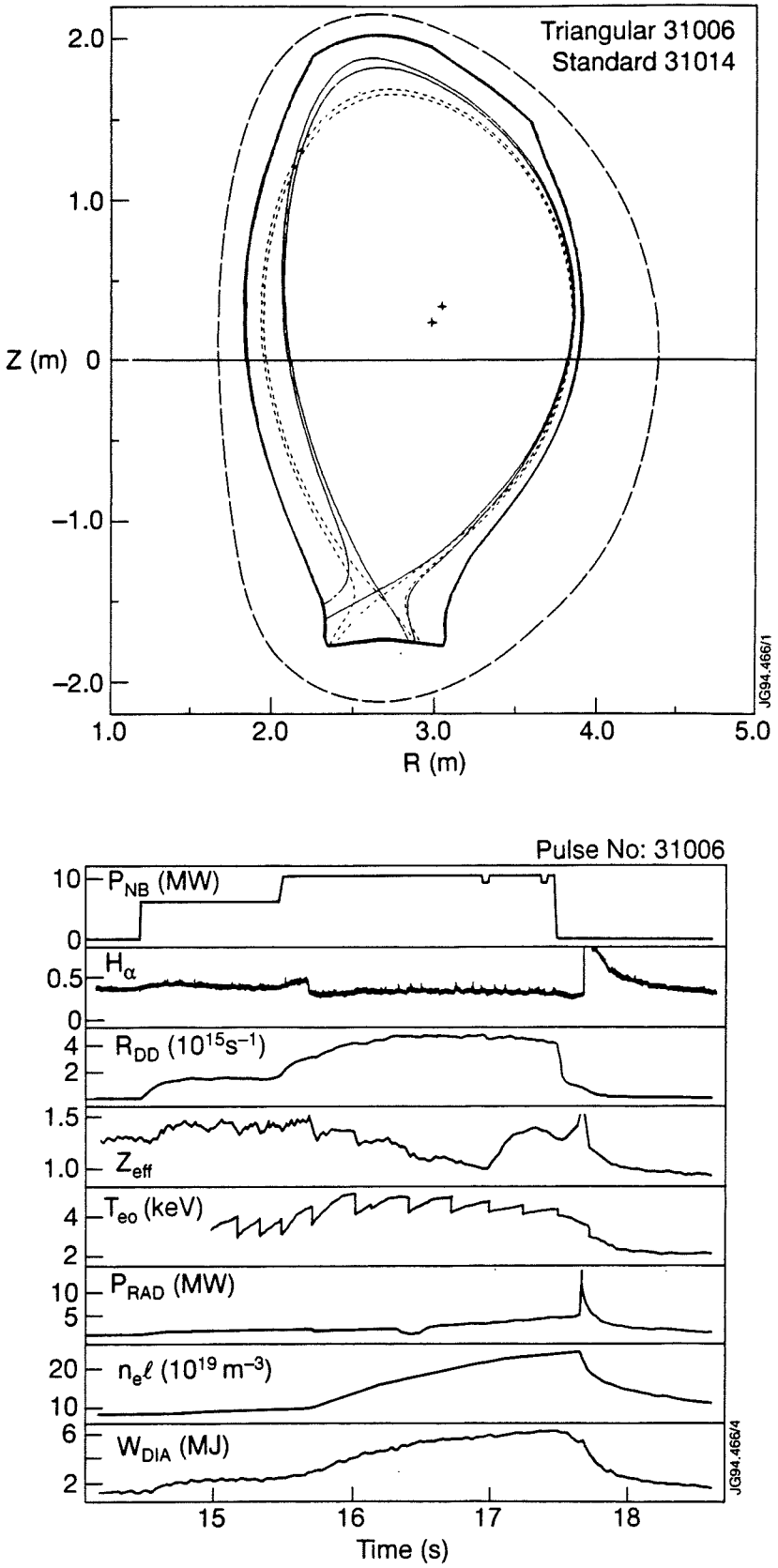

Fig. 3 *(a) The moderate triangularity configuration (solid) compared with the low triangularity FAT configuration (dashed). (b) time traces for the H-mode with moderate triangularity.*

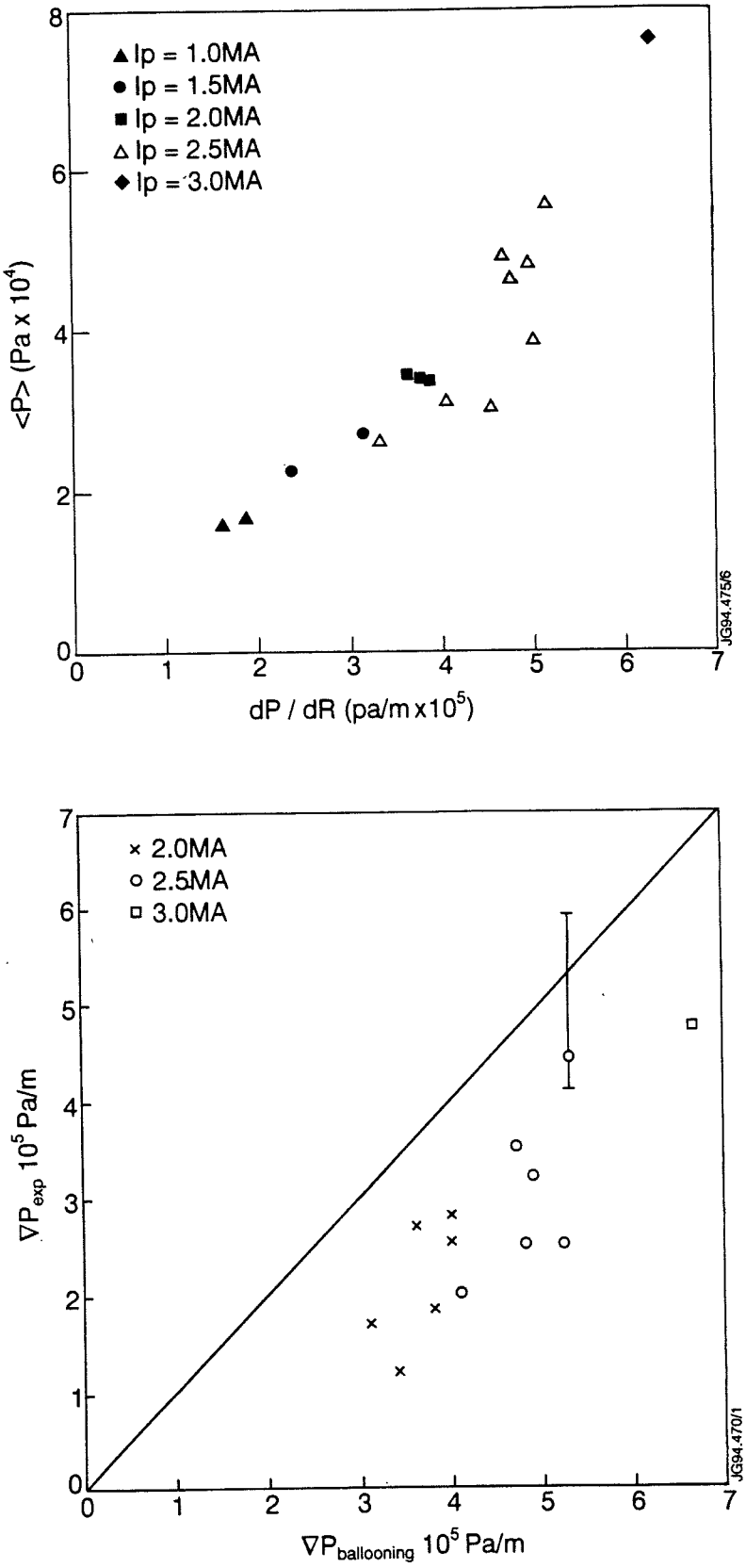

Fig. 4 *(a) The global stored energy plotted against calculated edge pressure limit for plasmas including the configuration scan and double null plasmas. (b) best estimate of edge pressure greadient plotted against the same calculated limit. See text for cautionary remarks.*

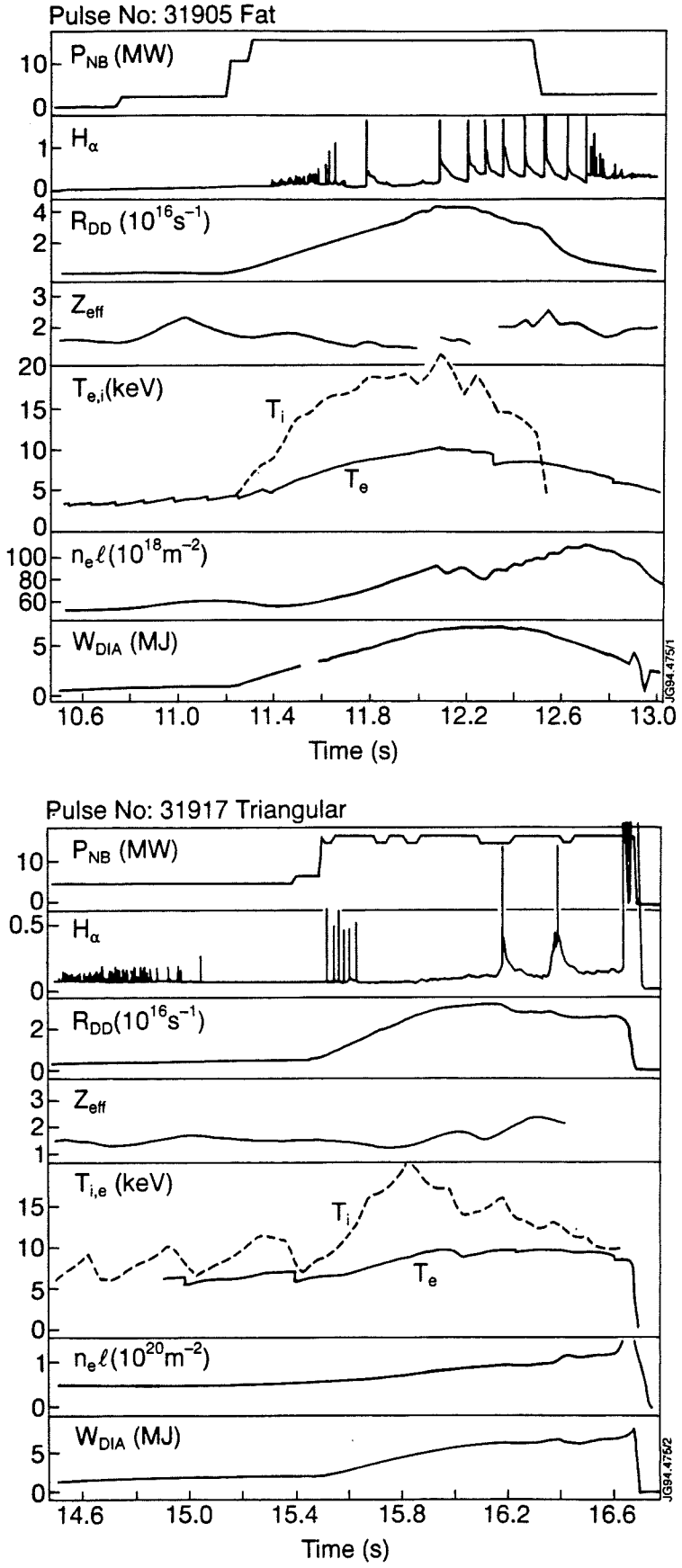

Fig. 5 Time traces for hot ion pulses with low main chamber recycling obtained by cryo pumping, (a) for the standard FAT plasma and (b) for the modest triangular configuration.

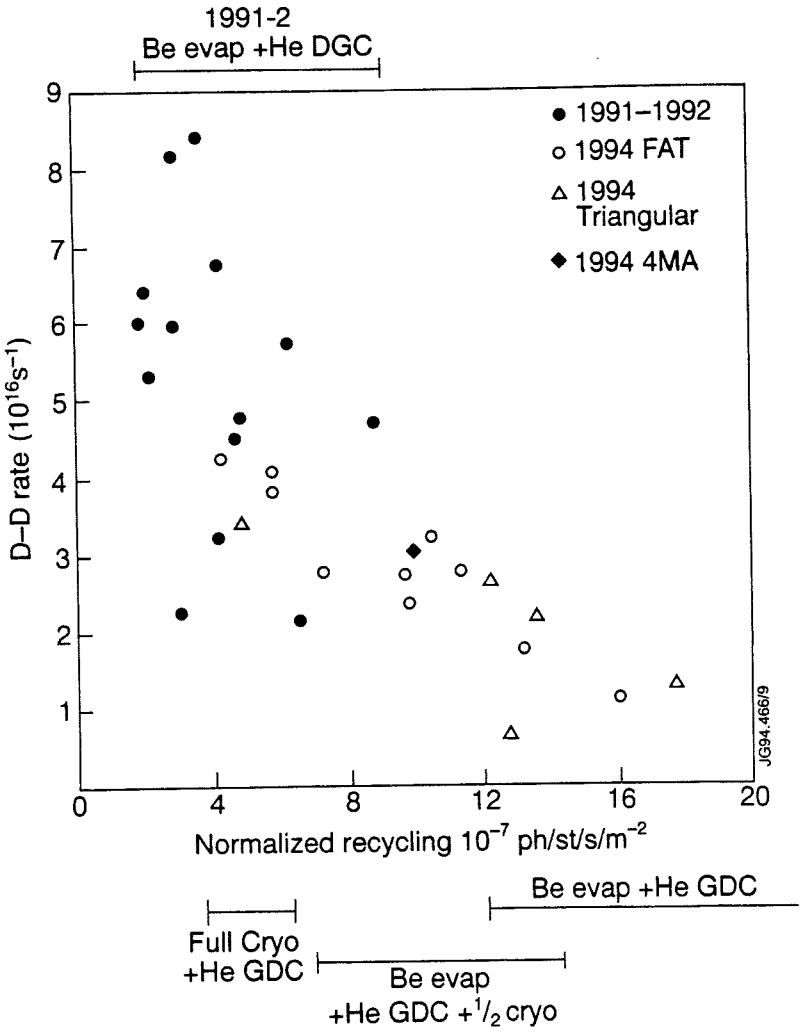

Fig. 6 *Trend of D-D yield versus main chamber recycling. Data from the new JET is compared with the high performance data from the old configuration.*

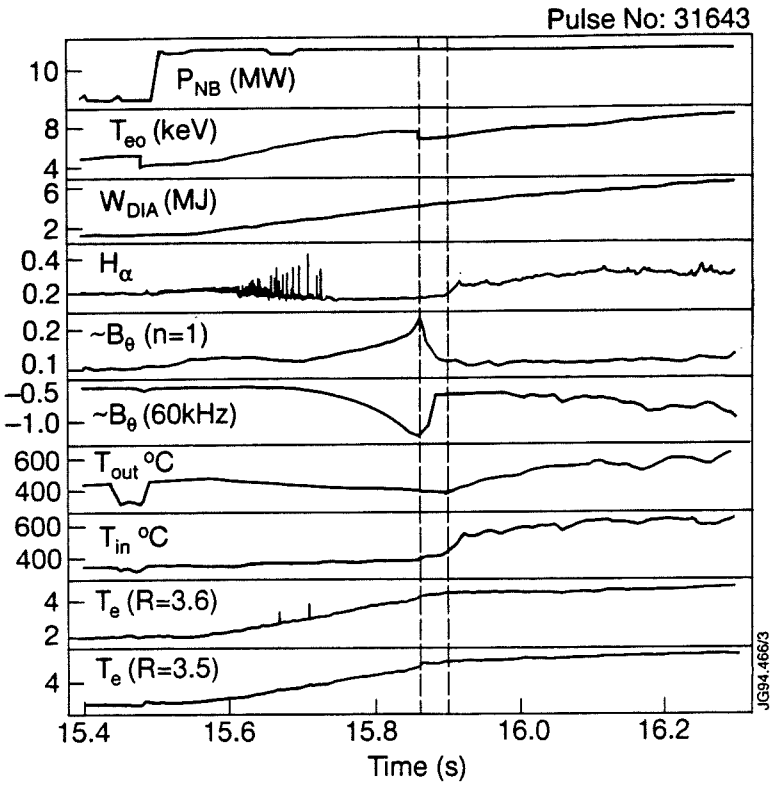

Fig.7 *Various time traces for a slow termination event following a sawtooth, see text.*

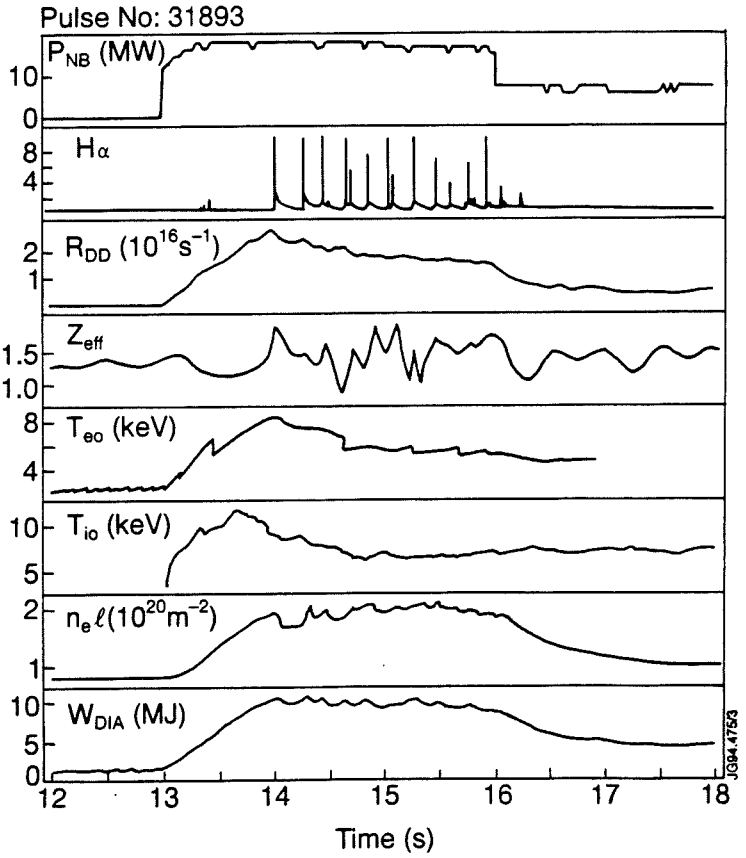

Fig.8 *Time traces for a 4MA/3.4T plasma in the new JET configuration showing both ELM free and stationary ELMy phase.*

Fast Wave Studies in JET

The JET Team
(presented by F G Rimini)

JET Joint Undertaking, Abingdon, Oxfordshire, OX14 3EA, UK.

FAST WAVE STUDIES IN JET

THE JET TEAM
(presented by F.G. Rimini)

JET JOINT UNDERTAKING
Abingdon, Oxon, OX14 3EA, U.K.

ABSTRACT

A new Fast Wave system has been installed at JET for Heating and Current Drive experiments in the new divertor configuration [1]. In this paper results from the initial operation of the system are presented. The different coupling characteristics of the inner and outer straps of each antenna are discussed. Coupled power in excess of 12MW has been achieved, both in ICRH only operation and in combination with NBI, with central electron temperature in the range of 8 keV and production of "monster" sawteeth as with the previous antenna.. With ICRH + NBI, total additional power in excess of 26 MW has been injected at 2 MA. The behaviour of the DD reaction rate for H-modes with combined heating is analysed in the framework of acceleration of beam ions by ICRH at $2\omega_{CD}$. Results from preliminary experiments of Direct Electron Heating are also presented.

1. INTRODUCTION

Application of Fast Waves to tokamak plasmas has proved to be a successful method for auxiliary heating. Since it is not limited by accessibility conditions and it relies on well known and tested technology for its power sources, Ion Cyclotron Resonance Heating (ICRH) is being considered as heating method for the next generation of Fusion Devices [2]. Fast Waves can also be used to generate Non-Inductive Current Drive, as shown in DIII-D [3] and Tore Supra [4], which may be used for profile control and continuous operation of a reactor. The study and assessment of reactor relevant Fast Wave Heating and Current Drive scenarios are part of the current experimental campaign in JET.

2. INITIAL OPERATION OF THE NEW JET FAST WAVE SYSTEM

In view of the operation in the divertor phase of JET, the ICRH system has been heavily modified. The new antennas (A2) consist of four straps, whose currents can be arbitrarily phased to allow directional waves to be generated for Current Drive experiments; each strap is fed by a single wide-band (25 - 52 MHz) tetrode amplifier capable of delivering up to 2 MW. The full system is made of four such antennas installed around the torus. The new arrangement into four straps yields a k// spectrum narrower by a factor 2-3 with respect to the previous ICRH system. Real time matching is achieved via feedback control of frequency, line length and stub length. Feedback control of the coupling resistance by plasma radial position control can also be used.

Details of the antenna conditioning and of the characteristics of the antenna-plasma coupling are presented in ref. [5]. More recent data have highlighted a difference in coupling between the two outer and the two inner straps of each antenna. In fig. 1 the power and coupling resistance RC for each strap of one particular antenna are shown. On average, it has been found that the value of RC on the outer straps is roughly twice that of the inner straps. The data indicates that the coupling increases and the coupling imbalance decreases with increasing frequency. One possible explanation for this asymmetry is the actual difference in the structure of the inner and outer straps, in particular the cross-over straps to the inner conductors. As a consequence of the uneven coupling, when the four straps are operated at the same power, the voltage along the transmission lines is

not balanced, thereby limiting the power that could be delivered by the outer straps. As an alternative, the antennas can be operated with balanced voltage, and imbalanced power, as shown in fig. 2. Comparison of these two methods has shown that, in dipole phasing, heating efficiency is not affected by imbalancing the power in the straps. The high power operation, discussed later in this paper, has been carried out using power imbalance between outer and inner straps.

Experiments with varying phasing between the straps have been carried out, including tests of the Current Drive phasings (+60° and +90°). The best heating efficiency is obtained with $0\pi0\pi$ (dipole) phasing; the 0000 phasing (monopole) has shown very poor heating efficiency and generates large carbon influxes from the limiter.

Actions are being taken to modify the antenna structure, in order to minimise the difference in coupling between inner and outer conductors and to reduce the impurity production observed with some phasing values.

3. HIGH POWER OPERATION

High power ICRH operation has been achieved in 2 MA divertor plasmas, with gradB away from the divertor target (reversed gradB counter current beams), and in 1.5 MA plasmas with gradB towards the divertor target (normal gradB). In dipole configuration at 42 MHz, for minority (H)D heating, up to 13 MW of power have been coupled, both with ICRH alone and in combined ICRH+NBI. In all the cases discussed here the coupling resistance R_C has been maintained constant at the desired value (3Ω to 3.5Ω) by feedback control of the plasma radial position.

With ICRH alone (fig. 2) the central electron temperature, measured via ECE, reaches 8 keV and the typical "monster" sawteeth are observed. At this power level, in reversed gradB and B_T = 2.8 T, no H-modes are produced; the stored energy is in excess of 3 MJ, while the fast ion energy content is estimated to be up to 0.6 MJ.

In combination with NBI (fig. 3), a total additional heating power in excess of 26 MW has been achieved, resulting in H-modes with a short ((200 msec) ELM-free phase followed by an ELMy phase lasting for the entire duration of the high power phase. During the ELMy phase the stored energy is of the order of 4.5 MJ, which is close to the JET/DIII-D H-mode scaling, as indicated in the figure. The quality of the H-mode appears to be insensitive to plasma-limiter distance. With ICRH + NBI the usual sort of behaviour is found, rather than the small sawteeth characteristic of NBI alone in counter current configuration.

A comparison of H-mode data, at I_p = 2 MA , B_T = 2.6 - 2.8 T, reversed gradB, shows that the measured DD reaction rate, R_{DD}, increases more than linearly with auxiliary power in cases of combined ICRH + NBI. In the database, the variation of ion temperature with ICRH power is negligible, while the electron temperature increases with ICRH power. The enhanced R_{DD} is likely to be caused by the fast deuteron population from NBI having higher energy than in cases with NBI alone. This could be due both to reduced collisionality and to direct acceleration by ICRH of the beam ions at $2\omega_{CD}$. The first effect can be taken into account by plotting R_{DD} as function of a parameter that accounts for the initial energy distribution of the NBI ions and the variation in their collisionality (fig. 4). The remaining enhancement can be attributed to interaction of the ICRH waves with the beam ions at $2\omega_{CD}$, as is confirmed by numerical simulations with the PION code [6].

4. DIRECT ELECTRON DAMPING EXPERIMENTS

There are several reactor relevant scenarios for Fast Wave Heating and Current Drive that can be studied in JET plasmas.

A scheme similar to the one proposed for ITER, i.e. injected wave frequency below all ion cyclotron frequencies in the plasma [2], is considered : in the new JET divertor configuration by using Fast Waves at 33 MHz in a 3.1 T Deuterium plasma only the fundamental ω_{He3}, resonance is present in the plasma. The single pass damping is predicted to be of the order of 10%, to be compared with about 50% for the ITER case. However, since there are no competing cyclotron absorption mechanisms, most of the injected power is expected to be absorbed by the electrons.

Experiments with predicted high single pass damping, comparable to what is expected in ITER, are also planned at low toroidal field, B_T~1.4 T, high frequency, ~48MHz; in similar conditions, non-negligible direct electron damping has already been demonstrated in JET [7].

Scenarios characterised by high fraction of mode conversion, in the central plasma region, of the launched Fast Wave to an Ion Bernstein Wave [8] are being considered and numerical simulations of the predicted damping and Current Drive efficiency for JET plasmas are being carried out.

A fourth scheme is also studied. In Deuterium plasmas at B_T = 1.8 to 2.1 T and wave frequency 42 to 48 MHz, the main resonance in the plasma centre is $3\omega_{CD}$ while ω_{CD} is either at the very edge or out of the plasma. In a similar scenario, significant Direct Electron damping and some Current Drive have been obtained in Tore Supra [4].

Preliminary experiments have been carried out at 2.1 T, 42 MHz in dipole phasing (fig. 5). The predicted single pass damping for this case, given the low initial temperature, is of the order of 5%; rising to 5% - 10% at the end of the ICRH pulse [9]. Gamma Ray radiation has been monitored to assess possible absorption by ions at $3\omega_{CD}$ and consequent tail formation [10]: no significant gamma ray emission has been measured, thereby excluding the presence of a high energy Deuterium tail and eliminating a possible competing mechanism for the direct electron damping. Absorption at ω_{CH}, located at ~0.7m off axis on the high field side is estimated to be of the order of 10%, with no Hydrogen tail formation expected [6] The fast decrease of the central electron temperature at the ICRH switch-off suggests that direct electron damping of the Fast Wave is a non-negligible heating mechanism for this scenario.

Further studies of FW Direct Electron Heating and Current Drive scenarios are planned for the remainder of the JET experimental campaign; precedence will be given to the high frequency scenarios, where higher ICRF power is likely to be available.

5. SUMMARY

Results from the initial operation of the new JET Fast Wave Heating and Current Drive system have been presented. With ICRH, with coupled power above 10 MW, high electron temperatures and "monster" sawtooth activity have been obtained as in the previous campaign. In combined ICRH + NBI operation total additional power in excess of 26 MW has been injected at 2 MA. In H-modes with combined heating acceleration of beam ions by ICRH at $2\omega_{CD}$ has been observed. Preliminary experiments of Direct Electron Heating have also been carried out.

REFERENCES

[1] Wade,T., et al., to be published in Fusion Engineering and Design, 1993
[2] Bhatnagar, V., Jacquinot, J.,NET Report 103 EUR-FU/XII/163/94 (1994)
[3] Petty,C.C.et al., IAEA-CN-60/A3.5-P-6, these Proceedings
[4] Saoutic, B., et al., IAEA-CN-60/A-3-I-6, these Proceedings
[5] Bures,M., Proc. of 21st EPS Conf. (Montpellier,1994)
[6] Eriksson,L-G., et al., Nucl. Fusion 33 (1993) 1037
[7] Start,D.F.H., et al., Nucl. Fusion 30 (1990) 2170
[8] Majeskij, R., et al., IAEA-CN-60/A-3-I-4, these Proceedings
[7] TFTR , this conference ....
[9] Fraboulet.,D.,Nguyen,F., private communication
[10] Adams,J.M., et al., Nucl. Fusion 31 (1991) 891

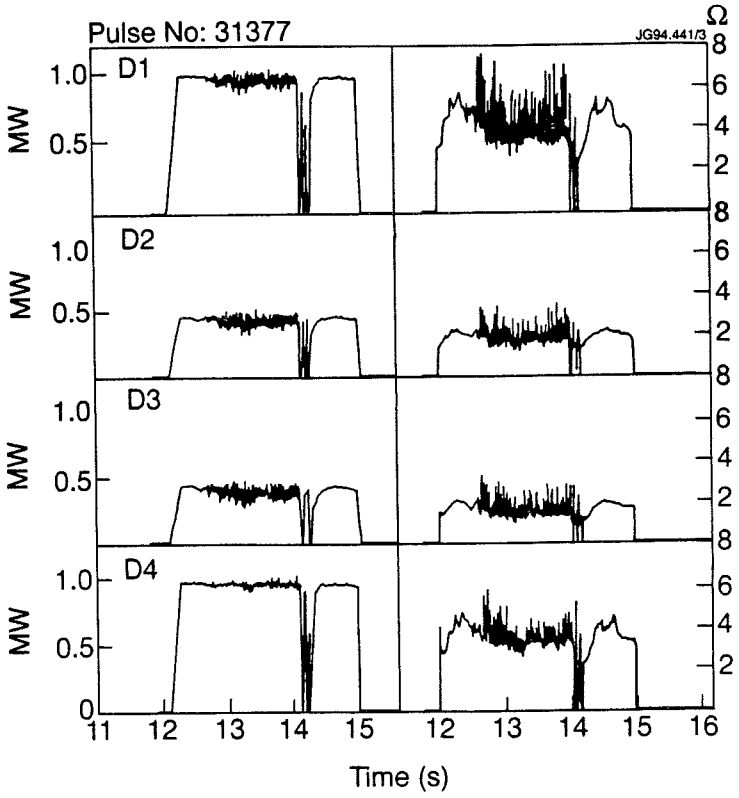

Fig.1 *Power (left and coupling resistance (right) for each strap of antenna D, in dipole phasing, during an ELMy H-mode*

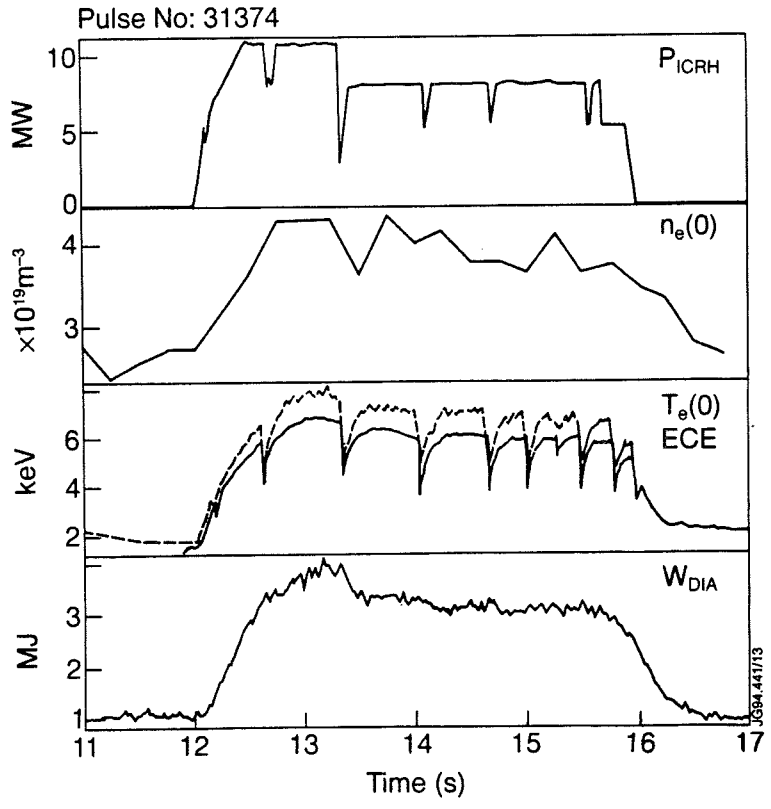

Fig.2 *High power pulse with ICRH alone*

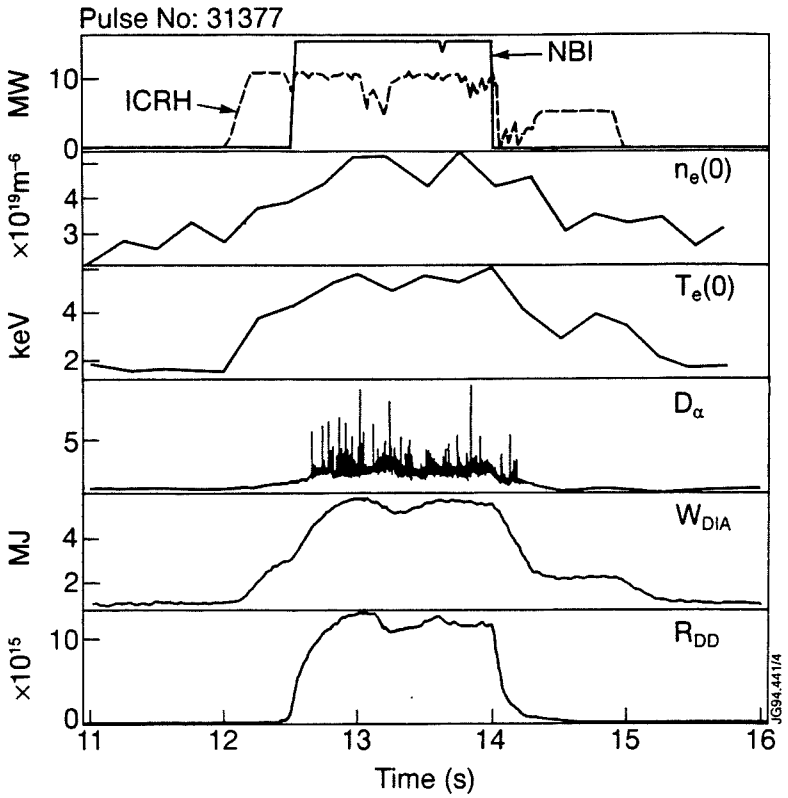

Fig.3 *High power combined ICRH + NBI pulse*

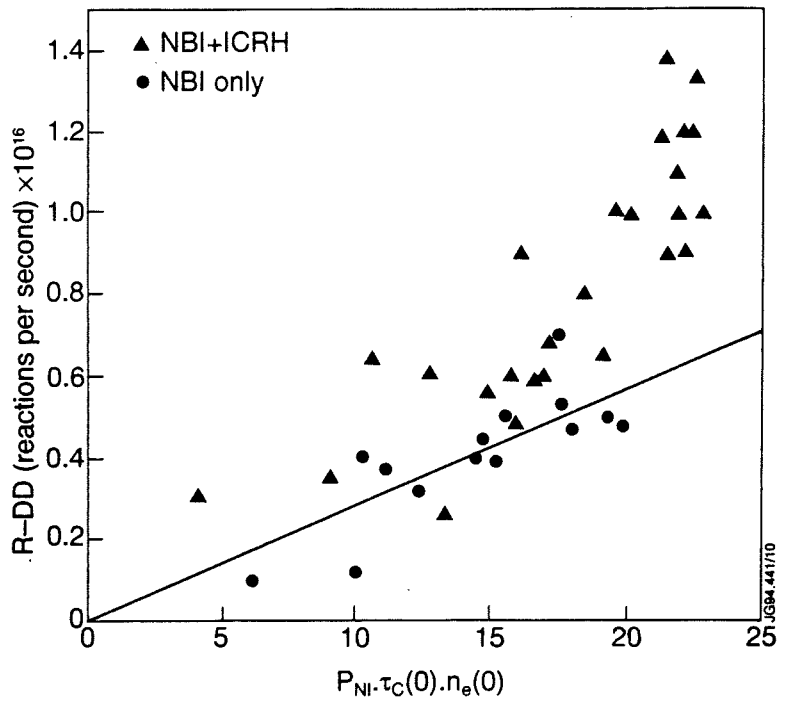

Fig.4 *DD reation rate vs $P_{NBI}*\tau_C(0)*n_e(0)$, where $\tau_C(0)$ is the beam ions collision time.*

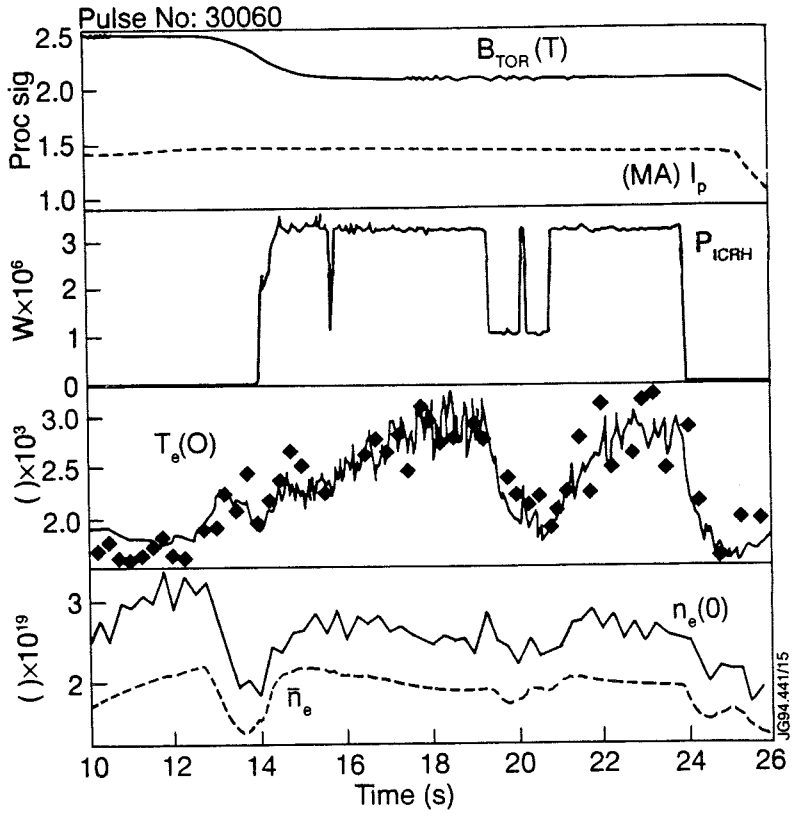

Fig.5 *Direct electron heating experiment*

Lower Hybrid Current Drive in JET and Reactor Applications

The JET Team
(presented by F X Söldner)

JET Joint Undertaking, Abingdon, Oxfordshire, OX14 3EA, UK.

LOWER HYBRID CURRENT DRIVE IN JET AND REACTOR APPLICATIONS

The JET Team
(presented by F.X. Söldner)

JET Joint Undertaking,
Abingdon,
Oxon, OX14 3EA, U.K.

ABSTRACT

Lower Hybrid current drive (LHCD) power up to 6 MW has been coupled with the new full system into JET plasmas. LHCD experiments have been performed in the range 0.7-3 MA. The current drive efficiency increases with the electron temperature. The same heating efficiency is obtained with LHCD and Neutral Beam Injection (NBI) in conditions of central power deposition (for LH at low densities with central density $n_{e0}<3x10^{19}m^{-3}$). The LH deposition profile has been varied between centrally peaked and strongly hollow shape. Central shear reversal over a wide plasma region has been achieved with combined operation of LHCD + ICRH during fast plasma current ramp-up, and maintained into high power NBI heating. The experimental current drive efficiencies and the form of the deposition profiles are reproduced by a ray tracing code validated on previous JET data. Calculations with TRANSP, including a new beam tracing LH code, describe well the experiment. The codes have been used to develop a scenario for steady-state operation of ITER with a high fraction of bootstrap current.

LOWER HYBRID CURRENT DRIVE EXPERIMENTS IN JET

The main goal of LHCD on JET is the active control of the plasma current profile in order to improve confinement and explore scenarios for steady state tokamak operation in combination with heating and current drive by Fast Waves and NBI. Lower Hybrid experiments started on JET during the previous experimental campaign with a prototype launcher, delivering up to 2.4 MW power to the plasma from one third of the final LHCD system [1]. The full LHCD system of JET has now come into operation. The LH plant consists of 24 klystrons with a maximum power output of 12 MW / 20s at 3.7 GHz. The power is coupled to the plasma through a single multi-waveguide grill type antenna, Wave spectra with the peak refractive index variable in the range $N_{||}$ = 1.4 - 2.3 can be launched by adjusting the antenna phasing. The launcher position is controlled by a hydraulics system which allows movements during plasma discharges. Real time coupling control by feedback on the launcher position, with the LH reflection coefficient as input has been used routinely. The reflection coefficient was kept below 5%, with a separatrix-launcher distance of up to 6 cm in standard X-point plasmas, and up to 10 cm in combination with NBI. Good coupling was maintained also during ELM´y and ELM-free H-modes.

Current drive experiments have been performed with the new LHCD system on JET in the range of plasma currents I_p = 0.7 - 3 MA. A maximum LH power of 6 MW and a maximum energy of 36 MJ have been coupled to the plasma so far. A representative 2 MA discharge at a line averaged density n_e = 1.8 x 10^{19} m^{-3} is shown in Fig.1. The LH-current drive with 4 MW coupled power replaces the Ohmic flux consumption (Fig.1b). The measured surface loop voltage $U_{l,surf}$ drops to zero (Fig. 1c). The corrected resistive loop voltage $U_{l,corr}$, taking into account changes of plasma current and internal inductance, stays slightly positive. The electron temperature rises from 3 to 5 keV (Fig. 1e) and the total energy content doubles

(Fig. 1f). A decrease of the internal inductance l_i indicates a broadening of the current profile (Fig 1g).

LHCD has been combined with ICRH and NBI in L- and H-mode discharges. In combined operation of LHCD with ICRH for up to 6s, a total energy of up to 55 MJ has been deposited into the plasma. The same incremental energy confinement time is obtained with both LHCD and NBI at comparative power levels in conditions of central power deposition. The heating efficiency of LH degrades with increasing density due to the broadening of the deposition profile.

The current drive efficiency η_{CD} increases with electron temperature, for LHCD alone and in combined heating/current drive scenarios. The scaling of η_{CD} with volume averaged temperature and the Z_{eff} term from theory is shown in Fig. 2 for a series of power scans with LHCD and ICRH combined. The variation due to Z_{eff} is negligible in these discharges, while the central electron temperature varied between 2 and 7 keV.

The current profile is broadened in most cases with LHCD, as seen from the reduction of the internal inductance l_i and a transient negative overshoot of the loop voltage after start of the LH. Hard X-ray measurements of the fast electron bremsstrahlung (FEB) give consistently broad or hollow emission profiles in these cases, suggesting off-axis LH power deposition profiles. The FEB profiles are peaked at low electron density and temperature and broaden with increasing density and temperature. A dependence of the LH deposition profile on the plasma current and the current profile is found. The FEB profiles broaden and the drop in l_i grows with plasma current, as seen from a comparison of 2 and 3 MA shots at constant magnetic field $B_t = 2.9$ T. The LH current deposition profile broadens with peaking of the plasma current profile, as seen in Fig. 3 from the FEB profiles at two stages of the discharge # 30779. LHCD was started at the end of the initial fast Ohmic current ramp-up. The current profile is slightly hollow in this phase, with a low value of $l_i = 0.6$. The FEB profile is then peaked in the center. It broadens during the current flat-top phase when the current profile is gradually peaking, with l_i rising up to 0.8. Electron density and temperature stay constant during the whole LH pulse at $n_{eo} = 2.3 \times 10^{19}$ m^{-3} and $T_{eo} = 2$ keV.

Current profile control experiments were performed with the aim to establish deep shear reversal over a wide region in the plasma center. A stable route to these configurations had been identified, with generation of shear reversal at low β_p during the plasma current ramp-up and freezing by subsequent high power heating. [2]. This method has been tested in first experiments on JET [3]. The evolution of the q profile in discharge # 31753 is shown in Fig. 4, as obtained from magnetic measurements. Direct current profile measurements have yet to be made. Shear reversal over about half the plasma radius is achieved in this case with combined application of LHCD + ICRH during a fast plasma current ramp-up (2s). The hollow current distribution is maintained with subsequent additional NBI heating (4s). At a later stage, after switch-off of LHCD, the q profile relaxes to a monotonic distribution (6s) and remains then nearly unchanged during the following NBI + ICRH phase (9s).

MODELLING OF LOWER HYBRID CURRENT DRIVE

The recent LHCD experiments on JET have been extensively modelled with two codes based on different approaches. The BARANOV ray tracing code had been validated on previous JET data, [4]. The current drive efficiencies in the new experiments are well reproduced over the whole parameter range. Calculation of the FEB signals in the code allows direct comparisons between calculated and experimental LH deposition profiles. The broadening of the profiles with increasing electron density and temperature is also found in the code calculations. The off-axis shift of the current deposition profile with increasing plasma current can be explained by a stronger $N_{||}$ upshift on longer wave trajectories in the outer plasma. Difficulties arise with modelling of experiments in conditions of multiple wave

reflections at the plasma boundary before absorption. An alternative code for the calculation of LH propagation and damping employs a beam tracing method based on a diffraction model developed by Pereverzev [5]. This code has been implemented into the predictive 1.5-D transport code JETTO and into the interpretive transport analysis code TRANSP. Time dependent calculations for the analysis of experiments and for predictive modelling have been performed with both codes. The time evolution of the loop voltage in discharge # 29711 (Fig. 1c) is well reproduced. The LH current deposition profiles, as calculated with both codes for this discharge are shown in Fig. 5. The ray tracing code gives a broader and smoother profile, as diffusion of fast electrons is included. The total driven current reaches 1.75 MA with the beam tracing code in the TRANSP calculation and 1.84 MA in the BARANOV ray tracing code. Reliable modelling can be expected from both codes for conditions with dominant single pass absorption.

LOWER HYBRID CURRENT DRIVE ON ITER

The models developed and validated on the basis of the experimental results on JET have been used to study the application of LHCD to ITER and reactor grade plasmas [6]. LH power and current deposition profiles are determined in these studies with ray tracing and beam tracing codes. The temporal evolution of the plasma profiles is calculated with the 1.5-D transport code JETTO. Full current drive and real time profile control on ITER can be achieved by a combination of LHCD and Fast Wave current drive (FWCD) with a high fraction of bootstrap current in the H-mode at high β_p. The off-axis current drive capability of LHCD is essential to establish and maintain stable shear reversal configurations. A scenario with 74% bootstrap current, 20% LH-driven current and a small fraction of FWCD-driven current for central q control has been developed. Steady-state operation at a plasma current of 13.5 MA is then provided by a combination of FW and LH systems, with 50 MW each.

REFERENCES

[1] C. Gormezano, et al., 14th Int. Conf. on Plasma Phys. and Contr. Nuclear Fusion, Würzburg, Vol. 1, p. 587 (1992).

[2] F.X. Söldner, et al., 21st Europ. Conf. on Contr. Fusion and Plasma Physics, Montpellier (1993).

[3] C. Gormezano, et al., this conference.

[4] Y. Baranov, et al., 20th Europ. Conf. on Contr. Fusion and Plasma Physics, Lisbon, Vol. III, 881 (1993).

[5] G.V. Pereverzev, Nuclear Fusion **32**, 1091 (1992).

[6] ITER Task Report IVA-LH (1994), to be published.

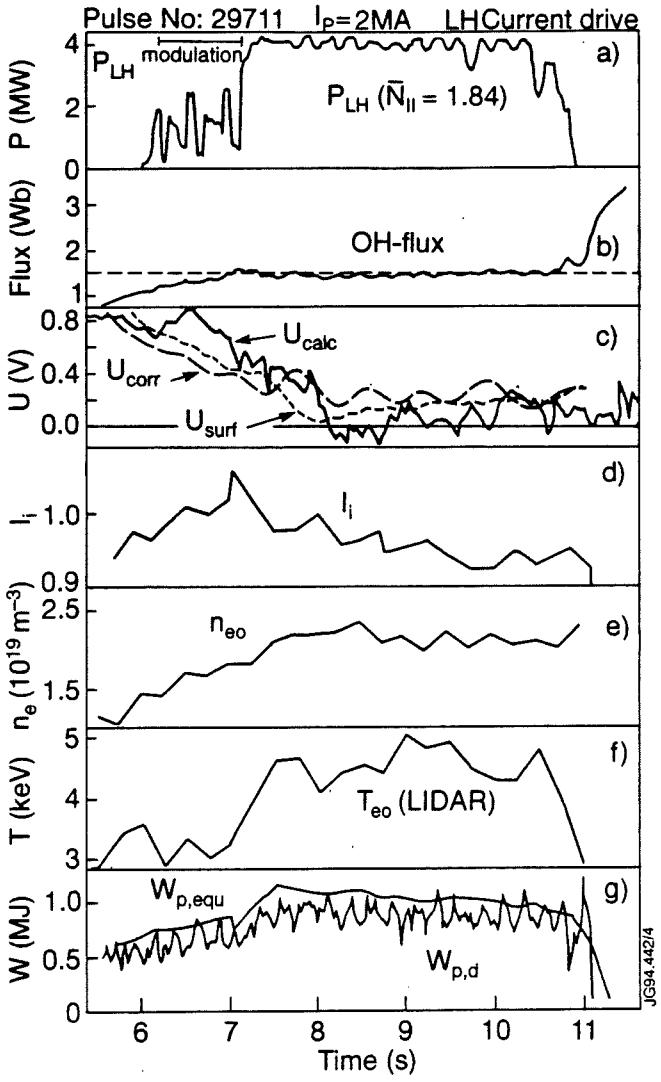

Fig. 1 *LHCD discharge at I_p = 2 MA, B_t = 2.8 T. LH power (a), OH flux consumption (b), measured, corrected and in TRANSP calculated loop voltage (c), central and line averaged electron density (d), central electron temperature (e), energy content from diamagnetic and equilibrium field measurements (f) and internal inductance (g).*

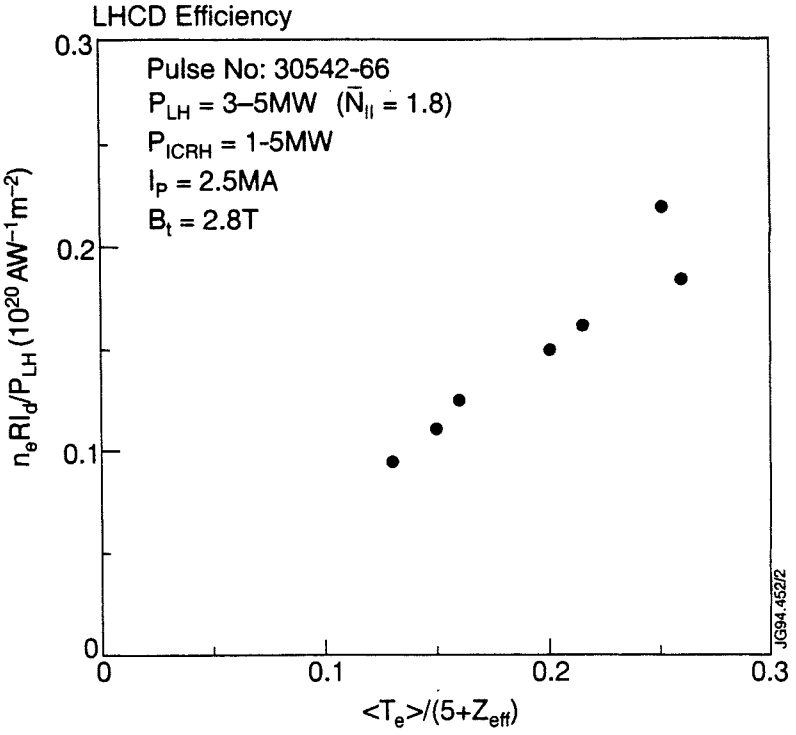

Fig. 2 *Scaling of the LH-current drive efficiency with volume averaged electron temperature and Z_{eff} in combined operation of LHCD + ICRH.*

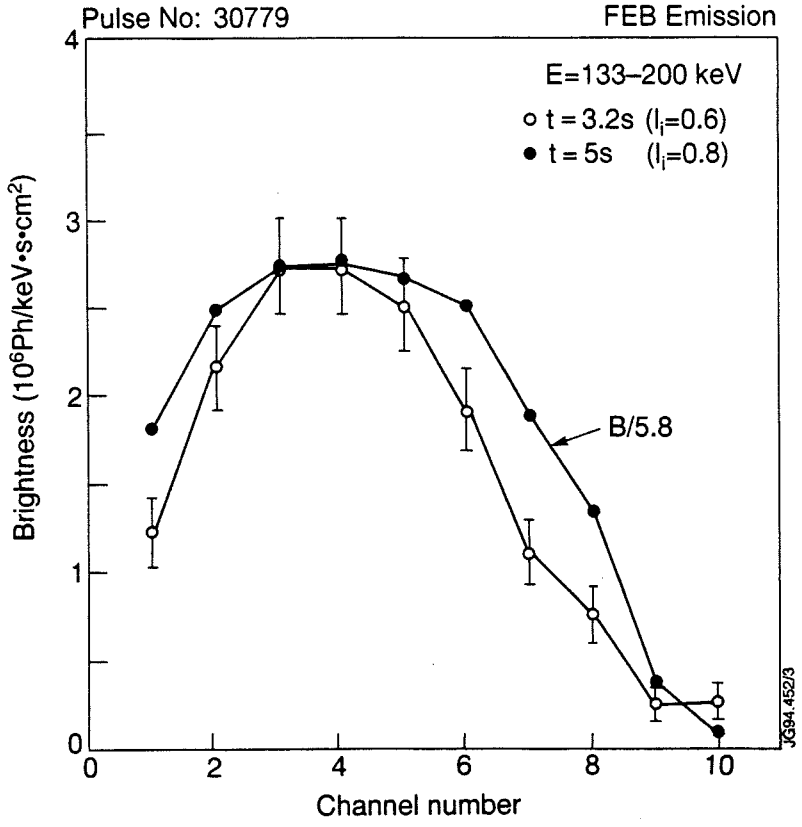

Fig. 3 *Fast electron bremsstrahlung (FEB) profiles during LHCD for two phases of a discharge with different current distributions. The FEB profile at 5 s is normalised to the profile at 3.2 s (scaling factor 5.8).*

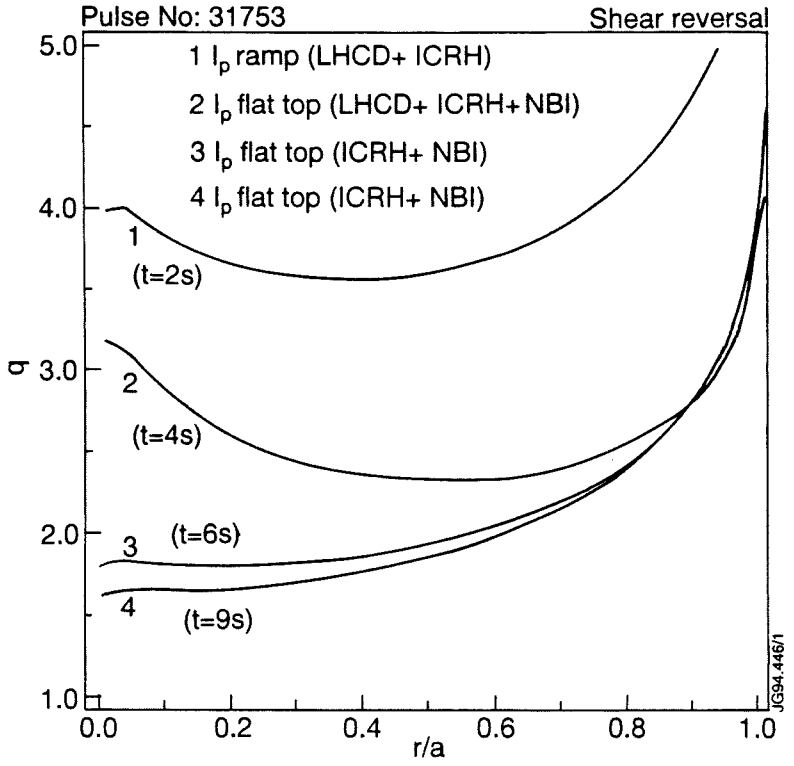

Fig. 4 *Temporal evolution of the q profile during a shear reversal discharge with combined application of LHCD, ICRH and NBI.*

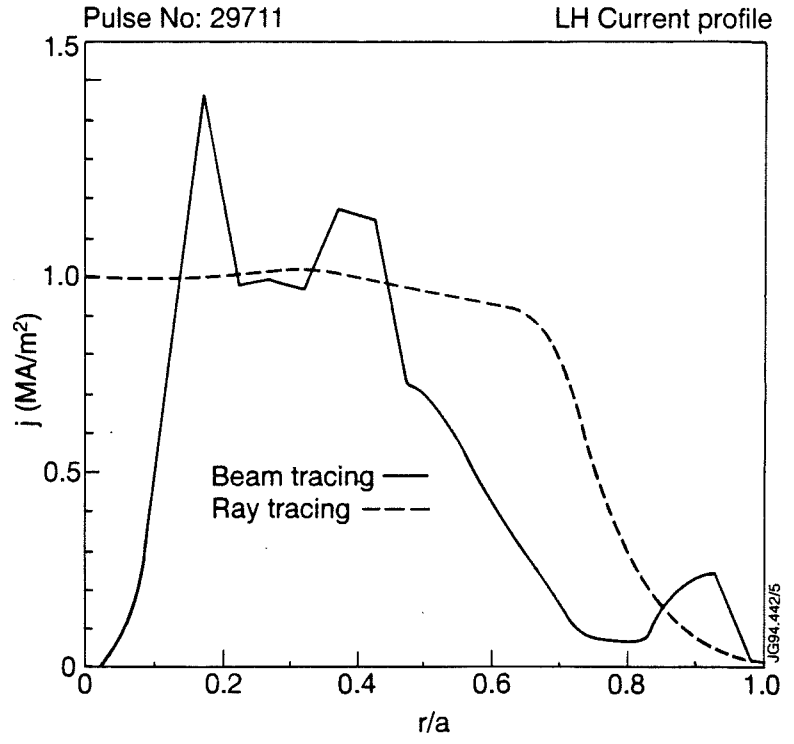

Fig. 5 *LH current deposition profiles from the BARANOV ray tracing code and TRANSP with the Pereverzev beam tracing code for discharge # 29711.*

Alfvén Eigenmodes and Alpha-Particle Losses in JET

W Kerner, L C Appel[1], M Cox[1], T C Hender[1], G T A Huysmans, M R O'Brien[1], S D Pinches[2], S E Sharapov[3], F S Zaitsev[4].

JET Joint Undertaking, Abingdon, Oxfordshire, OX14 3EA, UK.
[1] UKAEA/EURATOM Fusion Association, Culham, Abingdon, Oxfordshire, UK.
[2] University of Nottingham, Nottingham, UK.
[3] RRC Kurchatov Institute, Moscow, Russia.
[4] Moscow State University, Moscow, Russia.

ALFVEN EIGENMODES AND ALPHA-PARTICLE LOSSES IN JET

W. Kerner, L.C.Appel[1], M.Cox[1], T.C.Hender[1], G.T.A.Huysmans, M.R.O'Brien[1], S.D.Pinches[2], S.E.Sharapov[3], and F.S.Zaitsev[4]

JET Joint Undertaking, Abingdon, Oxon, OX14 3EA, UK.
[1]UKAEA/EURATOM Fusion Association, Culham, Abingdon, Oxon, UK.
[2]University of Nottingham, Nottingham, UK.
[3]RRC Kurchatov Institute, Moscow, Russia.
[4]Moscow State University, Moscow, Russia.

ABSTRACT

Fast α-particle losses in JET D-T discharges are studied in the context of neoclassical transport and anomalous losses of super-Alfvénic α-particles in the presence of unstable TAE's. It is found that in the Fokker-Planck treatment large orbit width effects need to be taken into account which leads to broader n_α profiles. In high performance JET discharges with $n_D \approx n_T$, typically, $n = 3$ TAE can be driven unstable. Such instabilities cause prompt α-losses scaling linearly with the TAE amplitude. Above the stochasticity threshold, which is fairly high in this case, anomalous α-particle diffusion sets in.

1. INTRODUCTION

The physics of α-particles in tokamaks is of particular interest and importance now that research into controlled fusion has reached thermonuclear parameters and D-T fuel has been used in JET and TFTR. One key issue for burning plasmas is transport. The magnitude of slow α-particle transport will determine the "Helium ash" content and therefore the dilution of the plasma. The level of fast α-particle transport, which is considered in this paper, will determine both the radial dependence of the source of Helium ash and the plasma heating profile. Studies of α-particle transport and losses feature in the TFTR D-T campaign [1] and are likely to feature in further D-T experiments in JET. In this paper we consider, for typical JET conditions, firstly fast α-particle neo-classical transport allowing for large drift orbit effects. Secondly, anomalous losses of super-Alfvénic α-particles in the presence of unstable TAE-modes are studied. The relevance of TAE-excitation in actual JET discharges can be verified experimentally by the Alfvén Eigenmode Active Diagnostic experiments in JET [2]. However, the problem whether unstable TAE's can cause significant anomalous losses of α-particles is of principal interest in itself. For this purpose we suppose some TAE's to be driven unstable and analyse the α-particle behaviour in the presence of finite-amplitude TAE's.

2. NEO-CLASSICAL ALPHA-PARTICLE TRANSPORT

The α-particle distribution f_α is calculated as a function of position, speed and pitch-angle using the FPP code [3]. The code solves the 3D trajectory-averaged Fokker-Planck equation [4] with terms for the α-particle source and the full collision operator including the neo-classical transport terms. The code has been tested by comparison with standard expressions for neo-classical ion fluxes, bootstrap current and toroidal conductivity, but is not restricted to large aspect ratios nor to distributions close to Maxwellian, unlike most neo-classical treatments. The collision operator can be integrated either over the full α-particle trajectories or over flux surfaces allowing an assessment of the importance of finite drift effects. Collisions are with background electron, deuterium and tritium Maxwellians. The α-particle source is isotropic in pitch-angle and monoenergetic (at 3.5MeV) with magnitude and profile determined by the background deuterium and tritium density and temperature profiles. Here we restrict the source to thermal-thermal fusion and neglect orbit losses. Also, the results here are steady-state, though a time-dependent simulation is used for the TFTR comparison and may be necessary for similar JET

comparisons. Parameters typical of JET were used for the simulations : R=3m; a=1.07m; κ=1.5; I_p=1, 3 and 5 MA; B_ϕ=3T; $n_e(r)=(0.9(1-r^2/a^2)^{1/2}+0.1)\ 5x10^{19}m^{-3}$; $n_D=n_T=0.4n_e$; $T_e(r)=(0.95(1-r^2/a^2)+0.05)$ x 10 keV; $T_D=T_T=2T_e$; $j(r)\sim(1-(r/a)^2)^2$ (which gives $q_o\sim1$ for I_p=3MA). Figure 1 shows the predicted profiles of α-particle density and plasma heating by the α-particles (which is largely electron heating) for I_p=1 and 3 MA.

On each graph the results of calculations with both flux surface- and trajectory-averaging are shown. As expected, the α-particle density rises with increasing I_p as the neo-classical transport drops. Also, the differences between surface- and trajectory-averaging reduce as I_p rises since the orbit widths drop. The trajectory-averaging gives a broader $n_\alpha(r)$ demonstrating the importance of including all large orbit width effects in the calculation. In the cases considered the transport time was long compared with the collision time and the α-particles had almost thermalised (energies $\sim10^2$ keV) by the time they left the plasma edge. Consequently the heating profile if orbit excursions are neglected is close to that deduced from the α-particle source (Figures 1(b) and 1(d)), though the orbit excursions significantly broaden the profile. These trends were confirmed by calculations for I_p=5MA (not illustrated).

Figure 2 shows, for the trajectory-averaged I_p=3MA case, velocity space contours of f_α at the inside and outside of the flux surface with r≈a/2. There is significant anisotropy in pitch-angle, unlike in standard slowing down approximations for f_α, showing that such approximations are inadequate for comparisons with α-particle measurements and that a fuller treatment as described here is required.

3. ALFVEN EIGENMODE SPECTRA AND PARTICLE LOSSES

In order to analyse the super-Alfvénic α-particle losses due to TAE's, the most unstable TAE's need to be identified. For typical JET parameters we calculate TAE-spectra, mode structure and continuum damping effect using the toroidal linear spectral code CASTOR [5]. For the analysis of driving and various damping mechanisms (ion Landau [6], trapped electron collisional [7,8] and radiative [9] dampings) a hybrid kinetic - MHD model is employed. The local TAE-stability analysis reveals that for low-m TAE-modes in JET ion Landau damping plays a dominant role; high-m TAE's are strongly suppressed by radiative and trapped electron collisional damping effects, and therefore TAE's of intermediate mode numbers, $m \sim 3 \div 6$, are the most dangerous. In particular, the TAE stability of a high performance deuterium JET discharge (#26087) was analysed, assuming $n_D = n_T$. It is found for this case that a modest decrease in density (and increase in temperature) destabilises the Alfven modes, and thus would permit their effects to be studied. The most likely candidates for TAE instability are found to be the n=3 modes. These n=3 eigenfunctions are used as input to a Hamiltonian guiding centre code with which collisionless losses due to TAE modes have been studied by Monte-Carlo simulations of 50,000 α-particles. The α-particles have a slowing down distribution with energies in the range 3.5MeV to 1.5MeV, a radial distribution varying as $(1-\Psi)^3$ and a random distribution in pitch, poloidal and toroidal angle. For these studies three n=3 TAE modes with normalised frequencies ω/ω_A=0.41, 0.51 and 0.58 have been used. Since these eigenmodes have been obtained from a linear simulation their amplitudes are arbitrary; here they are normalised so each eigenfunction has the same maximum radial field amplitude. As in Ref. [10] these Monte-Carlo simulations show two distinct classes of lost particles due to the n=3 TAE modes. Firstly there is a prompt loss of α-particles born near a loss boundary; co- and counter-passing particle prompt losses peak at ~3μs and trapped losses at ~6μs. These losses scale linearly with the applied TAE perturbation. Secondly above a stochastic threshold there is a steady long term loss of α-particles by stochastic diffusion into a loss boundary.

It can be seen from Fig 3 (d) that the majority of particles are lost just below the outboard mid-plane for the particular ∇B-drift direction used; this is due mainly to co-directed trapped particle orbits (see Fig 3(c)) intercepting the 'wall' (at $\theta \lesssim 0$).

We now examine the stochastic losses and diffusion in more detail. For passing particles the stochastic diffusion occurs in the presence of the TAE perturbations because the particle orbits and flux surfaces are relatively displaced causing side-band resonances. Stochasticity occurs when the particle excursions due to the primary and side-band [11] resonances overlap. With multiple TAE perturbations (of different frequency) stochasticity must be determined by the particle diffusion (or loss) which the TAE perturbations cause. As in Ref. [10] diffusion is measured by evaluating for an initially mono-energetic and mono-P_ϕ particle distribution, the spread of $\langle \Delta P_\phi^2 \rangle = \langle P_\phi^2 \rangle - \langle P_\phi \rangle^2$ in time (where $\langle\rangle$ denotes an ensemble average). Figure 4 (a) shows for the same n=3 TAE perturbations as used for Fig 3 the variation of $\langle \Delta P_\phi^2 \rangle$ with time for $\delta B_r/B=3\times10^{-3}$ and 5×10^{-4}; for these cases 500 particles are launched with an initial E=2.5MeV, $P_\phi=3.6\times10^{-19}$kgm^{2}s^{-1} and the particles are randomly distributed in pitch, poloidal and toroidal angles. For this case the stochasticity threshold is fairly high since the n=3 eigenmodes peak in a low shear region which increases the field amplitude required for island overlap [11]. Figure 4(b) shows for the $\delta B_r/B=3\times10^{-3}$ case the number of particles experiencing a given variation in P_ϕ. The smaller class experiencing a large variation are passing particles while the trapped particles have a small variation in P_ϕ.

ACKNOWLEDGEMENTS

The UKAEA authors were funded by the UK Department of Trade and Industry and by Euratom.

REFERENCES

[1] STRACHAN, J.D., et al., Physical Review Letters **72** (1994) 3526-3529. HAWRYLUK, R.J., et al., ibid. 3530-3533.
[2] FASOLI, A., et al. to be published, also: JET Progress Report 1993, EUR-JET-PR11, p.51.
[3] O'BRIEN, M.R., COX M., WARRICK, C.D., ZAITSEV, F.S., Proceedings of the IAEA Technical Committee Meeting on Advances in Simulation and Modelling of Thermonuclear Plasmas, Montreal 1992, IAEA (1993), p527.
[4] ZAITSEV, F.S., O'BRIEN, M.R., COX, M., Physics of Fluids B **5** (1993) 509-519.
[5] KERNER, W., et al., Plasma Phys. Contr. Fus. **36** (1994), 911.
[6] BETTI, R., FREIDBERG, J.P., Phys. Fluids B **4**, (1992) 1465.
[7] GORELENKOV, N.N., SHARAPOV,S.E. , Phys. Scr. **45**, (1992) 163.
[8] CANDY, J., ROSENBLUTH, M.N. Phys. of Plasmas 1, (1994) 356.
[9] METT, R.R. ,MAHAJAN, S., Phys. Fluids B4 (1992) 2885.
[10] SIGMAR, D.J., HSU, C.T., WHITE, R., CHEING, C.Z., Physics of Fluids B **4** (1992) 1506.
[11] BERK, H.L., BREIZMAN, B.N., Ye, H., Physics of Fluids B **5** (1993) 1506.

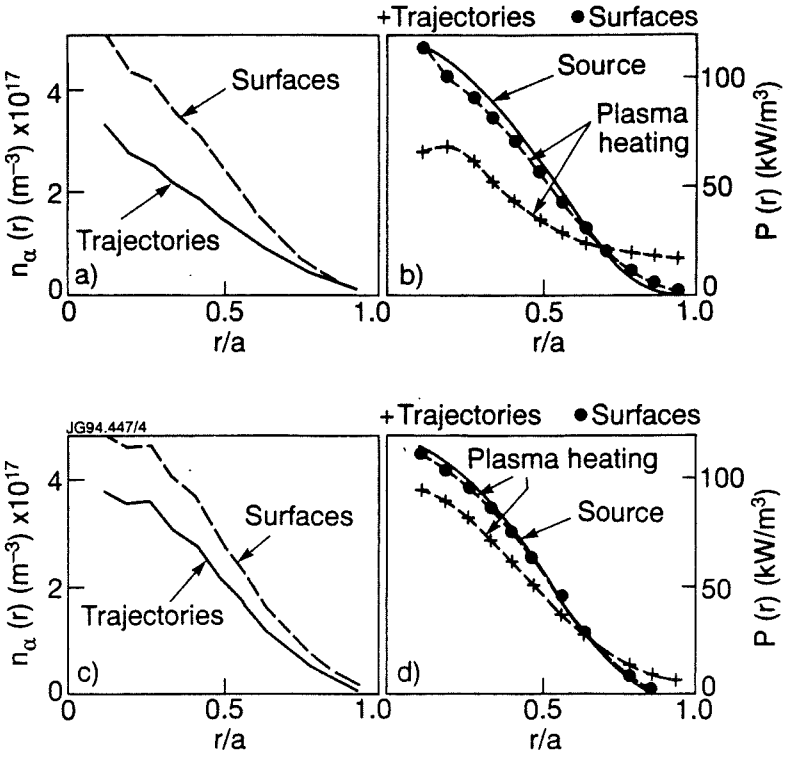

Fig. 1 *Comparison between surface- and trajectory-averaged calculations for I_p=1MA: (a) Alpha-particle density profile and (b) Alpha-particle source and plasma heating profiles, (c) and (d) as (a) and (b) but for I_p=3MA.*

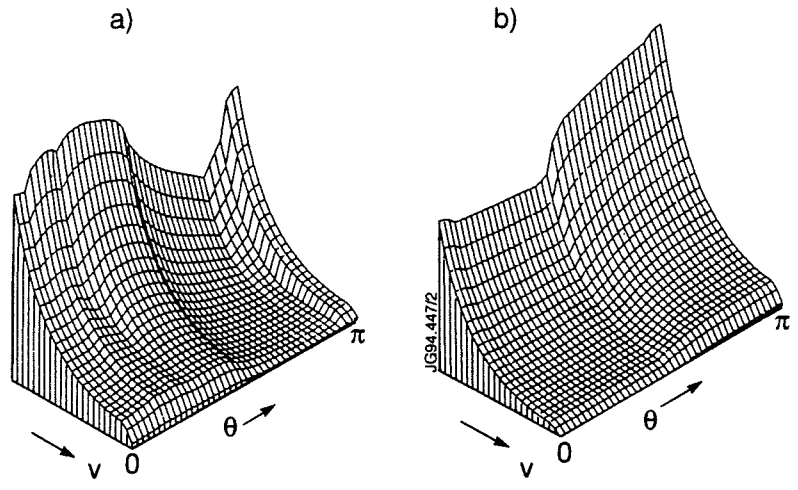

Fig. 2 *Contours of f_α as functions of speed and pitch-angle for I_p=3MA for the (a) outside and (b) inside of the flux surface with r≈a/2. The minimum and maximum energies plotted are 0.6 and 4 MeV.*

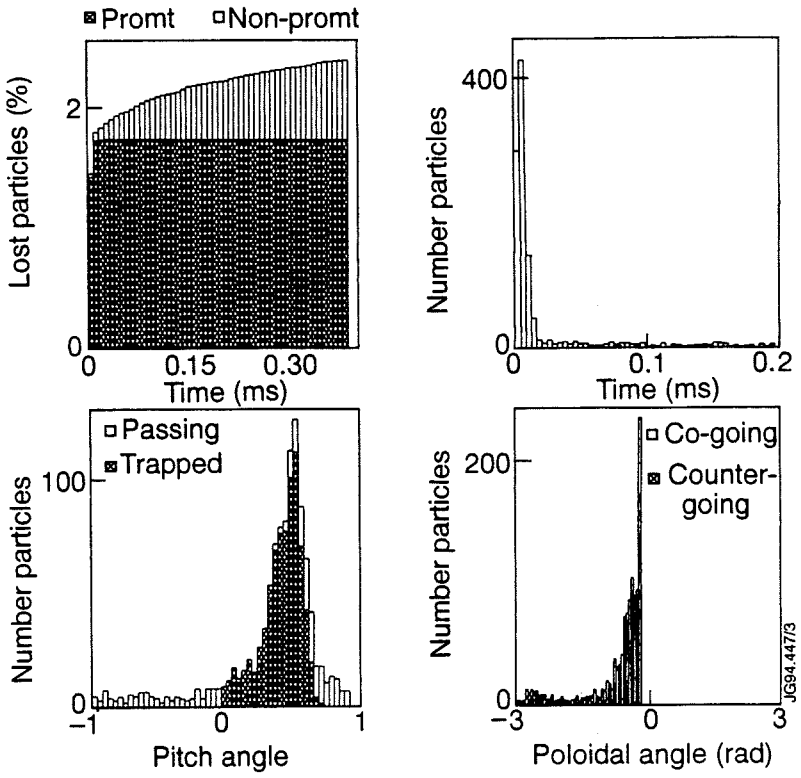

Fig. 3 *(a) Fraction of lost particles as function of time (b) Number of lost particles in 4μs bins with the birth type of the particles distinguished (c) and (d) total number of lost particles versus pitch angle and poloidal angle, respectively.*

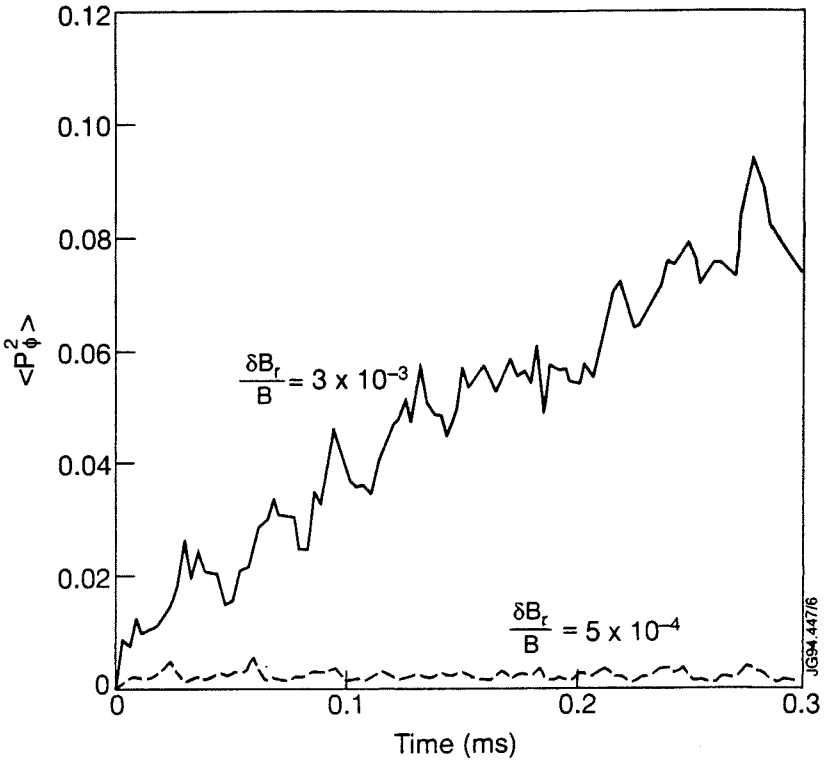

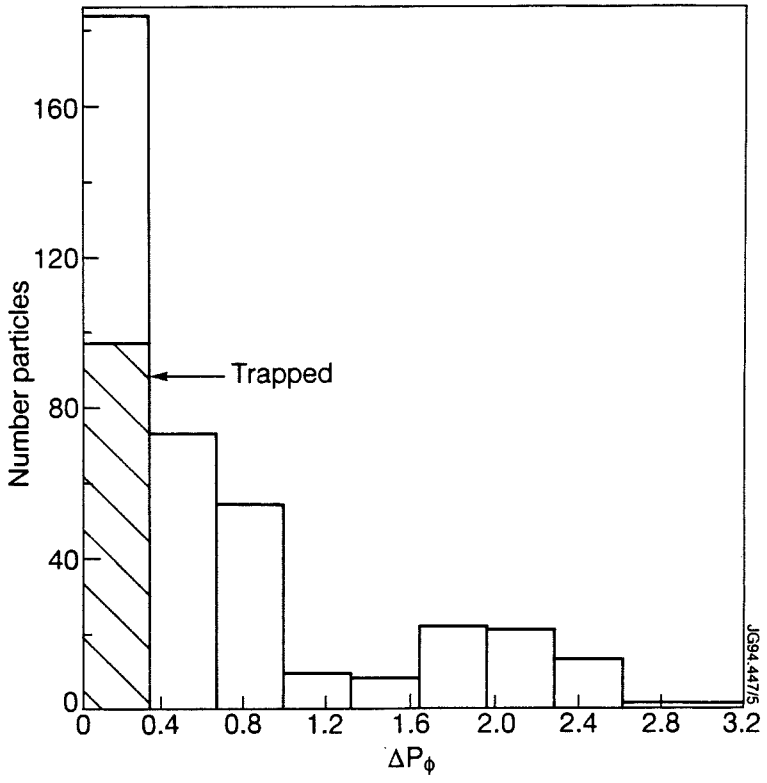

Fig. 4 *(a) Variation of $\langle \Delta P_\phi^2 \rangle x10^{+40}$ with time for $\delta B_r/B=3x10^{-3}$ and $5x10^{-4}$ (b) Number of particles with a given variation ΔP_ϕ for $\delta B_r/B=3x10^{-3}$, the shaded bars are trapped particles.*

The Physics of L and H-mode Confinement in JET

V V Parail[1], B Balet, P Bak, J G Cordey, N Deliyanakis, M Erba, R Giannella, D G Muir, M F F Nave, L Porte, E M Springmann, A Taroni, K Thomsen, G Vayakis.

JET Joint Undertaking, Abingdon, Oxfordshire, OX14 3EA, UK.
[1] Permanent Address: Russian Scientific Centre "Kurchatov Institute", Moscow, Russia.

THE PHYSICS OF L AND H-MODE CONFINEMENT IN JET

V.V. Parail[1], B.Balet, P.Bak, J.G. Cordey, N. Deliyanakis, M. Erba, R. Giannella, D.G. Muir, M.F.F. Nave, L. Porte, E.M. Springmann, A. Taroni, K. Thomsen and G. Vayakis.

JET Joint Undertaking, Abingdon, Oxon, OX14 3EA, UK
[1] Permanent address: Russian Scientific Centre "Kurchatov Institute", Moscow, Russia.

ABSTRACT

The results of numerical simulation of JET L, H and VH mode are presented. It is shown that L-H and H-L transitions are accompanied by a fast and large modification of the transport coefficients not only near the plasma edge but across a large fraction of the plasma cross section. Both experiments and numerical simulations show that giant ELMs on JET also have a global character and their penetration length increases with the amplitude of the D signal. Transport coefficients are of the order of the L-mode ones during these ELMs. Analysis shows also that within the experimental accuracy transport coefficients are the same for VH and ELM-free H mode JET discharges. The difference between them is mainly due to impurity radiation, power deposition profile and different in the plasma recycling and related convection.

1. INTRODUCTION

It has been shown[1], that the transport coefficients (electron and ion thermal diffusivities χ_e and χ_i, plasma diffusion coefficient D and perpendicular viscosity μ) in JET drop over a very wide radial region ($0.5 \le r/a \le 1$) in a very short time scale ($\Delta\tau \le 3$ms for χ_e) at the L-H transition. A possible explanation is that plasma turbulence is correlated in radial direction by the plasma toroidicity[2]. Therefore any modification of the anomalous transport coefficients (at L-H and H-L transitions and during ELMs) could propagate across the magnetic field with the group velocity of plasma turbulence (which is much faster than the velocity of heat pulse propagation). Results of transport analysis of JET discharges are presented which support this idea and allow us to develop transport models which can describe the evolution of plasma parameters in L, ELM-free and ELMy H-modes JET plasma.

2. EXPERIMENTAL RESULTS

Fig.1 shows the temporal evolution of the electron temperature at different radii measured by the new 48 channel ECE Heterodyne Radiometer for a typical low density discharge from the new campaign (#31078 with B_t=2.8T, I_p=2.5MA, $\bar{n}_e \cong 1.5 \cdot 10^{19} m^{-3}$, P_{NBI}=10MW) together with the D_α signal. It is seen that both L-H and H-L transitions are accompanied by an abrupt change of electron transport over a very wide radial region ($0.5 \le r/a \le 1$). The direct comparison of experimental evolution of electron temperature with one calculated under the assumption of either local or global modification of χ_e at the time of L-H transition for #31078 is shown in Fig. 2. This confirms our previous conclusion [4] about global modification of electron transport during the transition. To explain the fast response of the electron temperature using a local model for χ_e, one has to take an extremely nonlinear form for

$$\chi_e \sim \frac{|\nabla T_e|^{m+1}}{T_e^{\,m}} \quad \text{with } m \geq 20.$$

A global modification of plasma transport was also found to take place during giant ELMs. In particular it appears that each giant ELM on JET consists of a short (t≤1ms) broadband burst of MHD turbulence (Fig.3) followed by a much longer (t>>10ms) tail of enhanced transport which extends radially from the separatrix inwards for an extent depending on ELM's amplitude (Fig.4). This concept has been supported by recent measurements of density fluctuations during the L-H transition and giant ELMs, measured by a multi-channel, O-mode reflectometer, spanning the frequency range 18-70kHz, corresponding to critical densities in the range (0.4-6)x$10^{19}m^{-3}$. In the next section the result of numerical analysis of the plasma dynamics at the time of the L-H transition, during ELMs and in the ELM-free H and VH modes will be presented. The main objective of such analysis is to reveal the common and distinctive features of the transport in these regimes.

3. PREDICTIVE MODELLING

The evolution of electron and ion temperatures T_e and T_i was simulated while the plasma density, Z_{eff} and the radiated power were imposed from experiment. Power deposition profiles were taken from TRANSP analysis. The following model for electron and ion thermal diffusivities was used:

$$\chi_e = \frac{c^2}{\omega_{pe}^2}\frac{\varepsilon v_{Te}}{qR} + \alpha_e \frac{c|\nabla(nT_e)|}{eBn} aq^2, \quad \chi_i = \chi_i^{neo} + \alpha_i \frac{c|\nabla(nT_e)|}{enB} aq^2 \qquad (1)$$

where the first term on right hand side of χ_e reproduces neoalcator scaling, χ_i^{neo} is the ion neoclassical thermal conductivity and the second term on the right hand side of χ_e and χ_i is an empirical Bohm-like coefficient, proposed and used in [3] to reproduce L-mode confinement in JET. This analysis shows that the numerical coefficients α_e and α_i should be chosen $\alpha_i^{L} = 3\alpha_e^{L} = 9.9\cdot10^{-4}$ to fit JET L-mode discharges. We found that the best agreement with old and new JET shots is achieved if we assume that α_e and α_i are reduced from $\alpha_i^{L} = 3\alpha_e^{L} = 9.9\cdot10^{-4}$ in L-mode to $\alpha_i^{H} = 3\alpha_e^{H} = 0.54\cdot10^{-4}$ in H-mode plasmas. New boundary conditions for T_e and T_i were used in our analysis which correspond to an assumption that the longitudinal heat flux in the SOL is proportional to the particle flow: $\chi_{e,i} n \nabla T_{e,i}|_{r=a} = \beta_{e,i} D T_{e,i} \nabla n|_{r=a}$, where $D = \frac{\chi_e \chi_i}{\chi_e + \chi_i}$ and $\beta_e \sim \beta_i \sim 0.3$ are numerical parameters. These boundary conditions allow us to reproduce the formation of the temperature pedestal after the L-H transition (Fig.5) and to explicitly take into account convective losses.

In our analysis we also tried to quantify the difference between local energy transport in JET hot-ion VH mode and the ELM-free H-mode. To illustrate these points we chose the best hot-ion shot #26087 (B_t=2.8T, I_p=3.2 MA and P_{NBI} =14MW) from the previous campaign and two ELM-free H-mode from the current campaign- ##30591 (B_t=2.8T, I_p=2.5 MA and P_{NBI}=15MW) and 30725 (B_t=2.3T, I_p=3MA and P_{NBI}=7MW). The temporal evolution of the total measured plasma energy content and that calculated with our model during the ELM-free H-mode phase for all discharges are shown in Fig.6. They show that within the experimental accuracy we can fit both kind of shots with the same transport coefficients. The main differences between VH and ELM-free H-mode

lie not in transport properties but in the impurity radiation (the H-mode accumulates impurities much faster than the VH mode), power deposition profiles (centrally peaked for VH-mode and flat or even hollow for H-mode) and different level of convective losses (the latter is larger for #30591). This conclusion was recently confirmed by TRANSP analysis.

Finally we have used our transport model for numerical simulation of the giant ELMs. The idea was to find the radial and temporal distribution of enhanced transport during giant ELMs and the magnitude of the χ_e and χ_i increase. The analysis shows that giant ELMs can be modelled by assuming that the coefficients α_e and α_i have the following form: $\alpha_{e,i}^{ELM} = \alpha_{e,i}^{L} \exp\left\{-\frac{(t-t_0)}{\Delta t} + \frac{(r-a)}{\Delta r}\right\}$, where t_0 is the time of the beginning of ELM and Δt- its duration, Δr is the characteristic radial width of ELM. We chose shot #30952 from new campaign as a reference one because it contains ELMs of all sizes (see Fig.3). Our numerical analysis shows that we can reproduce the temporal and radial evolution of electron temperature by assuming that Δr increases as the D_α signal increases (Δr=40cm for ELM at t=51.47s and Δr= for ELM at t= 52.27s).

CONCLUSIONS

New experimental results from JET support the idea of a global character of plasma turbulence. Both transport analysis and predictive modelling show that the plasma transport coefficients (χ_e, χ_i, D and μ) experience very large (more than one order of magnitude) and very rapid reduction at a time of L-H transition not only near plasma edge but far inside plasma volume. The transport properties of ELM-free H-mode and VH mode on JET are very close. The difference between them is mainly due to the impurity radiation (which might be connected with plasma-wall interaction), power deposition profile and the different role of plasma convection. Finally experiment and numerical simulation show that giant ELMs on JET also have a global character and can be modelled as a temporary H-L transition triggered by an MHD event.

ACKNOWLEDGEMENT.

The authors are grateful to J.P. Christiansen, G. Fishpool, T.T.C. Jones, W. Kerner, K. Lawson, P. Lomas, O.P. Pogutse, R. Sartori, B. Schunke, P. Smeulders, P. Thomas and M.G. von Hellermann for fruitful discussions.

REFERENCES.

[1] Cordey, J.G., Muir, D.G., Neudachin, S.V., Parail, V.V., et al., Plasma Physics and Contr. Fusion, **36**, A267, (1994),
[2] Connor, J.W., Hastie, R.J., and Taylor, J.B. Proc. Roy. Soc. London Ser. A 365, 1 (1979),
[3] Taroni, A., Erba, M, Springmann, E., and Tibone, F. accepted for publication in Plasma Physics and Contr. Fusion,
[4] Parail, V.V., Cordey, J.G., Springmann, E. and Taroni, A. accepted for publication in Nuclear Fusion.

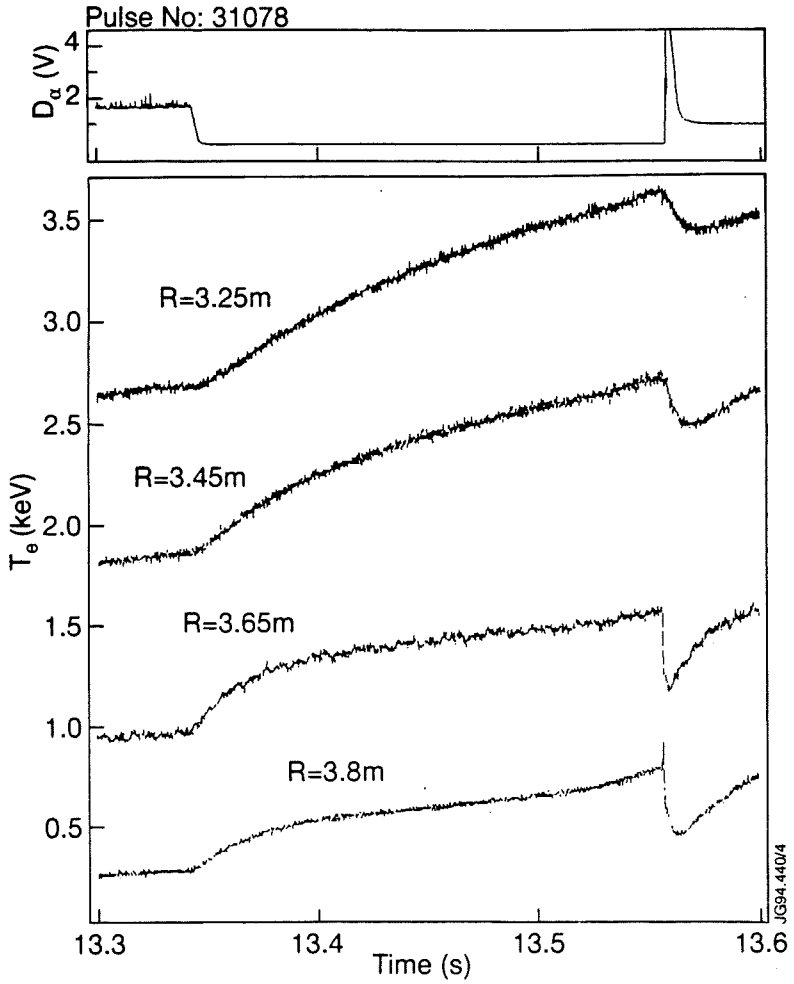

Fig. 1 *Temporal evolution of T_e at different radii and D_α signal for shot #31078.*

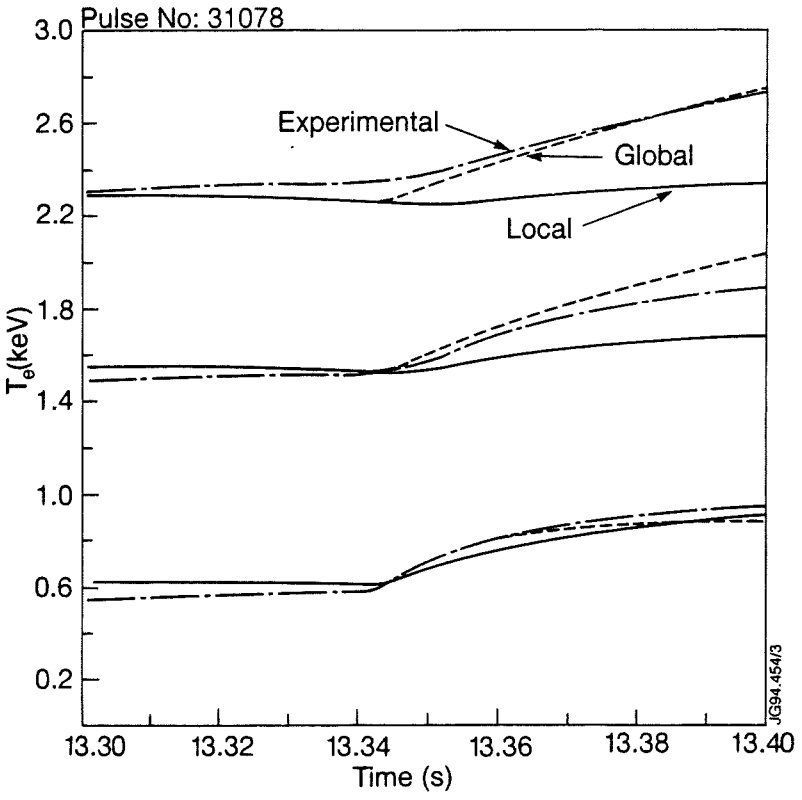

Fig. 2 *Temporal evolution of measured (chain) and calculated T_e under assumption of local (solid) and global (dotted) modification of χ_e.*

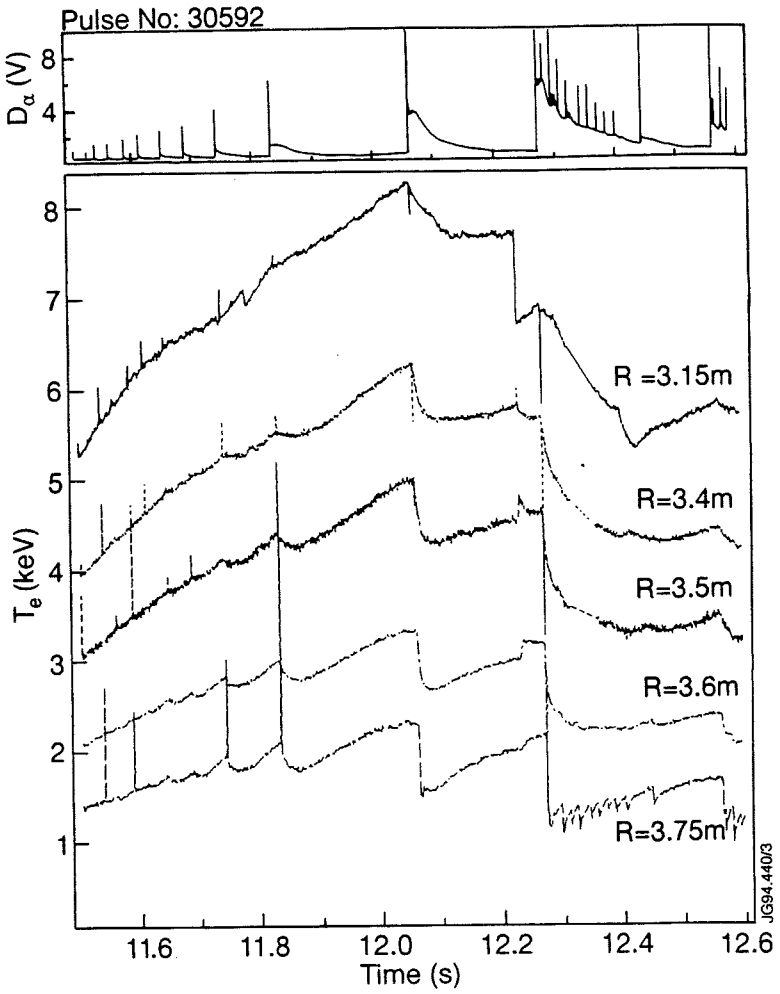

Fig. 3 *Evolution of D_α and fast MHD signals during giant ELM (shot #30929).*

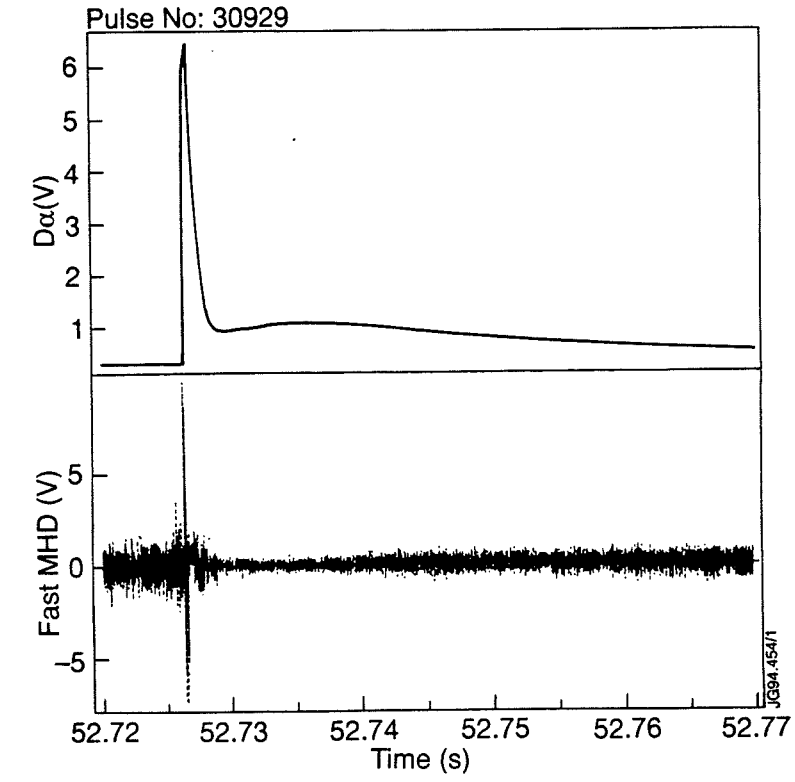

Fig. 4 *Temporal evolution of T_e at different radii and D_α signal for shot #30592.*

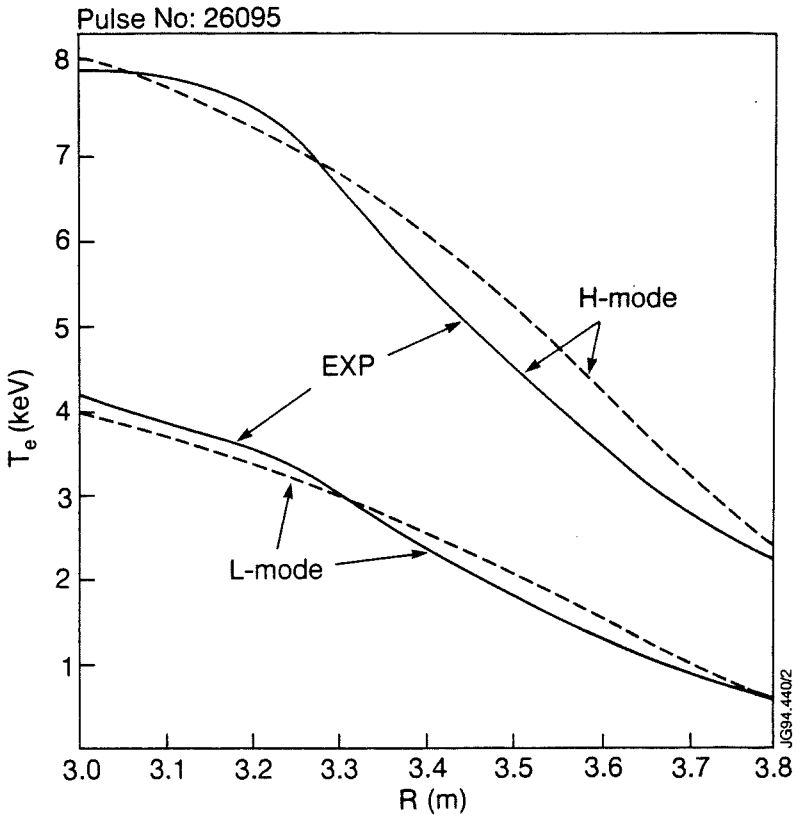

Fig. 5 *Measured and calculated T_e profile for L and H mode phase of shot II 26095.*

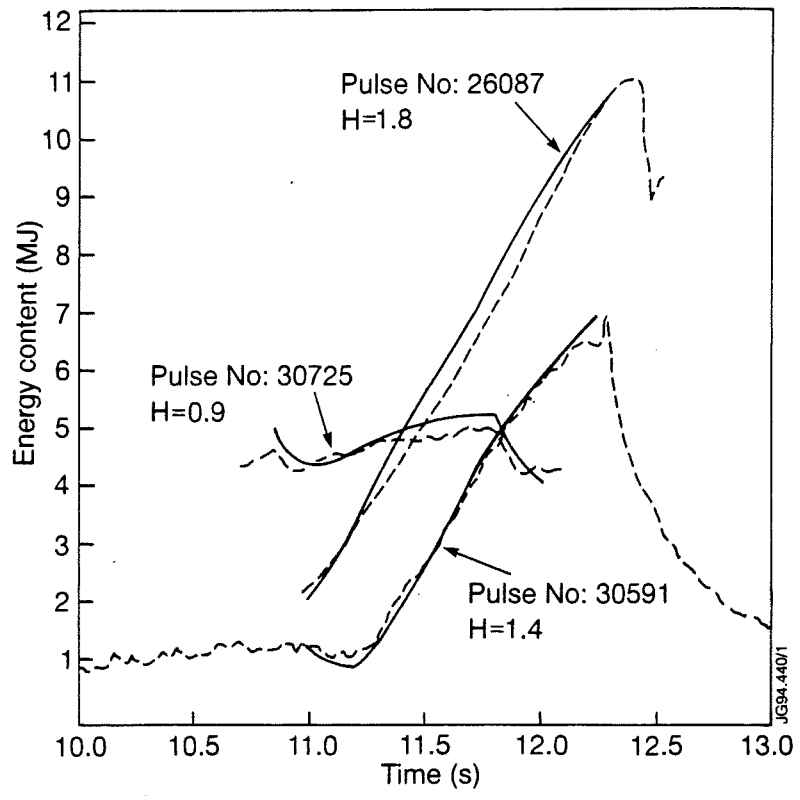

Fig. 6 *Temporal evolution of measured (dashed) and calculated (solid) plasma energy content for ELM free H-modes ($H=\tau_E/\tau_E^{ITER93\text{-}H}$)*

Nonlinear Collisionless Magnetic Reconnection and Fast Relaxations

M Ottaviani, F Porcelli.

JET Joint Undertaking, Abingdon, Oxfordshire, OX14 3EA, UK.

NONLINEAR COLLISIONLESS MAGNETIC RECONNECTION AND FAST RELAXATIONS

M. Ottaviani, F. Porcelli

JET Joint Undertaking, Abingdon, Oxon, OX14 3EA, UK.

ABSTRACT

We analyse the nonlinear stage of magnetic reconnection in collisionless and weakly collisional regimes. The reconnection time turns out at least an order of magnitude shorter than the Sweet-Parker-Kadomtsev time for values of the skin depth and of the magnetic Reynolds number typical of the core of large tokamaks.

INTRODUCTION

Laboratory plasmas close to thermonuclear conditions exhibit a variety of relaxation phenomena involving strong magnetic activity, the best studied being probably sawtooth oscillations[1]. A common feature of these phenomena is the fact that they become sharper in the largest, hottest devices like JET[2].

Renewed interest in the sawtooth crash problem was sparked by the observation that at the high plasma temperatures of these experiments sawteeth can occur on a time scale shorter than the electron-ion collision time. For example, Fig. 1 shows the position of the peak of the soft X-ray emissivity during a typical sawtooth crash in JET. By interpreting the position of the peak as the position of the magnetic axis, one can see that the displacement behaves roughly exponentially with time, covering a large fraction of the plasma radius in a timescale of order of $100\mu s$.

Since the sawtooth phenomenon is initiated by a reconnecting mode, the m=1 internal kink, those experimental findings have generated considerable interest in the problem of magnetic reconnection in collisionless or weakly collisional regimes, where electron inertia is responsible for the decoupling of the plasma motion from that of the magnetic field (See Refs.3-4 for an extended list of references).

The timescale predicted by the linear theory of m=1 kink-tearing modes is in good agreement with that observed in the experiments[3]. However the validity of the linear theory is limited by the condition that the displacement of the magnetic axis does not exceed the width of the reconnecting layer, in practice the electron skin depth or the ion Larmor radius, whichever is larger. In order to explain experimental results like those shown in Fig. 1, a nonlinear analysis is required. In particular one needs to understand the dynamics in the early nonlinear stage, $\delta_{linear} << \lambda << a$, where λ is the displacement, δ_{linear} the width of the reconnection layer as given by linear theory and a is the plasma radius.

MODEL AND RESULTS.

Our study of collisionless reconnection employs an extension of reduced MHD on a two-dimensional slab, where the electron inertia terms, proportional to the square of the electron skin depth $d_e = c/\omega_{pe}$ is added in Ohm's law. Larmor radius terms, although formally of the same order as the skin depth terms, are initially neglected as they are not sufficient to decouple the motion of the plasma from the magnetic field lines. We therefore consider the coupled equations:

$$\partial_t U + [\varphi, U] = [J, \psi] + \mu_i \nabla^2 U, \tag{1}$$

$$\partial_t F + [\varphi, F] = \eta \nabla^2 (\psi - \psi_o) - \mu_e \nabla^4 \psi, \tag{2}$$

where $[A,B] \equiv e_z \cdot \nabla A \times \nabla B$, with e_z the unit vector along the z direction. $U = \nabla^2 \varphi$ is the fluid vorticity, φ is the stream function, $J = -\nabla^2 \psi$ is the current density along z, ψ is the magnetic flux function, ψ_o is the equilibrium flux function, $F \equiv \psi + d^2 J$ is the total electron canonical momentum in the toroidal direction and d is the skin depth. The dissipative effects we have included are the ion viscosity μ_i, the electrical resistivity η and the electron viscosity μ_e. Since the equations are normalised these dissipation coefficients must be interpreted as the inverse of Reynolds-like numbers.

The co-ordinates x and y vary in the intervals $x \in [-L_x, L_x]$ and $y \in [-L_y, L_y]$, with the slab aspect ratio $\varepsilon \equiv L_x/L_y < 1$ (Here we choose $\varepsilon = 1/2$). Periodic boundary conditions are imposed at the edge of these intervals. Length and times are normalised to the slab width and to the (poloidal) Alfven time respectively.

The initial condition is a tearing-unstable equilibrium without flow, $J_o = \psi_o = \cos x$ ($L_x = \pi$) with the addition of a small $m = 1$ perturbation in the unstable direction. Most of our studies were carried out with $d/2L_x = 0.04$ so that the logarithmic jump Δ' of the linear eigenfunction across the reconnecting layers is such that $\Delta' d \geq 1$. In this *large-Δ'* regime the mode structure has global character, resembling the eigenfunctions of the $m = 1$ internal-kink, $\varphi_L \approx \varphi_\infty \operatorname{sign} x$ everywhere except in narrow layers near the reconnecting surfaces. Moreover, with our choice of ε, only the m=1 mode is unstable.

The collisionless equations ($\mu_i = \mu_e = \eta = 0$) were studied numerically and analytically in Ref.4. Here we only summarize the main results.

Initially, in the linear stage, the system evolves exponentially with a growth rate $\gamma \approx d$ until $\lambda \approx d$. By this time the current density perturbation $\delta J = J - J_{eq}$ around the X-point has become of the order of the equilibrium current density.

In the nonlinear stage a current spike of width *d*develops around the X-point. An analytic calculation based on the conservation of F shows that δJ behaves like $\delta J \approx (\lambda/d) \ln(d/x)$ at a distance x from the X-point, $x < d$. The logarithmic singularity is cut off by a new nonlinear time-dependent microscale $\delta(t) \equiv d \exp[-\lambda(t)/d]$ so that at the X-point $\delta J_X \approx (\lambda/d)^2$. No singularity occurs in the flux function to the leading order: $\delta\psi_X \approx \lambda^2$ for $x < \lambda$.

In the nonlinear stage the reconnection proceeds faster than exponentially as far as numerically observable and arguably until the displacement reaches a macroscopic size. This is confirmed by an analytic equation for λ which predicts

an explosive time dependence in the early nonlinear stage. Thus the overall reconnection time in the purely collisionless case scales like $\tau_{rec} \approx d^{-1}$, in substantial agreement with Ref.5.

The nonlinear microscale δ becomes rapidly small. Thus, additional physical effects not included in the simple collisionless model eventually come into play and δ is replaced by some other scalelength as a cutoff. In order to understand the experimental results one must identify which of the many possible cutoff mechanisms is relevant in a particular situation. Moreover it is crucial to verify whether the reconnection can proceed at a fast rate even in the presence of spike-limiting mechanisms.

Here we discuss the role of a small amount of dissipation in the form given in Eqs. (1-2). A variety of cases with $\mu_e \neq 0$ and/or $\eta \neq 0$ have been considered, all of them possessing the same linear eigenfunctions and growth rate but differing in the nonlinear phase (Fig. 2).

A pure resistive case ($\eta = 3.\times 10^{-3}$ and $d = 0$) is found to follow the Sweet-Parker scenario. By contrast, a moderate resistive case with finite electron inertia ($\eta = 1.5\times 10^{-3}$ and $d/2L_x = 0.028$) behaves essentially in a collisionless fashion: resistivity (at this value) is ineffective as cut-off mechanism. This is understood by inspecting Ohm's law (2) using the previously given expressions for the flux function and for the current. One can see that the resistive term in the spike region is bounded to $O(\eta\lambda^2/d^2)$ which is smaller than the l.h.s. of Eq. (2) as long as $\eta < \gamma_{linear} d^2$ (or $\eta^{1/3} < d$) (the resistivity term is a regular perturbation). When this occurs the resistivity can also be neglected in the linear theory and it is never important.

On the other hand, the electron viscosity term is $O[\mu_e(\lambda/d)(1/x^2)]$ and can balance the leading collisionless terms at a sufficiently close distance from the X-point for any value of μ_e. Thus the electron viscosity is an efficient cut-off mechanism. Note that not only the true (collisional) viscosity but also any process acting as a current hyper-resistivity would be an equally effective candidate. This idea has been confirmed by running simulations with μ_e in the range $4.\times 10^{-7} \leq \mu_e \leq 6.4\times 10^{-6}$ (with $d = 1/4$). One can see that the microscale (Fig. 2a) is strongly affected by the viscosity. On the other hand the growth of δJ_X is not slower than exponential even when the viscosity is switched on (Fig. 2b). Thus the total reconnection time is substantially unaffected. Therefore the presence of a viscous cutoff (as long as it is smaller than the skin depth) does not alter the conclusion that reconnection continues to proceed at a fast rate in the nonlinear stage.

For bigger resistivity, when $d < \eta^{1/3}$, the electron inertia is negligible in the linear phase and the displacement grows with $\gamma_{linear} \approx \eta^{1/3}$ until it is of order of the width of the linear layer $\lambda \approx \delta_{linear} \approx \eta^{1/3}$. In the nonlinear stage the system is expected to follow the Sweet-Parker scenario with the layer width shrinking as $\delta_{nonlinear} \approx (\eta/\lambda)^{1/2}$ while the displacement grows as a power law $\lambda \approx \eta t^2$. If $d < \eta^{1/2}$ (*strong collisionality*) the displacement reaches the macroscopic size $\lambda \approx 1$, where $\delta_{nonlinear} \approx (\eta)^{1/2}$, in the characteristic Sweet-Parker-Kadomtsev time $\tau_{SPK} \approx \eta^{-1/2} \approx (\tau_{Alfven}\tau_{Resistive})^{1/2}$. If however the skin depth falls in the intermediate range $\eta^{1/2} < d < \eta^{1/3}$ (*moderate collisionality*) the electron inertia becomes again important when $\delta_{nonlinear} \approx d$[6]. This occurs at some value of the displacement $\lambda^* \approx \eta/d^2$ after a time $t^* \approx d^{-1}$. Afterwards we expect that the

reconnection will proceed essentially in a collisionless fashion until $\lambda \approx 1$. The reconnection time is therefore controlled by the electron inertia, $\tau_{rec} \approx d^{-1} << \tau_{SPK}$, as long as $d < \eta^{1/2}$, throughout the collisionless and the moderate collisionality regimes. The borderline between these regimes is typical of large tokamak sawteeth and it is therefore of especial experimental interest. Here the reconnection time turns out at least an order of magnitude shorter than the Sweet-Parker-Kadomtsev time: $\tau_{rec} / \tau_{SPK} \approx \eta^{1/6} < 10^{-1}$.

For typical high temperature JET parameters, $\eta^{1/3} \approx d \approx 3.\times 10^{-3}$ (the skin depth is normalized to the $q = 1$ radius). After a linear phase, where resistivity and electron inertia are of comparable importance, the nonlinear evolution of $m = 1$ modes is controlled by collisionless effects. The reconnection time $\tau_{rec} \approx \tau_A / d$ is of order of 100μs. Ion Larmor radius effects can shorten this time by up to a factor three[3,8,9].

The fluid model we have investigated has a number of limitations, as discussed in Ref.7. However the indications from our analysis are that the occurrence of a rapid nonlinear stage, when the system evolves faster than the Sweet-Parker-Kadomtsev timescale, is a fairly general phenomenon in weakly collisional systems characterised by large values of the Δ' parameter.

REFERENCES

[1] S. von Goeler, W. Stodiek and N. Sauthoff, Phys. Rev. Lett. **33**, 1201 (1974).

[2] A. W. Edwards et al, Phys. Rev. Lett. **57**, 210 (1986).

[3] F. Porcelli, Phys. Rev. Lett. **66**, 425 (1991).

[4] M. Ottaviani and F. Porcelli, Phys. Rev. Lett. **71**, 3802 (1993).

[5] J. Wesson, Nucl. Fusion, **30**, 2545 (1990).

[6] M. Ottaviani and F. Porcelli, Proceedings of the 1994 EPS Conference, Montpellier.

[7] M. Ottaviani and F. Porcelli, Proceedings of the 1994 Int. Workshop on Theory of Fusion Plasmas, Varenna.

[8] L. Zakharov, B. Rogers and S. Migliuolo, Phys. Fluids **B5**, 2498 (1993).

[9] A. Y. Aydemir, Phys. Fluids **B4**, 3469 (1992).

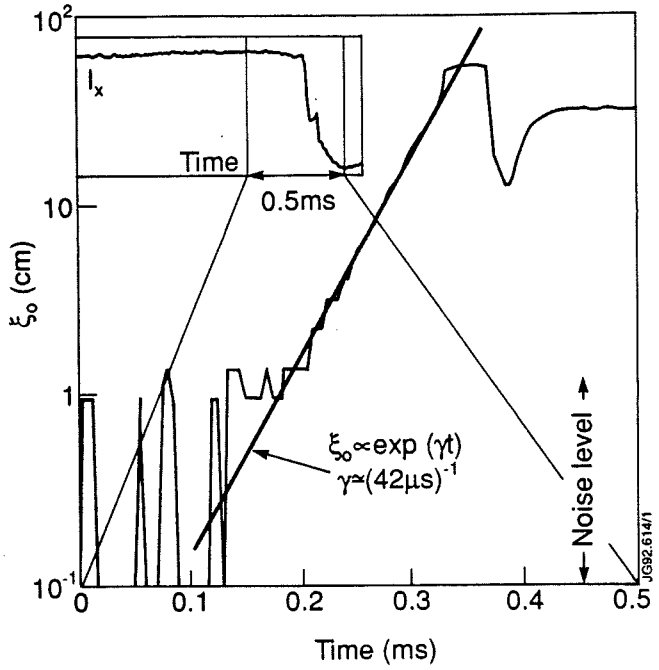

Fig. 1 *Evolution of the position of the peak of the soft X-ray emissivity during a fast sawtooth crash in JET.*

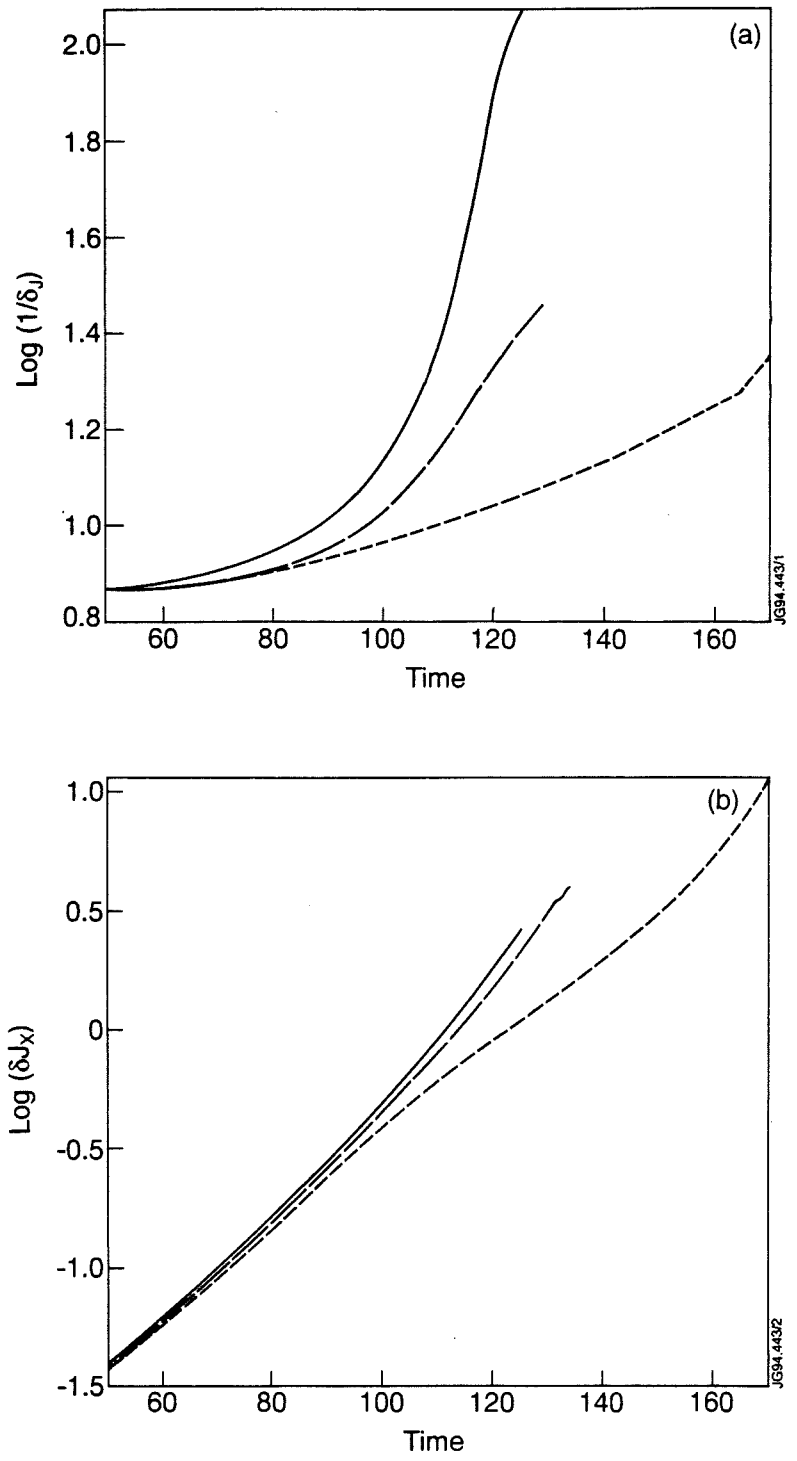

Fig. 2 *Decimal logarithm of a)* $\delta_J^{-1} = (\partial_x^2 \delta J)^{1/2}$ *and b)* δJ *at the X-point vs time. Solid lines: collisionless case. Long dash: with electron viscosity* $\mu_e = 6.4 \times 10^{-6}$. *Short dash: pure resistive case* $\eta = 3. \times 10^{-3}$.

Alfvén Eigenmodes Active Excitation Experiments in JET

A Fasoli[1], S Ali-Arshad, D Borba, G Bosia, D Campbell, J A Dobbing, C Gormezano, J Jacquinot, P Lavanchy[1], J Lister[1], P Marmillod[1], J-M Moret[1], A Santagiustina, S Sharapov.

JET Joint Undertaking, Abingdon, Oxfordshire, OX14 3EA, UK.
[1] CRPP/EPFL, 21 av. des. Bains, CH-1007 Lausanne, Switzerland.

ALFVEN EIGENMODES ACTIVE EXCITATION EXPERIMENTS IN JET

A.Fasoli[1], S.Ali-Arshad, D.Borba, G.Bosia, D.Campbell, J.A.Dobbing, C.Gormezano, J.Jacquinot, P.Lavanchy[1], J.Lister[1], P.Marmillod[1], J.-M.Moret[1], A.Santagiustina, S.Sharapov

JET Joint Undertaking, Abingdon, Oxon, OX14 3EA, UK
[1] CRPP/EPFL, 21 av.des Bains, CH-1007 Lausanne, Switzerland

ABSTRACT

The newly installed JET Alfven Eigenmodes (AE) active diagnostic is described along with the first experimental results. The aim of this diagnostic, which is based on external antenna excitation and synchronous detection of the plasma response, is a systematic study of the AE properties, in particular in terms of damping and stability. Direct information on frequencies, mode structures and, most importantly, damping rates of the excited global resonances can be obtained. TAE modes have been excited and identified by the dependence of their frequency upon magnetic field and density. The first direct measurements of the AE damping rates in different regimes corresponding to distinct dominant absorption mechanisms are reported.

1. INTRODUCTION

The understanding of the interaction between magnetically confined toroidal plasmas and fusion generated alpha particles is one of the key issues in the preparation of thermonuclear ignition experiments. In tokamaks and stellarators, energetic particles generated by fusion reactions or additional heating can excite via resonant interaction global Alfven Eigenmodes (AE), which can in turn trigger anomalous fast particle losses [1]. The parameter space over which ignition and safe operation can be achieved may be limited in the presence of these instabilities both by the induced degradation of alpha confinement and by the possible first wall damage due to localised energy deposition by the mode scattered resonant particles [2]. The natural occurrence of Alfven Eigenmodes is related to the balance between different damping mechanisms and the fast particle driving. AE spectra, mode structures and instability thresholds can be investigated by simply observing fluctuations in the appropriate frequency range [1]. Energetic particles driven AE activity has been reported for NBI and ICRH heated discharges in different tokamaks, including JET [3]. These passive measurements, however, cannot provide quatitative information concerning damping and driving effects. A more comprehensive understanding of the MHD activity in the Alfven regime can be reached via a study of the plasma response to externally driven perturbations. External antenna excitation and coherent detection of different probing signals at the edge and in the plasma core are combined in the Alfven Eigenmodes active diagnostic at JET. Such a diagnostic has the unique advantage of providing a direct measurement of the damping rates of the Alfven Eigenmodes in different plasma conditions.

2. EXPERIMENTAL SET-UP

i) Active antenna excitation

The JET saddle coil antennas are used to excite the Alfven Eigenmodes. The launching apparatus, developed to cover the frequency range of pressure, toroidicity and ellipticity induced AE (30 to 500 kHz), encompasses a remotely controllable function generator, a 3 kW broad band power amplifier, an impedance matching network, a power distribution and an isolation unit. The power distribution unit connects the amplifier output to the active antennas,

allowing different combinations of antenna phasing that can preferentially excite specific toroidal and/or poloidal mode numbers (n: all, odd, even, (2,6,...), (4, 8,...); m: odd, even). Input current and voltage are measured at the distribution unit, whilst the voltage measurements on both the active and passive saddle coils are taken at the isolation unit. Currents on the saddle coils are measured at the end of the 80 m transmission line. Maximum currents and voltages induced in the saddle coils by the AE exciter in the present configuration are of the order of 30 A and 500 V, respectively. Correspondingly, the magnetic perturbations in the plasma are predicted to be such that $\delta B/B<10^{-5}$. As a result, the excited AE amplitudes are not expected to enhance the transport of energetic particles.

ii) Diagnostic method

The excitation frequency is swept across the shear Alfven gap regions, where AE are expected. The plasma response is extracted from background signals via homodyne detectors, providing in phase and quadrature components of the signals, or, in a complex representation, their real and imaginary parts. Different probing channels are considered: The voltage and current of the excited saddle coils provide the antenna impedance. The induced voltage on the passive saddle coils and the fast magnetic coils measure the perturbation of the radial and poloidal B-fields, allowing a mode analysis both in the poloidal and toroidal conjugate planes. Other non-magnetic diagnostics, such as heterodyne ECE and reflectometry, will be coupled to the synchronous detectors to reconstruct the radial structure of the excited global mode.

3. DATA ANALYSIS AND REPRESENTATION

The antenna-plasma-detectors transfer function can be directly obtained by dividing the complex amplitude of the different probes response by that of the current driven in the active antenna. The individual AE manifest themselves as resonances in the transfer function, which can be expressed as

$$H(\omega)=\frac{a+ib\dfrac{\omega}{\omega_0}}{1-\left(\dfrac{\omega}{\omega_0}\right)^2+i\dfrac{2\gamma}{\omega_0}\dfrac{\omega}{\omega_0}}$$

where ω is the angular frequency of the exciter signal, ω_0 the resonance (real) frequency and γ the damping rate. a and b are real numbers that, for small damping ($\omega_0>>\gamma$), are proportional to the in phase and quadrature components of the detected signals. To represent the plasma resonance in terms of complex conjugated poles (p, p*) and residues (r, r*), the complex transfer function H is decomposed in partial fractions. If several (N/2) resonances occur in the measurement range, this representation reads

$$H(\omega,x)=\sum_{n=1}^{N/2}\frac{1}{2}\left(\frac{r_n(x)}{i\omega-p_n}+\frac{r_n^*(x)}{i\omega-p_n^*}\right)=\frac{B(x)}{A}$$

where $p=i\omega_0+\gamma$ and x indicates explicitly the space dependence of a diagnostic signal. B and A denote polynomials in $i\omega$ with real coefficients and degree N-1 and N, respectively. For a given resonance only the numerators (the residues) depend upon the position, whilst the denominators, i.e. the poles, are common. Since the signals may contain direct coupling with the antenna, an additional quantity, dependent upon position, must be added

$$H(\omega,x)=\frac{B(x)}{A}+D(x)=\frac{B'(x)}{A}$$

B'(x) can have a higher degree than B(x) to account for the antenna-probe coupling transfer function. The data analysis, based on the fit of a set of space resolved measurements of complex transfer functions with rational functions in $i\omega$ with real coefficients [4], leads to a representation of the eigenmodes in terms of complex poles and of the corresponding space dependent residues. The latter correspond to a measurement of the wave amplitude as a function of space, i.e. of the single mode structure. The pole provides two pieces of information. Its imaginary component gives the actual frequency of the mode, ω_0. When no fast particle driving terms are present in the plasma, the real part of the pole, γ, corresponds directly to the damping rate. For modes which are stable but for which a finite fast particle induced growth rate exists ($\gamma_{drive} \neq 0$, $\gamma_{damping} > \gamma_{drive}$), γ is the difference between the damping rate and the growth rate: $\gamma=\gamma_{damping} - \gamma_{drive}$. The cases of marginally stable ($\gamma_{drive} \sim \gamma_{damping}$) and unstable modes ($\gamma_{damping} < \gamma_{drive}$) are more complicate and would necessitate a data analysis in terms of non-linear models. Note that the synchronous detection chain can also be used in passive mode, with the reference frequency being swept across the expected AE frequency domain, but with no current driven in the saddle coils. In this case the frequency and amplitude of an unstable mode can be estimated, but, due to the lack of knowledge of the driving source spectrum, no information on its damping can be gathered.

4. FIRST EXPERIMENTAL RESULTS

i) Passive studies

Preliminary passive studies using two saddle coils and five magnetic probes indicated some broad band ($\Delta f>30$ kHz) activity around the TAE frequency, f_{TAE}, when neutral beam heating at moderate power is applied to the JET diverted plasmas ($f_{TAE} \cong v_{Alfven}/(4\pi qR_0)$ and $v_{Alfven}=B/(4\pi n_i m_i)^{1/2}$) . These studies helped in identifying the frequency domain of interest for the first phase of the active studies, which have subsequently been undertaken in the range 60-180 kHz.

ii) Results with active AE excitation

In this region several Eigenmodes have been clearly observed in the ohmic phases of JET pulses in different plasma configurations. An example of a resonance seen in an ohmic plasma is shown in Fig.1. When the frequency is swept across the resonance, the magnetic probe signal amplitude describes a circle in the complex plane. The maximum value of the perturbed magnetic field measured by the pick-up coil is of the order of 10^{-6} T. The relatively low damping rate ($\gamma/\omega \cong 1\%$) seems to suggest the absence of continuum damping.

iii) Eigenmode identification

To verify the 'Alfvenic' character of the observed resonance, the dependence of the observed resonance frequency upon the magnetic field and density was investigated. In the first case (Fig.2) only the toroidal magnetic field is varied. The measured frequency agrees with f_{TAE} calculated with the simplifying assumption that q=1.5, which for realistic JET profiles corresponds to the most unstable TAE mode [5]. The damping coefficient is not observed to vary throughout the scan. Fig.3 shows a case in which the density is varied, with toroidal field and plasma current practically constant. The observed mode frequency follows the calculated f_{TAE}. These two results clearly show that the observed resonances are related to the Toroidal Alfven Eigenmodes. Quality factors ($Q=\omega/\gamma$) of the order of ten at the beginning of the scan suggest that in this regime continuum damping can be responsible for the mode absorption. After $t \cong 49$s, the profiles are modified in such a way that $n(r)q^2(r)$ becomes approximately constant, and a second regime, in which the Alfven gaps are open and no continuum damping is possible, is entered.

iv) Effect of variations in the plasma current

A scan in the plasma current, for constant toroidal field, was performed in shot #31638. Variations in the mode frequency as well as in its damping coefficient clearly appear in the AE data (Fig.4). The observed frequency does not follow the simply calculated f_{TAE}, for fixed values of q and for densities taken at the corresponding radial position, but it increases as the plasma current is raised. The mode structure does not vary significantly throughout the scan, as shown in the poloidal reconstruction reported in Fig.5 for two different times. An increase in the plasma current produces an outward displacement of the resonant surface corresponding to a fixed value of q (e.g. q=1.5). The corresponding variation of the density along the radial profile would translate into a variation of v_{Alfven}, and thus of f_{TAE}, which is compatible with the observed Eigenmode frequency variation. A quality factor larger than 100 seems to exclude the presence of continuum damping for this shot and is consistent, for its order of magnitude and its variation with the density, with the predicted effect of electron Landau damping [6].

v) Effect of additional heating

Preliminary results concerning AE excitation in the presence of fast particles generated by NBI and/or ICRH indicate that the damping rate is changed by additional heating. Experiments with the AE active diagnostic in conjunction with NBI, IRCH and Lower Hybrid additional heating, current drive and profile control, are under way.

5. CONCLUSIONS

The combination of external antenna excitation and synchronous detection of the plasma response constitutes the basis of the Alfven Eigenmode active diagnostic at JET. The experimental apparatus has been installed and tested and the diagnostic method has been successfully demonstrated. MHD global modes have been excited and identified as Alfven Eigenmodes by the dependence of their frequency upon the density and the toroidal magnetic field. The damping rates of TAE modes have been experimentally measured for the first time. Control of antenna phasing and space resolved magnetic measurements allow a determination of the excited mode structure. These experimental investigations on the behaviour and specifically on the damping, of the Alfven Eigenmodes in JET, complemented by MHD and kinetic modelling, are expected to provide an important contribution to the assessment of the Alfven Eigenmode stability in future thermonuclear experiments.

REFERENCES:

[1] A.D.Turnbull et al., *Phys. Fluids B* 5, 2546 (1993).
[2] H.L.Berk et al., IAEA/D-P-II-1, *these proceedings.*
[3] S.Ali-Arshad and D.Campbell, to be published on *Plasma Phys. and Controlled Fusion.*
[4] J.-M.Moret, *CRPP Laboratory Report* LRP 498/94 (1994).
[5] L.Villard et al., *Proc. 20th Eur. Conf. on Controlled Fusion and Plasma Physics,* ed. by J.A.Costa Cabral, M.E.Manso, F.M.Serra, F.C.Schuller, EPS Lisbon, (1993) IV, 1347, and G.T.Huysmans et al., *ibidem,* I, 187.
[6] R.Betti and J.P.Freidberg, *Phys. Fluids B* 4, 1465 (1992).

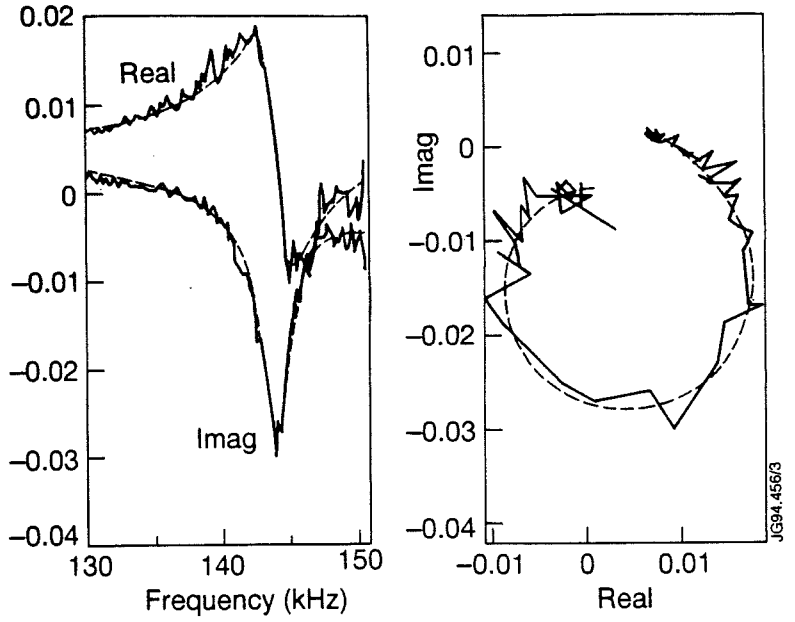

Fig.1 *Example of experimentally observed TAE resonance in the ohmic phase of JET shot #31638. Left: Real and imaginary part of a magnetic probe response. Right: Complex plane representation of the same signal. In both cases the signal is normalised to the exciter current. A fit with a rational fraction of order 5/2 is also shown. The fit gives f=144.2 kHz ($\delta f<100$ Hz), $\gamma=1400\ s^{-1}$ ($\delta\gamma<100\ s^{-1}$). $B \cong 2.8$ T, $I_p \cong 2.2$ MA, line integrated density $\cong 7x10^{19}\ m^{-3}$. Two active saddle coils (on the top of the machine, in opposite octants, 1 and 5) with the same phase are used.*

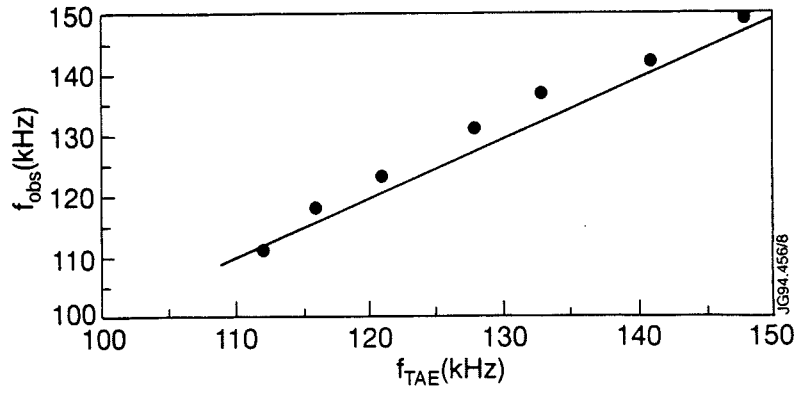

Fig.2 *Variation of the measured Eigenmode frequency with toroidal magnetic field (#31591). In the interval considered B is varied linearly between 2.2 T and 3 T. The density and plasma current are kept constant. The same saddle coils as in Fig.1 are active, but with opposite phase. Here and in Fig.3, f_{TAE} is calculated for constant q (q=1.5).*

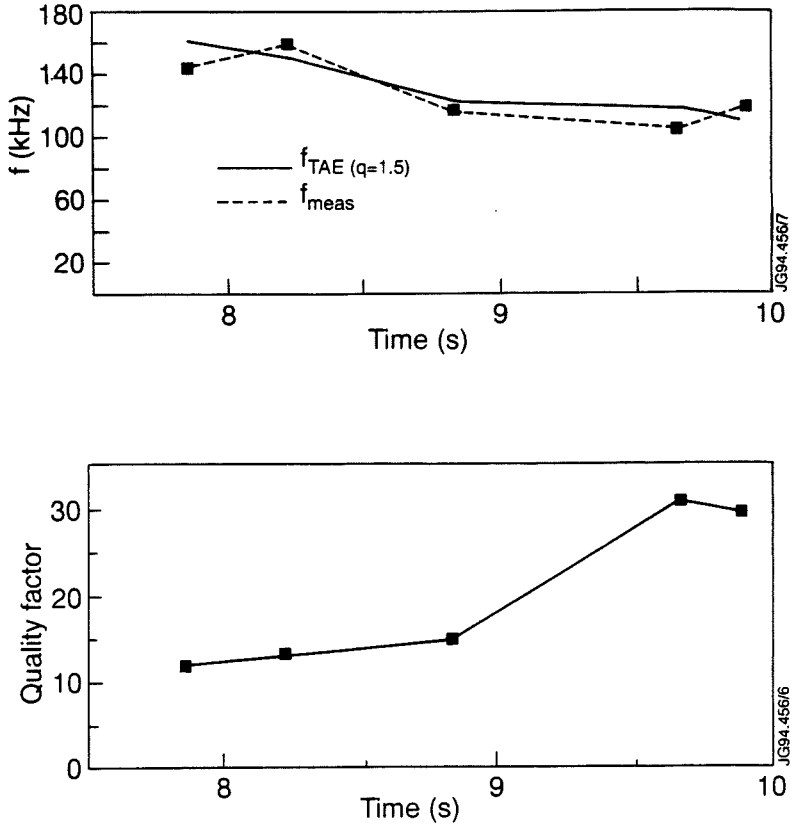

Fig.3 *TAE frequency (top) and quality factor (bottom) for different densities within JET shot #31150. The line integrated density varies between $5.2x10^{19}$ m^{-2} and $11x10^{19}$ m^{-2}; $B \cong 2.7$ T, $I_p \cong 2$ MA. One active saddle coil on the top is used.*

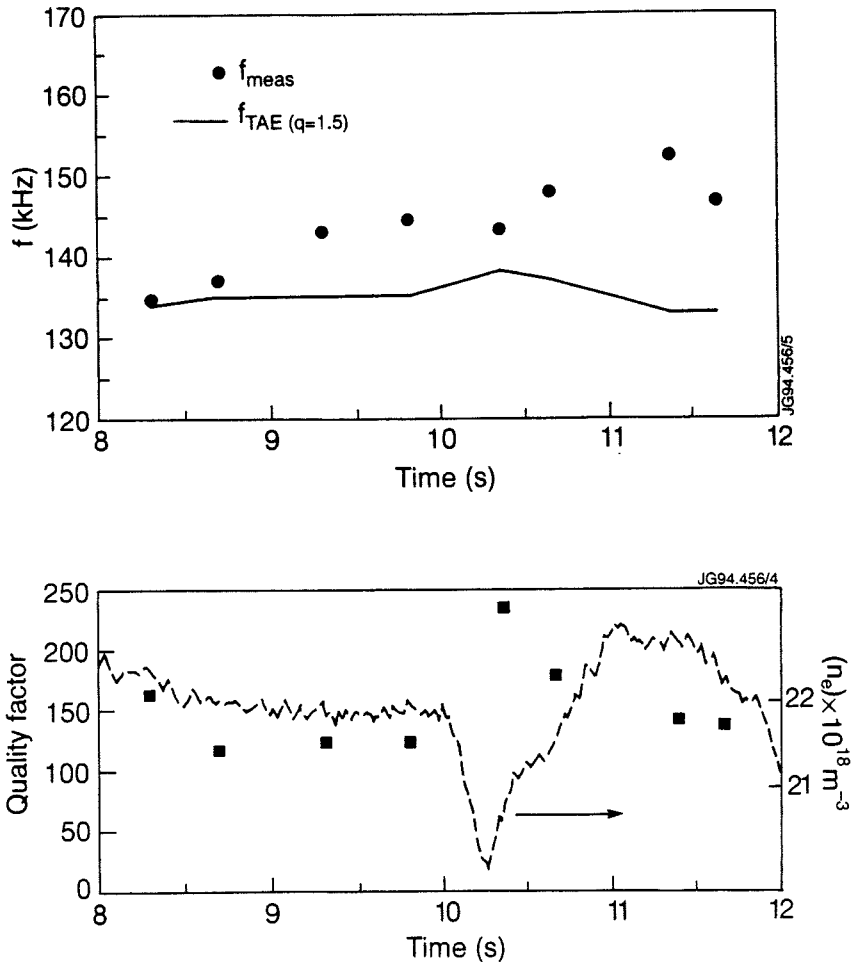

Fig.4 *Evolution of the observed frequency (top) and quality factor (bottom) of a global Alfven mode with increasing plasma current (JET shot #31638, as for Fig.1). The variation of density is also indicated (bottom). I_p is scanned linearly from 2.17 MA to 2.6 MA; $B \cong 2.8$ T.*

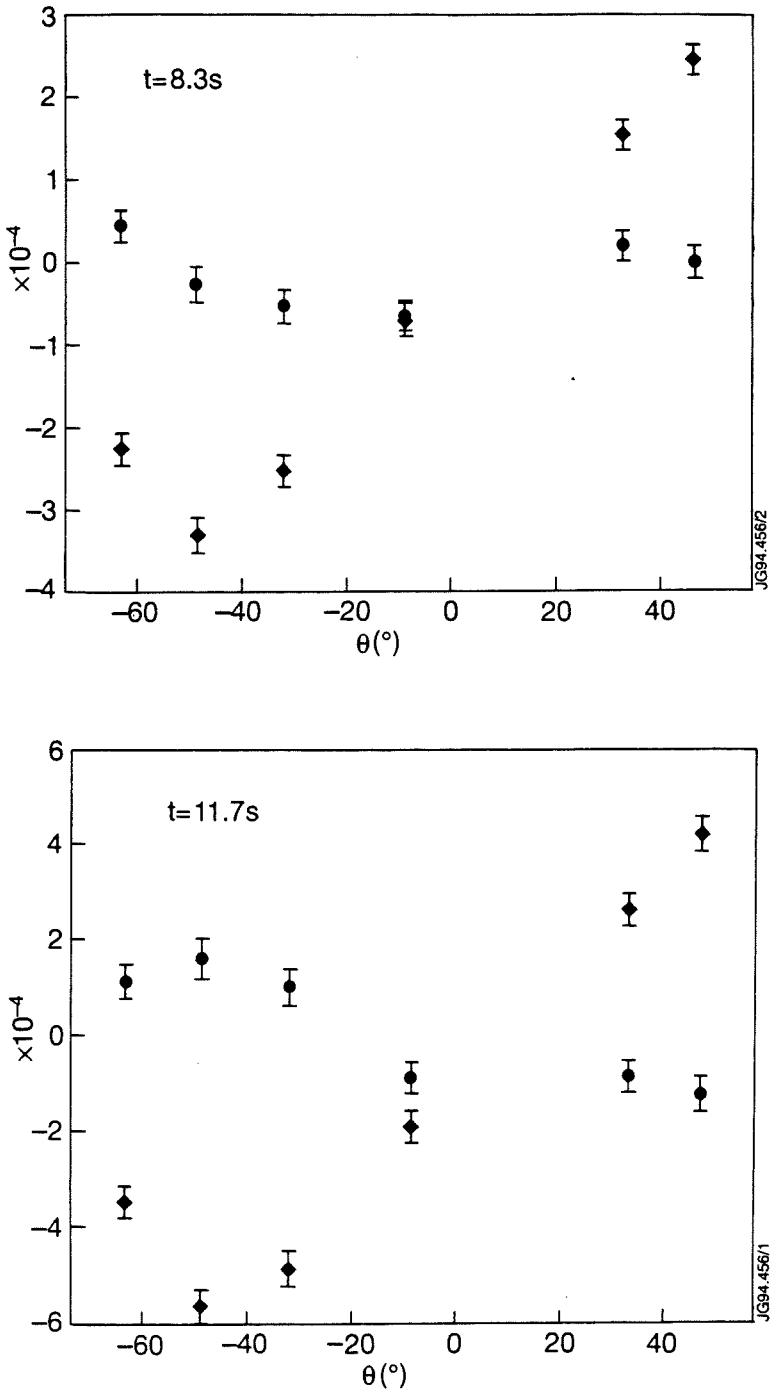

Fig.5 *Poloidal mode structure reconstruction for two different times of the current scan reported in Fig.4. Top: t=8.3 s; Bottom: t=11.7 s. Real (•) and imaginary (◆) components of the Eigenmode residues are plotted vs. the poloidal angle. As in Fig.1 the magnetic signals are normalised to the active saddle coil current.*